

# Adding anisotropy to the standard quasi-harmonic approximation still fails in several ways to capture organic crystal thermodynamics

Nathan S. Abraham and Michael R. Shirts\*

*Department of Chemical and Biological Engineering, University of Colorado Boulder,  
Boulder, CO 80309, USA*

E-mail: michael.shirts@colorado.edu

## Abstract

We evaluate the accuracy of varying thermal expansion models for the quasi-harmonic approximation (QHA) relative to molecular dynamics (MD) for 10 sets of enantiotropic organic polymorphs. Relative to experiment we find that MD, using an off-the-shelf point charge potential gets the sign of the enthalpic contributions correct for 6 of the 10 pairs of polymorphs and the sign of the entropic contributions correct for all pairs. We find that anisotropic QHA provides little improvement to the error in free energy differences from MD relative to isotropic QHA, but does a better job capturing the thermal expansion of the crystals. A form of entropy–enthalpy compensation allows the free energy differences of QHA to deviate less than 0.1 kcal/mol from MD for most polymorphic pairs, despite errors up to 0.4 kcal/mol in the entropy and enthalpy.

Deviations in the free energy of QHA and MD do not clearly correlate with molecular flexibility, clarifying a previously published finding. Much of the error previously found between QHA and MD for these flexible molecules is reduced when QHA is run from a lattice minimum consistent with the same basin as MD, rather than the energy-minimized experimental crystal structure. Specifically, performing anisotropic QHA on lattice minimum quenched from low-temperature replica exchange simulations reduced the error previously found by 0.2 kcal/mol on average. However, these conformationally flexible molecules can have many low-temperature conformational minima, and the choice of an inconsistent minima causes free energies estimated from QHA to deviate from MD at temperatures as low as 10 K. We also find finite size errors in the polymorph free energy differences using anisotropic QHA, with free en-

ergy differences as large as 0.5 kcal/mol between unit and supercells loosely correlated with differences in anisotropic thermal expansion. These larger system sizes are computationally more accessible because our cheaper 1D variant of anisotropic QHA, which gives free energies within within 0.02 kcal/mol of the fully anisotropic approach at all temperature studied. The errors between MD and experiment are 1–2 orders of magnitude larger than those seen between QHA and MD, so the quality of the force field used is still of primary concern, but this study illustrates a number of other important factors that must be considered to obtain quantitative organic crystal thermodynamics.

## Introduction

Solid organics can pack stably in multiple forms, each of which can have significantly different chemical and materials properties from each other. The ability of a molecule to arrange in multiple solid forms, or polymorphs, can change crystal solubility,<sup>1,2</sup> charge mobility,<sup>3,4</sup> hardness,<sup>5</sup> and reactivity.<sup>6–8</sup> Relative stability of crystals can change with temperature<sup>2,9–19</sup> and pressure,<sup>20–23</sup> so we must consider entropic effects and crystal lattice changes when modeling the crystal thermodynamics.

Methods such as molecular dynamics (MD) and the quasi-harmonic approximation (QHA) are important for understanding the relative stability of crystals. QHA estimates the thermodynamics as a function of temperature and pressure by computing free energy due to harmonic vibrations around each crystal lattice minimum, and then determining the lattice geometry that minimizes the Gibbs free energy at each temperature as the crystal is expanded from the initial crystal lattice min-

imum. It is common to model thermal expansion isotropically, where the lattice vectors remain proportional and angles fixed. MD provides a more accurate description of the entropy and therefore free energy by generating the full conformational ensemble of the crystal, rather than neglecting anharmonic motions. Additionally, QHA assumes a single lattice is representative of the crystal at low temperatures whereas MD samples an ensemble of lattice configurations.

Our previous studies show that an isotropic QHA model can often yield free energy differences between polymorphs that fall within numerical error of the polymorph free energy differences computed by MD for small and rigid molecules. However, free energies from QHA deviates from those generated by MD by  $> 0.1$  kcal/mol at 300 K for dynamically disordered crystals or crystals with greater conformational flexibility.<sup>24</sup> The small-molecule crystals examined in our previous study all showed some level of anisotropic expansion, and the error in the QHA free energy qualitatively increased with the degree of anisotropy. We concluded that the deviations of the isotropic QHA from MD were either due to 1) an inaccurate thermal expansion model or 2) anharmonic motions in the crystal lattice, or 3) some combination of the two. Without modeling QHA anisotropically, we could not definitively determine the source of the deviations of QHA from MD.

We recently developed a method to efficiently determine the true anisotropic free energy minimum within the quasi-harmonic framework.<sup>25</sup> This method relies on determining gradient of the lattice parameters with respect to temperature. Our gradient approach identifies high temperature free energy minimum that are 0.01–0.23 kcal/mol lower than the minimum identified with an isotropic model, altering the polymorph free energy differences of pirac-

etam and resorcinol by 0.02–0.12 kcal/mol for unit cells of 4–8 molecules.<sup>25</sup> Our fully anisotropic approach and even a simplified 1D-anisotropic approach outperformed the accuracy of current quasi-anisotropic methods that only consider the anisotropy due to the potential energy as a function of crystal lattice vectors.<sup>26–30</sup>

In this paper we re-evaluate the 10 of the 12 polymorph pairs previously studied with MD and isotropic QHA to determine whether an anisotropic thermal expansion model can improve the performance of QHA relative to MD.<sup>25</sup> Specifically, we:

- evaluate the use of an off-the-shelf point charge potential in modeling the entropy, enthalpy, stability, and thermal expansion of organic polymorphs;
- determine how well our 1D-QHA variant compares to QHA using full anisotropic expansion over a larger data set than our initial anisotropic methods paper;<sup>25</sup>
- determine if finite size effects significantly contribute to the free energy ranking of polymorphs;
- discuss the appropriate ways to compare QHA and MD;
- determine if anisotropic QHA can reduce errors with respect to MD found previously with isotropic QHA;
- evaluate if entropy–enthalpy compensation plays a significant role in differences between QHA and MD; and
- highlight crystal behaviors found in MD that QHA cannot account for.

## Methods

In this study we examine the experimentally known polymorphs of the 10 molecules shown in Figure 1 using QHA and MD. All 10 of these molecules were examined in our previous study.<sup>24</sup> Most MD results in this study are from our previous publication,<sup>24</sup> and a methodological discussion of MD can be found there.<sup>24,31</sup> Modifications of the MD procedure and where these modified simulations are used will be discussed in the context of the paper. All isotropic QHA results have been updated from that previous study and we describe those changes made here. In our previous study we examined 12 enantiotropic pairs of polymorphs, but have excluded two molecules due to the experimentally known plastic phases with dynamic disorder at each molecular site. The dynamic disorder was confirmed with MD, both by others and ourselves, for the rotation of cyclopentane<sup>15,24</sup> and trans/gauche isomerization of succinonitrile<sup>24,32</sup> in the disordered crystals. This behavior is inherently anharmonic, meaning there is no chance that QHA can properly model them, and hence they are left out of this study. Furthermore, both plastic phase crystals had their lattices constrained for stability in MD in previous studies,<sup>24</sup> so they were not modeling fully anisotropic thermal expansion.

### Quasi-Harmonic Approximation

In the quasi-harmonic approximation (QHA) the Gibbs free energy is computed by determining the lattice geometry that minimizes the sum of the potential and the energy of the static, harmonic lattice vibra-

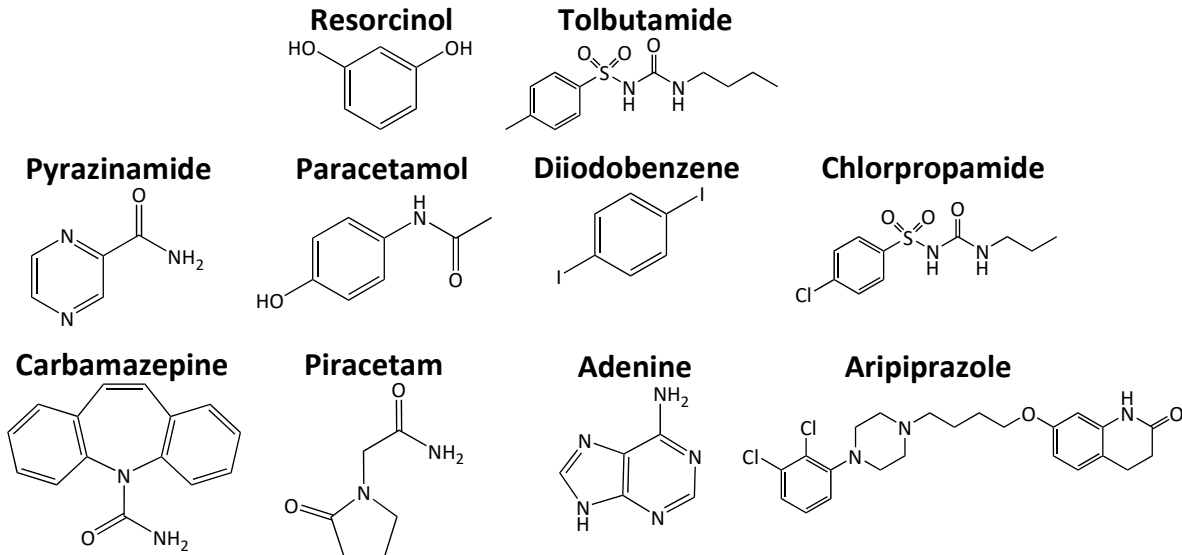


Figure 1: Molecules examined in this study.

tions, as shown in eq 2.

$$\begin{aligned}
 G(T) &= \min_y f(y, T) & (1) \\
 f(y, T) &= \min_{\mathbf{x}} (U(y, \mathbf{x}) \\
 &\quad + A_v(y, T) + PV & (2) \\
 y &= V, \mathbf{C}, \lambda
 \end{aligned}$$

where  $T$  is the temperature,  $P$  is the pressure,  $\min_{\mathbf{x}} (U(y, \mathbf{x}))$  is the lattice energy of the minimum energy cell geometry  $y$  and geometry optimized lattice coordinates  $\mathbf{x}$ , and  $A_v$  is the Helmholtz vibrational free energy of a harmonic oscillator. We define the cell geometry as  $y$ , which for isotropic expansion is the volume  $V$ , anisotropically with the six dimensional lattice tensor  $\mathbf{C}$ , or using our modified 1D-anisotropic expansion defined by  $\lambda$ .

The Helmholtz free energy ( $A_v$ ) of the lattice harmonic vibrations contribute to the entropic portion of QHA. We use the classical version of  $A_v$  for comparison to

MD, shown in eq 3.

$$A_v(V, T) = \sum_k \beta^{-1} \ln(\beta \hbar \omega_k(V)) \quad (3)$$

where  $\beta$  is  $(k_B T)^{-1}$ ,  $\hbar$  is the reduced Planck constant, and  $\omega_k$  is the frequency of the phonon of the  $k^{th}$  vibrational mode of the crystal lattice.

## Grüneisen Parameters

There are two common methods within the QHA framework to estimate the phonon frequencies of the crystal lattice at each lattice geometry of interest. The first way is to compute and diagonalize the mass-weighted Hessian of every crystal structure, which is computationally demanding. The second way is to use the Grüneisen parameter approach assumes that the changes in the frequencies of a particular phonon are constant as the crystal is strained in a particular direction. Use of the Grüneisen parameter to calculate the thermodynamics of organic and inorganic material is common.<sup>24,33–36</sup>

This assumption can introduce errors, but we have shown for polymorph free energy differences that those errors are generally less than 0.02 kcal/mol.<sup>25</sup> This is smaller than the experimental error in most cases, so we will exclusively use the Grüneisen parameter approach for QHA calculations in this paper when calculating polymorph free energy differences.

The standard definition of the Grüneisen due to a volume change is in eq 4, which is directly applicable only for constant strains, such as isotropic expansion, is:

$$\gamma_k = -\frac{V}{\omega_k} \frac{\partial \omega_k}{\partial V} \quad (4)$$

where  $\gamma_k$  is the Grüneisen parameter for the  $k^{\text{th}}$  vibrational frequency. Eq 4 is solved numerically, which requires diagonalization of the mass-weighted Hessian at two volumes to produce reference frequencies. The corresponding Grüneisen parameters can be used to solve the frequencies at all isotropic volumes relative to a reference point, generally the lattice minimum structure.

The Grüneisen parameter for the volume can be extended to a crystal placed under any strain,<sup>25,37</sup> which we will use for anisotropic expansion. Eq 5 is the anisotropic version of the isotropic equation (eq 4).

$$\gamma_{k,i} = -\left. \frac{1}{\omega_k} \frac{\partial \omega_k}{\partial \eta_i} \right|_{\eta_j \neq \eta_i} \quad (5)$$

Here, the Grüneisen parameter for the  $k^{\text{th}}$  vibrational mode due to the  $i^{\text{th}}$  strain ( $\eta_i$ ) applied to the crystal is  $\gamma_{k,i}$ . The symmetric  $3 \times 3$  strain matrix  $\boldsymbol{\eta}$  allows us to compute 6 sets of Grüneisen parameters numerically. With the Grüneisen parameters and reference frequencies, we can compute the frequencies of the lattice parameters at any cell geometry of interest, by integrating

eq 5. A full discussion of the use of both the isotropic and anisotropic Grüneisen parameters can be found in previous work.<sup>25</sup>

## Thermal Expansion

We previously implemented a method to determine the crystals thermal expansion,<sup>25</sup> which can be used to solve bi-optimization problems,<sup>38</sup> such as QHA. Eq 6 gives the general formulation for determining the crystal thermal expansion. If we have a reference structure, the 0 K minimum (i.e. classical lattice minimum), we can compute the thermal expansion and numerically integrate with temperature.

$$\begin{aligned} \frac{\partial y}{\partial T} &= \left( \frac{\partial^2 G}{\partial y^2} \right)^{-1} \frac{\partial S}{\partial y} \\ y &= V, \lambda, \mathbf{C} \end{aligned} \quad (6)$$

In eq 6,  $T$  is the temperature,  $S$  is the entropy, and  $G$  is the Gibbs free energy. By computing the numerical derivatives of the entropy and Gibbs free energy we can determine the gradient of  $y$ , the cell geometry, with respect to temperature.

### *Isotropic Expansion*

Isotropic expansion assumes that the lattice vectors remain proportional to one another and the lattice angles remain fixed. Due to these constraints the solution to QHA in eq 2 requires minimization of a single variable, the volume ( $y = V$ ). We compute the rate of isotropic thermal expansion using eq 6 and replacing  $y$  with the crystal volume ( $V$ ).

### *Anisotropic Expansion*

Anisotropic expansion allows the crystal lattice to relax to the harmonic free energy minimum structure by removing all constraints in isotropic expansion. In eq 2 we minimize the free energy as a function of all six crystal lattice parameters ( $y = \mathbf{C}$ ), which makes the problem of minimizing the

Gibbs free energy for QHA more complex. We compute the thermal expansion for all six parameters by using eq 6 and replacing  $y$  with a array of the six lattice parameters ( $\mathbf{C}$ ).

#### *1D-Anisotropic Expansion*

Computing eq 6 for anisotropic expansion ( $\mathbf{C}$ ) requires 73 lattice optimizations to determine a single six-dimensional gradient, which becomes increasingly expensive to compute for the entire temperature range of interest. In our previous work,<sup>25</sup> we found if the ratio of anisotropic expansion was kept constant at all temperatures we could achieve the same free energy differences within 0.005 kcal/mol of full anisotropic expansion. In that paper, we presented eq 7,

$$C_i(\lambda) = C_i(\lambda = 0) + \kappa_i \lambda(T) \quad (7)$$

where the lattice parameter  $C_i$  is a function of the variable  $\lambda$  and  $\kappa_i$ . In this case,  $\lambda$  is a single parameter describing the expansion in eq 2, which is zero at the 0 K lattice minimum value of  $C_i$ .  $\kappa_i$  is the gradient computed in eq 6 for  $y = \mathbf{C}$  at 0 K.

## Molecular Dynamics

A more complete approach to compute the thermodynamics of the crystals, including the free energy difference between polymorphs, is molecular dynamics (MD), which generates (in theory) the full configurational ensemble at a given temperature of interest. For our method, there are two necessary steps for computing the free energy differences of polymorphs using MD: 1) determine  $\Delta G$  between polymorphs at a reference temperature with simulations of a series of non-physical intermediate states and 2) determine  $\Delta G$  as a function of temperature for each polymorph using simulations at range of temperatures. For the first step, we can drive each crystal along a reversible

thermodynamic path to an ideal gas state by turning off intermolecular energies to determine the reference free energy differences. Then, with simulations at intermediate temperatures we can relate each temperature point back to the reference energy difference between polymorphs using the Multistate Bennett Acceptance Ratio (MBAR). A full discussion of this approach can be found in our previous work.<sup>24,31</sup>

## Computational Details

We have provided as supporting information a .zip file including all computational details to re-run simulations for both MD and QHA. For specifications on how we chose certain parameters we refer the reader back to our previous publications that present the methods for MD<sup>24,31</sup> and QHA.<sup>25</sup>

#### *Molecular Dynamics*

For a number of crystals, we found that the lattice parameters from the previous study<sup>24</sup> did not continuously change with temperature at low  $T$  for MD, so we reran the crystals with temperature replica exchange (REMD) to better escape from metastable states and thus allow for better convergence to the 0 K lattice energy minimum. Replica exchange parameters were chosen to give an average exchange probability of  $\sim 0.3$  between temperature samples from 10 K up to 350 K. Temperature replica exchange allows the simulations at different temperatures to exchange with one another, which causes the crystal to be heated up and reannealed throughout simulation while maintaining the proper ensemble distribution at all temperatures.<sup>39</sup> Temperature replica exchange was required to compute the low-temperature ensembles of for tolbutamide, chlorpropamide, and aripiprazole. We provide input files for both MD and QHA all within the input\_files.zip,

which contains all parameters for individual crystals and simulation settings for GRO-MACS 2018.

#### *Quasi-Harmonic Approximation*

All QHA calculations were performed using our Python based lattice dynamics code available on GitHub at [http://github.com/shirtsgroup/Lattice\\_dynamics](http://github.com/shirtsgroup/Lattice_dynamics). The code currently wraps around a number of molecular modeling packages. In this paper, all lattice vibrations, energy evaluations, and optimizations were performed using Tinker 8.1 molecular modeling distributed TINKER code to correct for errors in the Hessian calculation. Those modifications are discussed in the main paper and supporting information of our previous work and have since been updated in Tinker 8.7.<sup>25</sup>

Lattice structures were retrieved from the Cambridge Crystallographic Data Center (<https://www.ccdc.cam.ac.uk/structures/>) and a unit and supercell were lattice optimized. Supercells were created assuring that the three lattice vectors were twice the van der Waals cutoff, (8 Å). Specifications on cell size can be found in the Table S3. Each molecule was parameterized using the OPLS-AA<sup>40,41</sup> classical fixed point charge potential:

$$U_{total} = U_{bond} + U_{angle} + U_{dihedral} + U_{vdw} + U_{coulombic} \quad (8)$$

where the exact forms of the each of the energy terms are defined in the references.

The crystal structures were geometry and lattice optimized to the lattice minimum structure. Optimization of the crystal structure was performed with Tinker’s `xtalmin` executable to an RMS gradient/atom of  $10^{-5}$ . The molecules centers of mass, keeping the coordinates relative to the center of mass constant constant. The crystal was then geometry optimized using

Tinker’s `minimize` executable to an RMS gradient/atom of  $10^{-4}$ . These values were chosen to maximize convergence and numerical stability for the gradient method, and this choice is discussed fully in the supporting information of our previous work.<sup>25</sup>

To determine  $y(T)$  across the entire temperature range we use a 4<sup>th</sup> order Runge-Kutta integrator using the thermal gradient approach to satisfy eq 1. For most crystals, we found that 3 steps of 100 K each up to 300 K ensures that the crystal was at a locally metastable free energy minimum at all temperatures. If the structure is not at a free energy minimum with respect to box geometry variables at 300 K, the structure was re-run with 6 Runge-Kutta steps. For the unit cells only, if 6 steps could not maintain the crystal at a free energy minimum then 20 steps were run. All results shown are for the maximum temperature step that could be achieved while assuring that it remained at a free energy minimum with respect to box geometry under expansion (temperatures given in Table S4). Results for the graphed intermediate points between Runge-Kutta steps were calculated with a third order spline that was fit to the lattice parameters with temperature.<sup>25,42</sup>

## **Details of experimental data used for comparison**

We have exhaustively collected experimental results reported in literature to compare thermal expansion and thermodynamic stability to for MD. In previous work we compared entropic and enthalpic contributions to polymorph relative stabilities, but have found some inconsistencies in those reported results<sup>24</sup> and reevaluate these calculations here. Provided with our supporting information are two files, `experimental_expansion.csv` and `experimen-`

tal\_stability.csv, containing the literature results we used for comparison. In the expansion results file we provide the reported experimental lattice parameters, citation references and links, reported temperatures, and reference codes if the structure was submitted to the CCDC. For the stability results we report the values seen in Figure 2 along with the reported temperatures and literature references.

## Results and Discussion

The approaches presented above allow us to evaluate the effectiveness of QHA methods with different treatments of thermal expansion relative to MD for polymorph thermodynamics, including free energy differences between polymorphs, and lattice expansion. The differences between approaches for estimating the temperature dependence are greatest at high temperatures, so all comparisons are shown at the maximum temperature at which QHA is stable.

For QHA, we found that discontinuous readjustment of the molecules within the lattice occurs frequently during expansion, causing the method to expand to a structure that no longer corresponds with free energy minimum of the chosen expansion variable. As the crystal expands, the free volume around the molecules increases, allowing molecules to readjust into alternate minima more favorable to the lattice energy than the minima found by continuous deformation of lower temperature minima. These structural disruptions are problematic for the numerical stability of the gradient approach and generally cause the crystal to expand to a structure that is not a free energy minimum. For example, upon expansion of tolbutamide, at a certain point the alkyl tail can move into a newly created free volume, causing the quasi-harmonic free energy to

become discontinuous with temperature.

We determine if the crystal is at a free energy minimum with respect to the geometry parameter  $y$  by checking if:

$$\left(\frac{\partial G}{\partial y}\right)_{Backward} < 0 < \left(\frac{\partial G}{\partial y}\right)_{Forward} \quad (9)$$

If our crystal is at or near a free energy minimum, then the forward and backward numerical solution to eq 9 must be positive and negative respectively. If both are the same sign, then we must no longer be at a minimum.

All results using QHA are shown at the maximum temperature ( $T_{max}$ ), which is the highest temperature to satisfy eq 9. The values of  $T_{max}$  are reported in Table S4 and Table S5. Plots of the polymorph free energy differences and lattice expansions versus temperature for the 10 molecules studied are provided (Figures S20 – S56). Further quantification of the numerical and structural instability is discussed in the work where we initially presented the gradient method.<sup>25</sup>

## Comparisons to Experimental Results

We found that the OPLS-AA point charge potential is a poor predictor of the sign of enthalpic differences for polymorphs relative to experiment, as is expected for the simplicity of the energy function, but does accurately estimate the sign of the entropic differences. In Figure 2a and 2b the enthalpic and entropic contributions to the polymorph free energy differences at 300 K for the supercells using MD are shown relative to their experimental values, which are reported at varying temperatures that generally corresponding with the polymorph transition temperature.<sup>2,9,10,14,16,18,43–46</sup> The sign of the enthalpic contributions is only

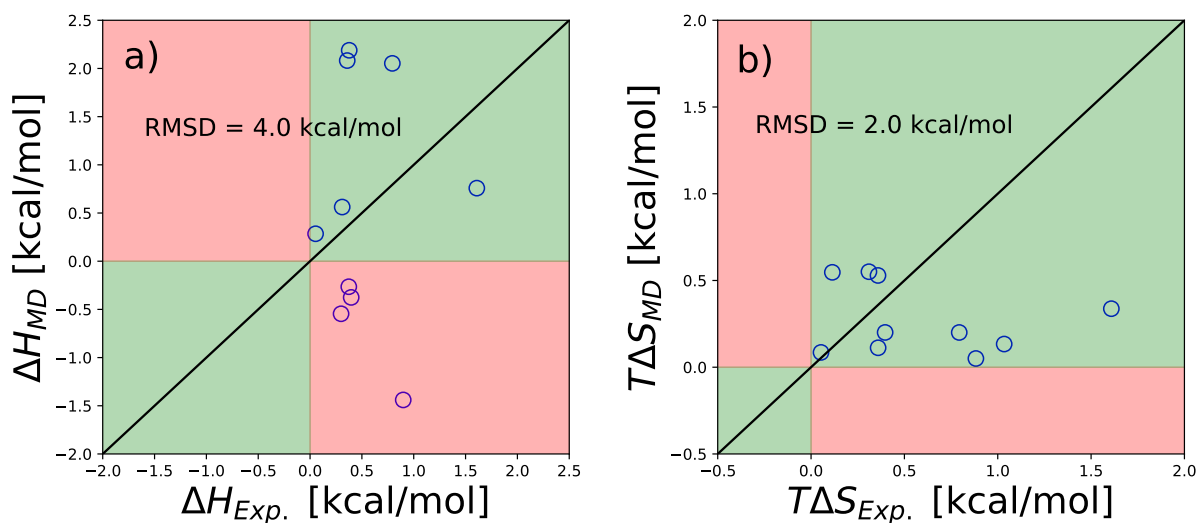


Figure 2: 300 K polymorph differences from MD for a) enthalpy and b) entropy versus experimental values taken from literature.<sup>2,9,10,14,16,18,43–46</sup> The sign of the enthalpy is only correct for MD for 6 of the 10 molecules, with no clear distinguishing molecular or crystallographic features separating the crystals with the incorrect sign. This contrasts with the entropy, which is correct in sign for all 10 molecules. If the polymorph pairs fall in the green quadrants than MD has the same sign as experiment, and the wrong sign in the red quadrants.

correct for 6 of the 10 polymorph pairs. The 4 molecules where the simulation has the wrong enthalpic ranking are piracetam, pyrazinamide, resorcinol, and paracetamol, and none of the enthalpic errors in these molecules have obvious correlations to chemical groups present, flexibility, crystal  $Z$  and  $Z'$  values, or relative packing. This contrasts with the polymorph entropy differences, where the sign is correct for MD for all 10 molecules. The RMSD between theory and experiment are 4.0 and 2.0 kcal/mol for  $\Delta H$  and  $T\Delta S$ , respectively. The most likely large sources of deviation from experiment could be due to 1) the experimental values coming from the polymorph transition temperature, not 300 K and 2) the use of a point charge potential to model the crystal energetics.

The lattice geometries for MD differ moderately from experiment, though the volumes match experiment more closely. We can quantitatively compare to experiment using exhaustive experimental results from Brandenburg and Wilson for carbamazepine form III and paracetamol form I, respectively.<sup>47,48</sup> The expansion of the lattice vectors, angles, and volume are shown for carbamazepine form III (Figure 3) and paracetamol form I (Figure 4). Prediction accuracy of lattice vectors varies both with crystal and lattice vector. We find that if the lattice vectors are orthogonal for experiment, MD always gets the corresponding angle correct or within error as seen with  $\alpha$  and  $\beta$  angles for carbamazepine and paracetamol. Despite errors in the individual lattice parameters, the crystal volume is similar between MD and experimental values. In the case of paracetamol (Figure 4) the experimental volume is within error of MD.

The change in the lattice vectors and orthogonal angles in MD generally agrees with experiment despite errors in the actual geometry. In Figures 3 and 4 we provide the

thermal expansion of each parameter by fitting a linear fit to MD and experimental data at all temperatures. In carbamazepine the change in the slope of experimental lattice parameters at low temperatures could be indicative of quantum behavior from the zero point energy, so for this crystal we perform the linear fit on values above 100 K. For all of the lattice vectors we see that the thermal expansion between MD and experiment are the same order of magnitude and sign. For the orthogonal angles there is no expansion. However, the thermal expansion of the  $\beta$  angle in both polymorphs has the wrong sign and in the case of paracetamol form I is an order of magnitude different. For carbamazepine, we see larger divergence between experiment and MD at low temperatures ( $T < 100$  K), which would be indicative of quantum zero-point energy effects. For both polymorphs there is also good agreement with experiment for the volumetric thermal expansion. Accurately modeled thermal expansion helps to explain why we also get the correct sign of the entropic differences for all 10 polymorph pairs in Figure 2b.

## Testing the Validity of 1D-Anisotropic QHA

Anisotropic expansion is relatively expensive compared to isotropic expansion, though still 2 orders of magnitude cheaper than free energy estimation with MD. Our previous work shows that a 1D-variant of anisotropic expansion can be a sufficient substitute to speed up the method with little effect on the accuracy of computed free energy differences.<sup>25</sup> Fully anisotropic expansion requires 73 structure optimizations every time the thermal gradient is computed. This contrasts with the 1D-approach, which requires the initial 73 op-

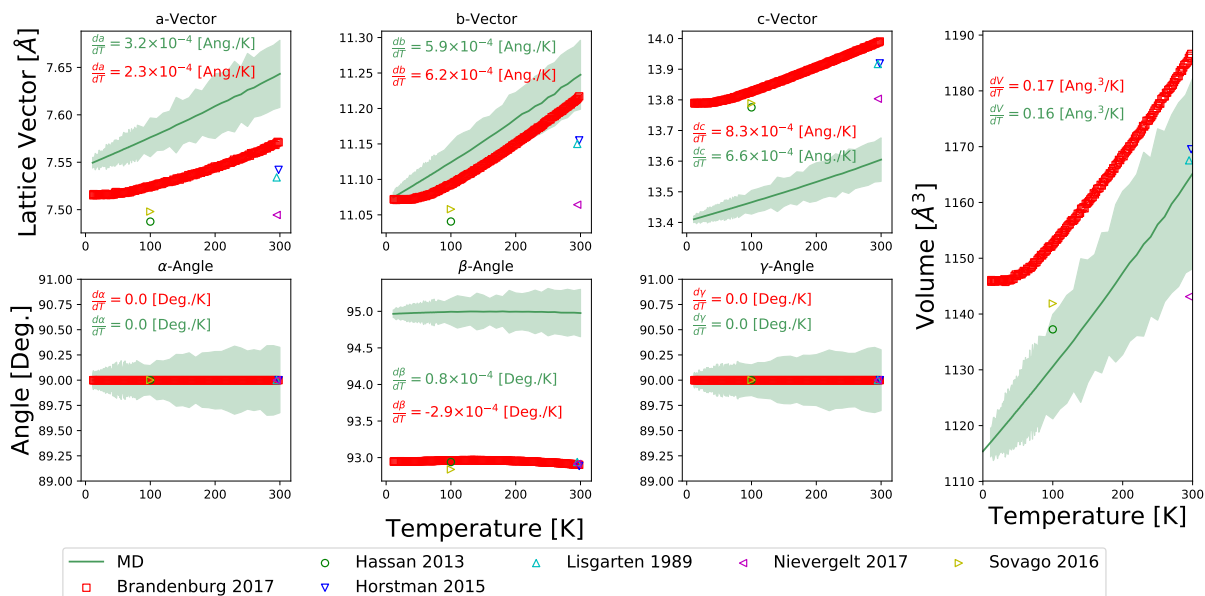


Figure 3: Thermal expansion of carbamazepine form III comparing MD to experimental results provided in literature.<sup>47,49–53</sup> While the lattice parameters differ between theory and experiment, the thermal expansion is similar between MD and experiment for all lattice parameters and volume. At low temperatures we find the largest deviation between experiment and MD. The shaded green area is the standard deviation in the lattice parameter during the MD simulation.

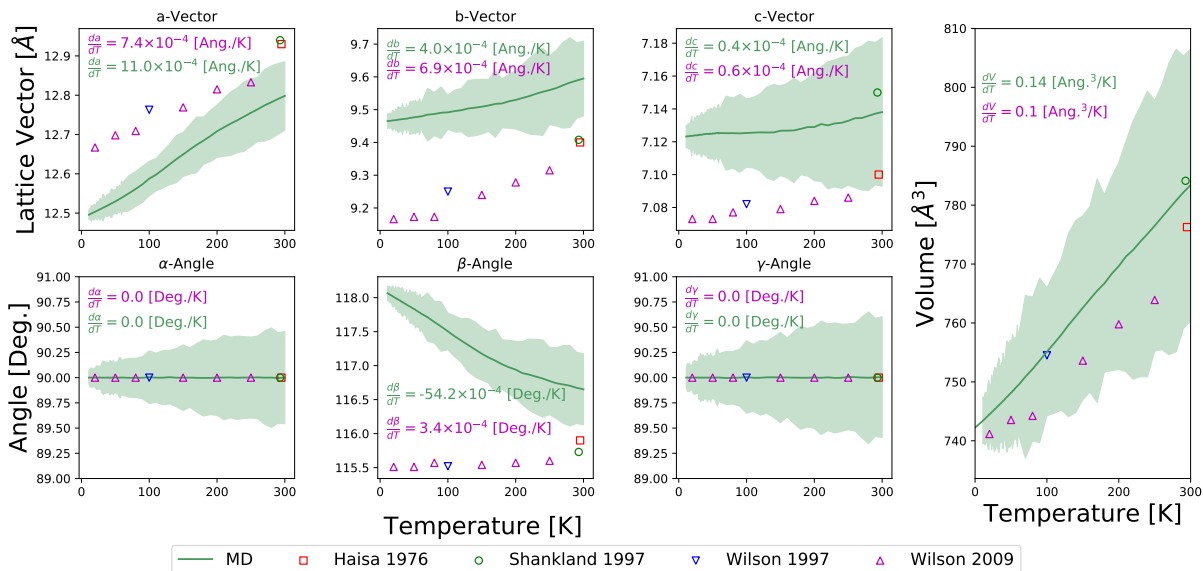


Figure 4: Thermal expansion of paracetamol form I comparing MD to experimental results provided in literature.<sup>48,54–56</sup> While the lattice parameters differ between theory and experiment, the thermal expansion is similar between MD and experiment for all lattice parameters and volume, except for the  $\beta$  angle. The shaded green area is the standard deviation in the lattice parameter during the MD simulation.

timizations at 0 K followed by 3 optimizations at all subsequent points for numerical integration. When we first presented the gradient approach we found that the 1D-anisotropic QHA approach computed polymorph free energy differences within 0.01 kcal/mol of full anisotropic expansion for the two sets of polymorphs tested. For this study, we ran both 1D-QHA and anisotropic QHA on unit cells of the quenched experimental structures (independent of MD) to evaluate the effectiveness of the 1D constraint.

The constraints applied to 1D-anisotropic approach provide numerical stability, allowing eq 9 to be satisfied at 300 K more frequently. At each integration step for expansion our program checks if eq 9 is satisfied, verifying if the crystal is at a free energy minimum. We will only report result up to the temperature ( $T_{max}$ )

where eq 9 is satisfied. When using fully anisotropic expansion, only 11 of the 20 crystals were able to satisfy eq 9 at all temperatures ( $T_{max} = 300$  K). This contrasts with the 1D-approach, where 19 of the 20 crystals remained at a free energy minimum up to 300 K. The only molecules where the fully anisotropic approach remained at a free energy minimum for both polymorphs were the relatively rigid resorcinol, adenine, and carbamazepine, suggesting that rigid molecules are less likely to experience numerical disruptions in QHA.

For the 10 molecules in this study, the RMSD in polymorph free energy difference between 1D-anisotropic and anisotropic QHA is 0.0066 kcal/mol, which is well below physically meaningful sensitivity thresholds. Figure 5a shows the polymorph free energy differences computed with 1D-QHA versus those computed with anisotropic

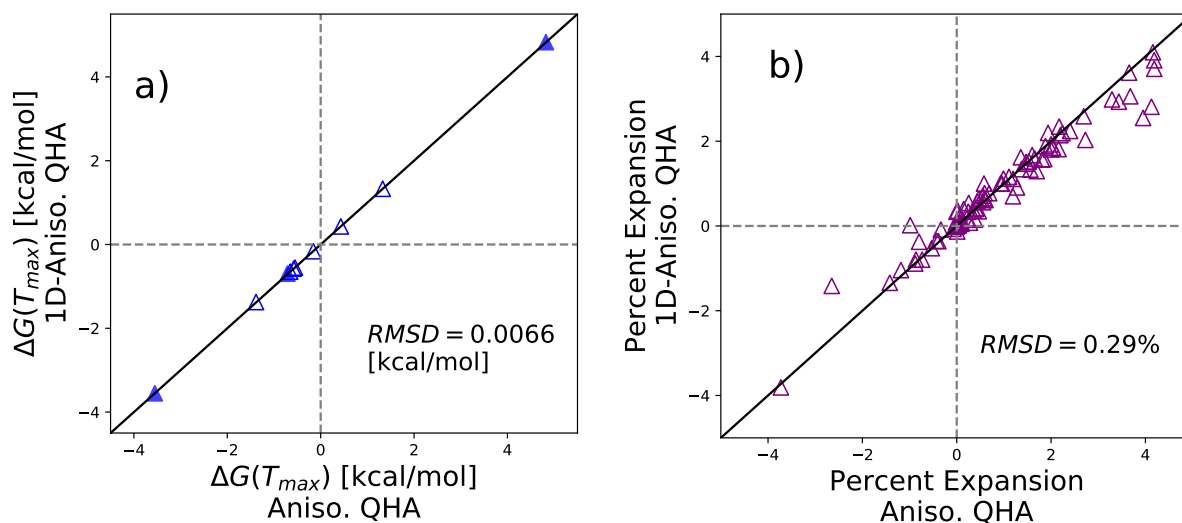


Figure 5: Comparison of the results of 1D- and fully-anisotropic QHA applied to the polymorphic unit cells. In all plots, the filled-in markers are the molecules with multiple molecular conformers (tolbutamide, chlorpropamide, and aripiprazole). a) Polymorph free energy differences ( $\Delta G(T_{max})$ ) computed with 1D and full anisotropic approaches are nearly equal. The black line is plotted as  $y = x$  and the data has a  $RMSD = 0.0066$  kcal/mol relative to that line. b) The percent expansion from 0 K to  $T_{max}$  for the three lattice vectors and angles are plotted. The  $RMSD$  in percent expansion between 1D and anisotropic QHA is 0.29%.

QHA at  $T_{max}$ . The free energies of most polymorphic pairs vary by less than 0.010 kcal/mol between 1D-QHA and anisotropic QHA. The only exception is aripiprazole, where the two QHA methods for determining  $\Delta G$  between polymorphs differ by 0.016 kcal/mol. The error in aripiprazole comes primarily from form X. The error in the individual free energies of polymorphs between 1D and fully anisotropic QHA is  $< 0.006$  kcal/mol (excluding aripiprazole form X), whereas the error in isotropic expansion is between 0.01–0.21 kcal/mol (Figure S11). Similarly, the high temperature lattice geometries of the two approaches have an RMSD of 0.29% for the expansion relative to lattice minimum structure.

For the molecules studied, 1D-anisotropic QHA is thus a sufficiently accurate approach to model anisotropic expansion for most purposes, and is much more efficient. The 1D approach produces polymorph free energy differences within 0.02 kcal/mol of the fully anisotropic approach at about 10% of the computational cost. More importantly, the 1D approach has greater numerical stability than full anisotropic expansion, allowing us obtain results at higher temperatures. The close numerical agreement between the 1D and fully anisotropic approach up to  $T_{max}$  shows that the 1D approach is a realistic constraint for these molecules. We will therefore use the 1D approach for all further evaluations for anisotropic QHA.

## The Cell Size Has a Non-negligible Effect on Polymorph Stability

We observe differences in the quasi-harmonic free energy differences between unit cells and supercells ranging from 0.04–0.5 kcal/mol and are loosely correlated to

differences in the high temperature cell geometry. In our previous study we assumed that an energy contribution less than 0.12 kcal/mol would give us 90% confidence that a re-ranking in crystal stability would not occur,<sup>24</sup> a number based on a previous much larger study of lattice energies versus quasi-harmonic free energies.<sup>57</sup> Six of the ten polymorphic pairs in Figure 6 exceed that cutoff, showing that finite size errors are sufficiently large to affect the stability ranking of polymorphs. All unit cells were quenched from the experimental crystals prior to running QHA and the supercells were constructed from the quenched unit cells. These results used the 1D-anisotropic approach for QHA.

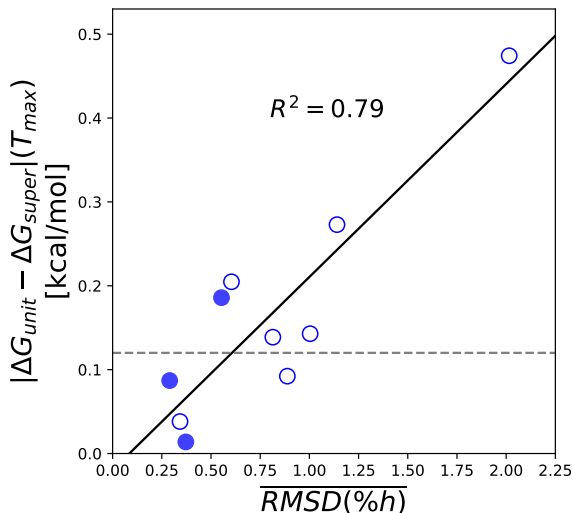


Figure 6: Differences between 1D-QHA in unit and supercells are shown for polymorph free energy differences against the average RMSD in percent expansion at  $T_{max}$ . There is a moderate ( $R^2 = 0.79$ ) correlation between the difference in unit and supercell percent expansion and the finite size error in free energy. The grey line is the 0.12 kcal/mol threshold, where values below the line have a 90% estimated confidence that re-ranking in crystal stability would not occur.<sup>57</sup> In all plots, the filled-in markers are the molecules with multiple molecular conformers (tolbutamide, chlorpropamide, and aripiprazole).

The error in the free energy differences between unit and supercells is correlated to the difference in expansion of the lattice parameters between unit and supercells. In Figure 6 we plot the deviations in the polymorph free energy differences versus the average RMSD of the percent expansions in both crystals. We found that there was a moderate linear correlation ( $R^2 = 0.79$ ) between percent expansion and deviations in the free energy due to finite size effects. Tolbutamide and chlorpropamide (filled-in markers) still fall under the cutoff suggest-

ing, though with a limited data set, that there is not necessarily significant correlation between molecular flexibility and finite size error. The largest error (0.47 kcal/mol) is for paracetamol where the supercell is only 6 times the size of the unit cell. This is the smallest difference between unit and super cell used in this study, with the largest being 24 times. Furthermore, we looked at the correlation between finite size errors and the ratio of unit and super cell and find that there is no correlation ( $R^2 = 0.109$  in Figure S13). The cell dimensions of supercells relative to unit cells can be found in Table S3.

## Performing QHA with a Lattice Minima Consistent with MD Ensembles

The lattice minimum structure quenched from experiment does not always coincide with the low temperature structures found from MD simulation of the same model, raising the question of what it means to compare QHA to MD. For some of the polymorphs studied here, we have found that the crystal supercells clearly reorganized into different configurational ensembles when heated up to 300 K using MD and can be quenched to a number of lattice minimum.<sup>24,58</sup> This suggests than QHA can be performed either independent or dependent of MD equilibration. QHA independent of MD equilibration, using a minimized experimental structure, has the potential risk of occupying a different basin than the MD simulation does, leading to potentially large differences in both lattice energy and configurational entropy between the approaches. In contrast, if QHA is run from a thermally annealed structure of the MD simulations, we have a better chance of matching the high-temperature MD ensemble with QHA,

as the lattice energy and vibrational modes will be more nearly the same, giving a purer test of whether the high temperature behavior is indeed quasi-harmonic.

To maximize the chance that we can identify the free energy minimum at low temperature, we performed temperature replica exchange molecular dynamics for the polymorphs of tolbutamide, chlorpropamide, and aripiprazole. For these six polymorphs, five frames from the equilibrated 10 K REMD simulation were quenched in order to find a lattice minimum for QHA consistent with the MD ensemble. All frames from the MD trajectory quenched to minima that had their potential energy within 0.02 kcal/mol, lattice vectors within 0.2 Å, and angles within 1.0° from one another. Differences in minima arose from conformations of the alkyl tails in both polymorphs of tolbutamide and chlorpropamide form V. In Table 1 we report the potential energy of the polymorphs when quenched from experiment, the lattice minimum used in our 2017 paper,<sup>24</sup> and the lowest energy structure quenched from REMD, relative to minimum found using REMD. Quenching from REMD produces the lowest lattice energy structure for all polymorphs. Overlaid structures of restructured crystals are provided in Figures S14–S19.

When the lowest lattice energy minimum is chosen, the error between isotropic QHA and MD is reduced by 0.083 kcal/mol from the error previously reported.<sup>24</sup> The error previously reported for these three systems was 0.083 – 0.397 kcal/mol, but with the new minima is 0.014 – 0.247 kcal/mol. In Table 2 the error of QHA for polymorph free energy differences relative to MD using replica exchange is shown at  $T_{max}$  for

the minimum found from our previous study and the minimum quenched from the 10 K REMD simulation. We exclude the lattice minimum quenched from the experimental structure since the lattice energy differences are so large. For isotropic QHA, the minimum quenched from REMD reduces the error relative to MD by 0.15 kcal/mol for tolbutamide and chlorpropamide. We see an increase in the error for aripiprazole, which is minimal compared to the reduction in error for the other two sets of polymorphs.

When using the lower lattice energy minimum, anisotropic QHA determines the stability of chlorpropamide and aripiprazole within 0.05 kcal/mol relative to MD. The error in QHA for tolbutamide, 0.206 kcal/mol, is still large, but is half the magnitude of what was previously reported.<sup>24</sup> Despite the new minimum of aripiprazole producing higher error in isotropic QHA, using anisotropic expansion reduced the error to 0.045 kcal/mol, implying that an isotropic constraint is inappropriate. The small increase in error when switching to anisotropic treatments seen in chlorpropamide for anisotropic QHA is most likely due to cancellation of error between polymorphs. For these polymorphs, all further analysis of QHA will be shown for the restructured crystals found from quenching low-temperatures replicas of REMD simulations.

## Comparison of thermal expansion and thermodynamics using QHA and MD

Anisotropic QHA allows the crystal lattice to relax into geometries that are more similar to MD, but there are still persistent errors in the high temperature geome-

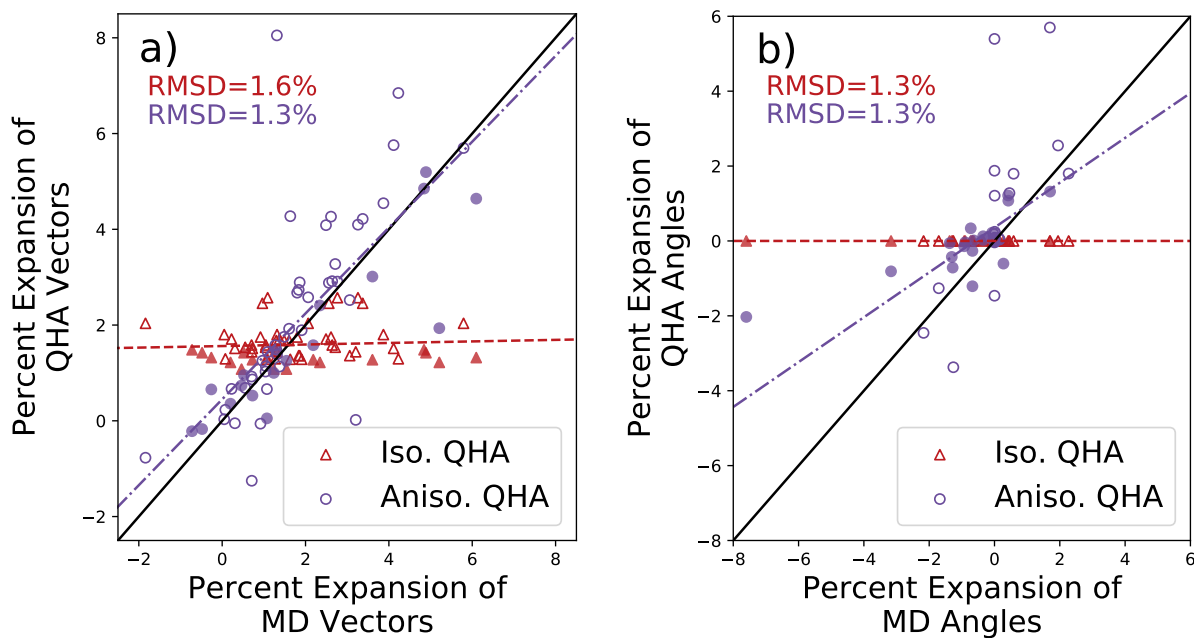


Figure 7: Scatter plots of the percent expansion of QHA versus MD for the lattice a) vectors and b) angles for isotropic and 1D-anisotropic QHA lattice parameters. The RMSD to MD is marginally improved for the lattice vectors and not improved for the angles when using anisotropic expansion over isotropic expansion. A least square fit between MD anisotropic QHA shows that anisotropic expansion provides a better  $y = x$  fit (black line) to MD than isotropic expansion. The slopes for anisotropic and isotropic expansion are a)  $0.89 \pm 0.22$  and  $0.02 \pm 0.06$  and b)  $0.60 \pm 0.14$  and 0.0 (exact), respectively. In all plots, the filled-in markers are the molecules with significant internal conformational freedom (tolbutamide, chlorpropamide, and aripiprazole).

Table 1: Potential Energy of Lattice Minimum Relative to 10 K REMD Quenched Structure

	Tolbutamide		Chlorpropamide		Aripiprazole	
	I	II	I	V	I	X
$\Delta U_{\text{Exp.}}^a$	1.837	0.250	0.000	3.095	1.989	0.302
$\Delta U_{\text{Previous}}^b$	0.442	0.250	0.000	0.294	0.048	0.000
$\Delta U_{\text{REMD}}$	0.000	0.000	0.000	0.000	0.000	0.000

<sup>a</sup> Potential energy differences of the lattice minimum quenched from the experimental structure and quenched from a 10 K REMD simulation; <sup>b</sup> Potential energy difference of the lattice minimum quenched from the restructured crystal found in our previous study<sup>24</sup> and quenched from a 10 K REMD simulation.

Table 2: Error of QHA Relative to MD at  $T_{max}$  Previously Reported<sup>24</sup> and Using a Lattice Minimum Quenched from REMD

QHA	Tolbutamide		Chlorpropamide		Aripiprazole	
	Iso.	Aniso.	Iso.	Aniso.	Iso.	Aniso.
$\delta(\Delta G_{\text{Prev.}})^c$	0.397	–	0.159	–	0.083	–
$\delta(\Delta G_{\text{REMD}})^d$	0.247	0.206	0.014	0.033	0.128	0.045

<sup>c</sup> Error between QHA and MD using the lattice minimum in our previous study;<sup>24</sup> <sup>d</sup> Error between QHA and MD using the lattice minimum quenched from the 10 K replica of REMD.

tries computed with QHA. In Figure 7a and Figure 7b we show the percent expansion of QHA lattice vectors and angles against MD, respectively. The black line represents a perfect agreement between the QHA method and MD, while the dashed lines are least squared fits between the two QHA methods and MD. For the lattice vectors, there is marginal improvement in the RMSD when using anisotropic expansion (1.3%) over isotropic QHA (1.6%). There is no improvement to RMSD for the lattice angles (anisotropic 1.3%, isotropic 1.3%). Despite there being little-to-no reduction in the RMSD’s, the least square fit between anisotropic QHA and MD is similar to the  $y = x$  line for both lattice vectors and angles. This contrasts with isotropic QHA, which is essentially independent of MD box vectors, which is expected for the fixed isotropic angles. Quantitatively, the

slopes for anisotropic and isotropic expansion are  $0.89 \pm 0.22$  and  $0.02 \pm 0.06$  for the box vectors ( $a$ ,  $b$ , and  $c$ ) and  $0.60 \pm 0.14$  and  $0.0$  (exactly) for the box angles ( $\alpha$ ,  $\beta$  and  $\gamma$ ), indicating that while anisotropic expansion may over or undershoot the changes, the directions of change are generally being properly predicted.

Anisotropic expansion provides minimal improvement in the error of polymorph free energy differences between QHA and MD. In Figure 8a we plot the Gibbs free energy differences of both QHA methods against the results for MD at  $T_{max}$ . The RMSD of  $\Delta G$  for isotropic and anisotropic QHA relative to MD are 0.113 and 0.079 kcal/mol, respectively. There is only a 0.034 kcal/mol improvement to the RMSD when using an anisotropic thermal expansion model, which is comparable to the bootstrapped error in the RMSD. Anisotropic QHA in

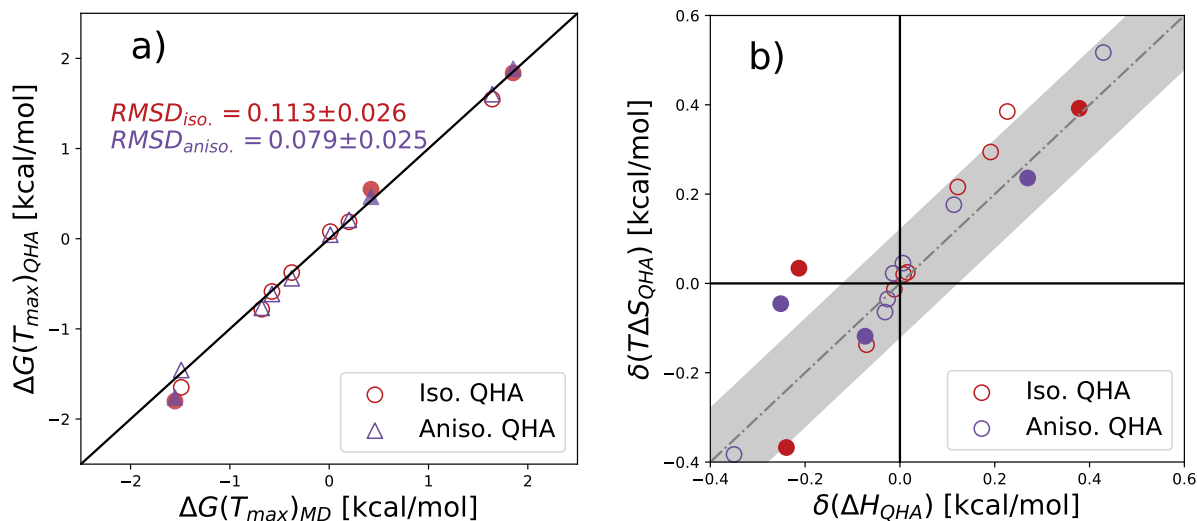


Figure 8: a) Gibbs free energy differences between polymorphs for QHA relative to MD and b) entropy–enthalpy compensation in errors of QHA relative to MD. a) Overall, there is a slight improvement of RMSD in the Gibbs free energy when using anisotropic expansion over isotropic expansion. This improvement is only slightly larger than the bootstrapped error in the RMSD. b) Grey shaded area indicates free energy differences  $< 0.12$  kcal/mol between QHA and MD, which for most of the graph indicates significant entropy–enthalpy compensation. The only molecule to fall outside of these bounds for anisotropic QHA is tolbutamide, which has the largest error in QHA relative to MD. In all plots, the filled-in markers are the molecules with multiple molecular conformers (tolbutamide, chlorpropamide, and aripiprazole).

fact has a larger deviation from MD than isotropic QHA for 3 of the 10 molecules, though the deviation from MD is small. Those molecules and their deviation of anisotropic QHA from MD ( $\delta(\Delta G_{1D})_{MD}$ ) are pyrazinamide (0.037 kcal/mol), resorcinol (0.062 kcal/mol), and chlorpropamide (0.033 kcal/mol). These results demonstrate that the deviations in the free energy differences between MD and QHA are due to something other than an insufficiently accurate thermal expansion model. Summary results for each molecule is provided in the Figure S57.

The difference between QHA and MD is minimized when a lattice minimum corresponding the sampled MD lattice parameters and anisotropic QHA is used. The largest errors for anisotropic QHA is seen for tolbutamide ( $\delta(\Delta G_{1D})_{MD} = 0.206$  kcal/mol), paracetamol (0.088 kcal/mol), and resorcinol (0.062 kcal/mol) with all other molecules  $< 0.045$  kcal/mol. Under the condition that a more consistent minimum with MD is used, we no longer find that the error in QHA trends with molecular size and flexibility.<sup>24</sup> However, molecular size and flexibility are correlated with a greater number of alternative lattice minima.<sup>58</sup> We also see no correlation between the error in QHA and the number of hydrogen bonds in the crystal ( $R^2 < 0.1$  in Figure S67 and Figure S68). Tolbutamide form II has a  $Z'$  of 4 and all other polymorphs are  $\leq 2$ , while this is not statistically significant it could explain why the error in QHA is an outlier. We also compared the gas and crystal phase torsions, but found no differences that distinguish tolbutamide from the rest of the molecules (Torsions shown in figures S60–S66).

We see entropy–enthalpy compensation in the differences between anisotropic QHA and MD of up to 0.12 kcal/mol for all molecules except for tolbutamide. Despite

the entropy and enthalpy for QHA having errors up to 0.5 kcal/mol from MD, the cancellation of those errors allows QHA to give free energy differences within 0.09 kcal/mol of the MD-calculated free energy differences for all systems except tolbutamide. In Figure 8b the error in the entropic differences of polymorphs is plotted versus the error in enthalpic differences of QHA relative to MD. We define a set of polymorphs demonstrating entropy–enthalpy compensation (gray shaded area) if the differences between errors in entropy and enthalpy (i.e. the error in the free energy difference) is  $< 0.12$  kcal/mol, giving us 90% confidence that a re-ranking in crystal stability would not occur due to this error.<sup>24</sup> Anharmonic motions may be important for computing the enthalpy and entropy differences of polymorphs, but for most of the systems studied here the error is minimal for computing the free energy. The only molecule that falls outside of this region for anisotropic QHA is tolbutamide. Out of the 10 molecules, 8 have larger entropic error in QHA than enthalpic error, which is most likely due to anharmonic motions. The only two sets of polymorphs that have larger enthalpic error in QHA are tolbutamide and chlorpropamide, which are further explained in the next section.

## Molecular Conformational Ensembles Can Still Exist Low Temperatures

Even at low temperatures, some crystals have substantial conformational degeneracies allowing quenched structures to settle into lattice minima that break the symmetry of the supercell. In figure 9b we show frames of the trajectory of chlorpropamide, with each frame taken 0.1 ns apart for the last 5 ns of the 10 K ensemble produced

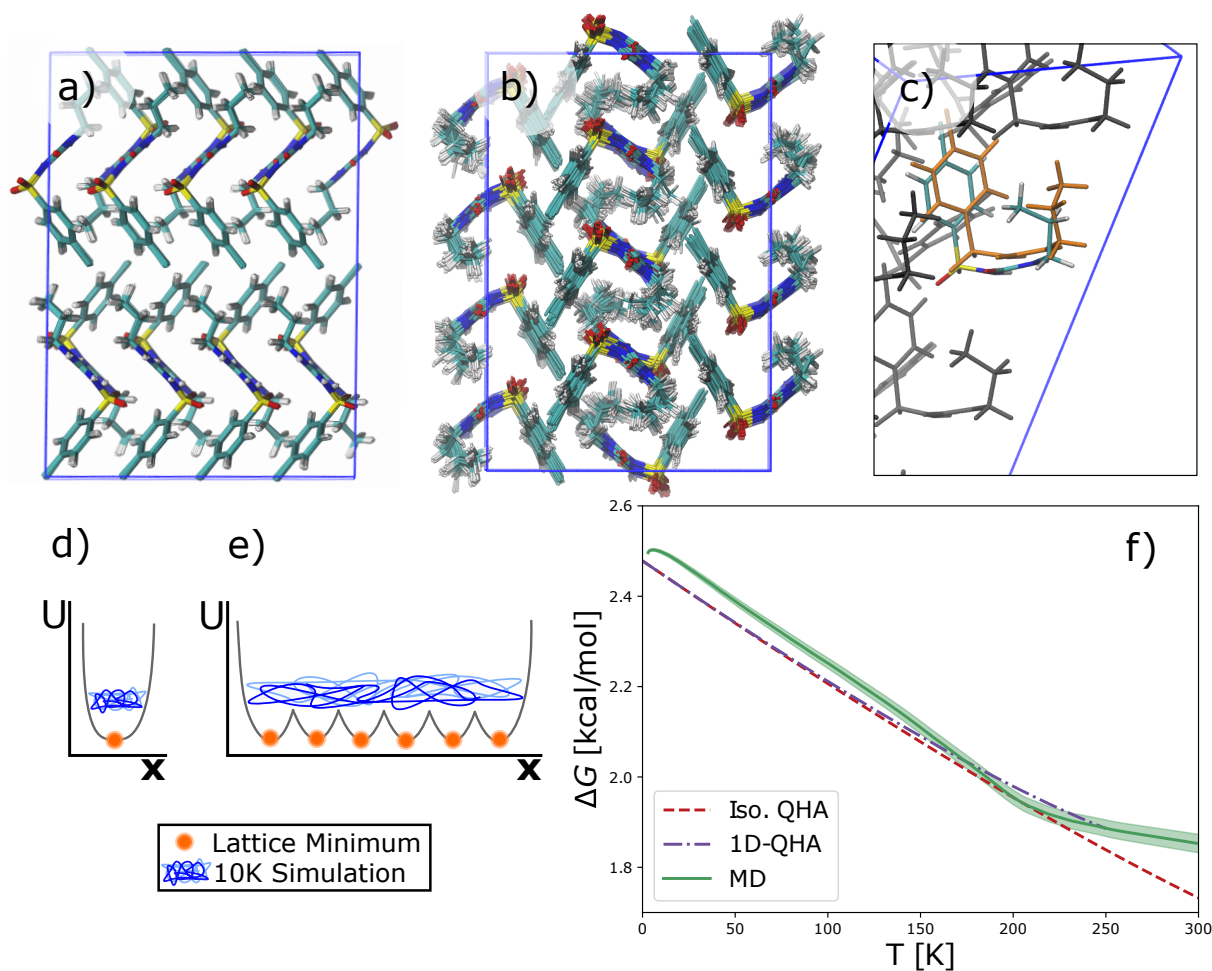


Figure 9: Snapshots of the 10 K ensemble for chlorpropamide form a) I and b) V taken from the last 5 ns of the replica exchange simulation, with 0.1 ns between each frame. Even at low temperatures, this crystal structure samples a surprisingly diverse conformational ensemble, with the greatest variability in the fluctuations around the alkyl tail. The RMSD of the entire 10 K simulation ensemble relative to the lattice minimum for form I is  $0.165 \pm 0.02 \text{ \AA}$  and form V is  $0.691 \pm 0.21 \text{ \AA}$ . c) Two frames of chlorpropamide form V that are 150 ps apart, showing that the position of the terminal carbon is sampling two torsional conformations at 10 K. Graphical representation of a crystal with d) a single configurational minima and e) multiple configurational minima drawn on a potential energy ( $U$ ) against the configurational space ( $\mathbf{x}$ ). f) Gibbs free energy difference of chlorpropamide form V relative to form I.

during replica exchange. From this low temperature ensemble, molecules are able to sample a number of configurations due to the degrees of freedom accessible to the alkyl tail, and the low energy differences between different alkyl rotamer configurations. When quenched, the tails fall into mostly independent conformations, breaking the crystal symmetry.

The thermodynamic accessibility of many configurations at low temperatures is a result of the existence of many configurationally diverse lattice minima with similar low energies. In Figure 9b the RMSF of form V is  $0.69 \pm 0.21 \text{ \AA}$  at 10 K, which is four times greater than form I where the RMSF is  $0.17 \pm 0.02 \text{ \AA}$  (Figure 9a). The more configurationally diverse behavior of form V helps to explain why quenching the MD simulations leads to so many different lattice minima. Figure 9d provides a graphical representation of the single lattice minimum and small configurational spaced covered at 10 K for form I, which contrasts with Figure 9e representation of form V.

The number of accessible low-energy minima causes a rapid deviation of QHA of up to 0.06 kcal/mol in the free energy difference relative to MD for chlorpropamide as low as 10 K. Figure 9f shows the polymorph free energy differences for chlorpropamide form V relative to form I for QHA and MD. Based on the  $G(T)$  plot from MD, between 0 and 10, the polymorph free energy difference for MD quickly changes, causing QHA to diverge by 0.06 kcal/mol at 10 K. While QHA can accurately model form I at low temperatures, it cannot capture the behavior of the alkyl tails in form V, which is why we see the immediate divergence of the two methods as  $T$  increases from zero. At temperatures greater than 10 K the deviation of the free energy from MD does not grow because of the entropy–enthalpy compensation, but we cannot necessarily con-

clude that this would be the case for other crystals that could have alternate configurational minimum. Both polymorphs of tolbutamide also sample a large number of conformations at low temperatures, causing a similar divergent behavior in  $\Delta G$  for QHA and MD at low temperatures (Figure S48).

The concavity in the free energy of chlorpropamide at low temperatures is due to dominating enthalpic changes close to 0 K, which quickly diminish relative to the entropic contributions as the temperature increases. Surprisingly, although form V has a larger low T configurational ensemble, it initially becomes less stable as a function of T relative to the more constrained form I. Up to 10 K, form V expands faster than form I (Figure 10a) causing an unfavorable enthalpic contribution to form V relative to form I (Figure 10b). Since  $T\Delta S$  is small at low temperatures, the changes in the enthalpic difference dominates the free energy differences. At temperatures greater than 10 K the difference in volume and enthalpy between polymorphs is constant. The initial expansion of form V allows the alkyl tails to have more conformational space than form I and by 20 K the entropic contributions in form V are large enough to switch the stability of the polymorphs.

## Conclusions

Although we have studied a relatively small number of enantiotropic polymorphs in this study, we find there here are persistent shortcomings of QHA that highlight the importance of anharmonic configurational sampling in determining accurate free energy differences of crystal polymorphs. The shortcomings identified in this study are: 1) that including anisotropic expansion provides minimal improvement in the error of polymorph free energy differences between

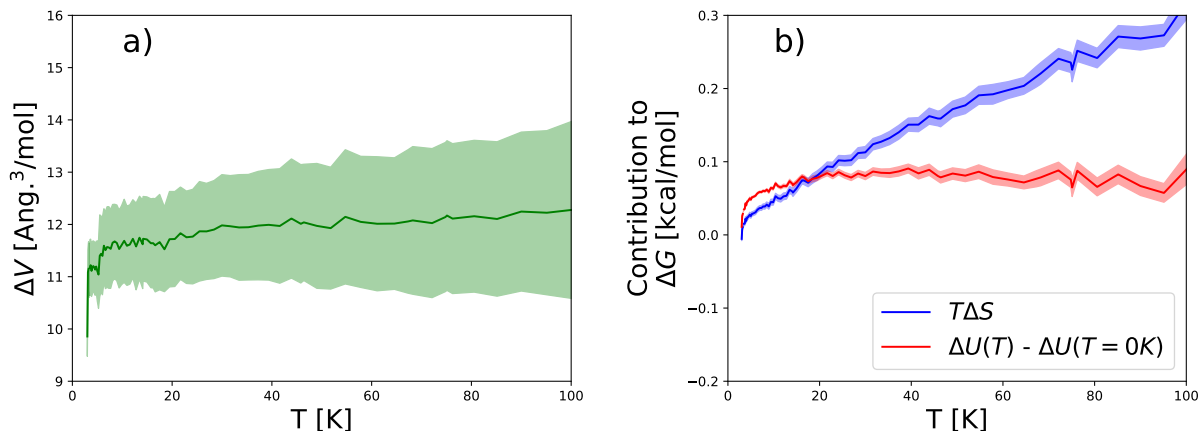


Figure 10: (a) Volume differences of chlorpropamide form V relative to form I using MD. Initially, form V expands much faster than form I. Above 10 K, the difference in volume between the forms is almost constant. (b) The entropic and enthalpic contributions to the Gibbs free energy difference of chlorpropamide form V relative to I. Below 10 K, the potential energy is the dominating free energy contribution making form V less favorable, explained by the sudden expansion of form V seen at low temperatures.

QHA and MD, 2) the number of accessible low-energy minima causes a rapid deviation of QHA relative to MD for temperatures as low as 10 K, 3) some crystals reorganize into clearly different structures when heated up to 300 K using MD, and 4) polymorph restructuring prevents QHA from being run independently of MD because the minimum energy configuration is likely to be inaccessible from an arbitrary low-energy starting point.

We found that the OPLS-AA point charge potential incorrectly ranked 4 of the 10 enthalpic differences of polymorphs relative to experiment, but correctly ranked the entropic differences of all 10 molecules. Despite the lattice geometries for MD differing moderately from experiment, the expansion of vectors and orthogonal angles for MD generally agree with experiment. The RMSD of both enthalpic and entropic differences between MD and experiment were 4.0 and 2.0 kcal/mol, respectively, which is roughly 2 orders of magnitude larger than

errors seen of QHA relative to MD if properly performed.

Our one-dimensional approach to model anisotropic thermal expansion predicts essentially identical high temperature lattice geometries and polymorph free energy differences as the full anisotropic QHA for the 10 polymorph pairs studied. Specifically, the computed polymorph free energy differences are within 0.02 kcal/mol at  $T_{max}$  for our 1D- and fully-anisotropic QHA methods for the 10 molecules studied. The lattice geometries of the two approaches remained essentially the same, with an RMSD of 0.29% for the expansion relative to lattice minimum structure. Additionally, 1D-anisotropic QHA is able to find a free energy minimum up to 300 K for all but one crystal unit cell, whereas the fully anisotropic approach fails to reach those desired temperatures for 50% of the crystals, due to the larger likelihood of a rearrangement into an alternate minimum when multiple derivatives are used, resulting in numerical insta-

bility of the approach.

Finite size effects do not always cancel out for polymorph free energy differences; instead, differences between unit cells and supercells can be up to 0.5 kcal/mol and therefore must be accounted for when attempting to accurately rank crystal stability. We found that this error is correlated with the error in the lattice geometries ( $R^2 = 0.79$ ), meaning they are reduced but not eliminated if the high temperature lattice geometries are the same between unit and supercells.

Anisotropic QHA only marginally improves the error in free energy differences from MD for the polymorph pairs studied. Using anisotropic QHA reduces the RMSD of  $\Delta G$  relative to MD by 0.034 kcal/mol, which is only slightly larger than the standard error in the RMSD. The errors in QHA with respect to MD are due primarily to anharmonic motions, because using an anisotropic thermal expansion model does not improve the deviations between QHA and MD. Differences between anisotropic QHA and MD do not appear strongly correlated with molecular flexibility. Tolbutamide with both a large deviation and high flexibility is an exception, and this difference could also be due to the large  $Z'$  value of 4 for form II. The free energy difference in tolbutamide had an error of 0.21 kcal/mol between anisotropic QHA and MD, whereas all other molecules deviated  $< 0.09$  kcal/mol.

The degree of flexibility of the molecules can result in a more significant chance of crystal restructuring upon annealing with replica exchange. Once a lower energy lattice minimum was found, the error in isotropic QHA was on average 0.08 kcal/mol lower than previously reported.<sup>24</sup> Anisotropic QHA from the new minimum was able to reduce the free energy differences between chlorpropamide and aripipra-

zole to  $< 0.05$  kcal/mol. We were consistently able to find lower lattice minimum than those quenched directly from experiment for more flexible molecules by running replica exchange molecular dynamics and quenching frames from the low temperature replica.

The polymorphs of conformationally flexible molecules exhibit differences in  $\Delta G$  of QHA relative to MD on the magnitude of 0.06 kcal/mol even as low as 10 K, despite the 0 K lattice energies being within 0.01 kcal/mol at 0 K, showing that agreement between QHA and MD cannot be assumed even at very low temperatures. These differences are due to either one or both of the polymorphs expanding quickly at low temperatures, which provides enough free volume to access a diverse number of conformations around the alkyl tail. We note that the temperature at which a crystal can access these conformations is structure dependent, as seen with the different polymorphs of chlorpropamide.

## Acknowledgments

The authors thank Eric Dybeck for producing majority of the MD results used from our previous paper. Final results for QHA were performed on the Extreme Science and Engineering Discovery Environment (XSEDE), which is supported by National Science Foundation grant number ACI-1548562. Specifically, it used the Bridges system, which is supported by NSF award number ACI-1445606, at the Pittsburgh Supercomputing Center (PSC). This work was also supported financially by NSF through the grant CBET-1351635.

# Supporting Information for “Adding anisotropy to the standard quasi-harmonic approximation still fails in several ways to capture organic crystal thermodynamics”

## Systems Studied

In Table 3 we provide the systems studied, their polymorphs names/numberings, and corresponding Cambridge Structure Database reference code (CSD Refcode), and the dimensions of the unit and super-

cells relative to the symmetric cell pulled from the database. The supercell sizes are the same as our previous study and the unit cells are the smaller cell size that assures that both crystals have the same number of molecules.

<b>Piracetam</b>	Form I	Form III
CSD Refcode	BISMEV03	BISMEV02
Space Group	P2 <sub>1</sub> /n	P2 <sub>1</sub> /n
Z / Z'	4/1	4/1
Unit cell Dimensions	1 × 1 × 1	1 × 1 × 1
Supercell Dimensions	4 × 2 × 3	2 × 3 × 4
<b>Carbamazepine</b>	Form I	Form III
CSD Refcode	CBMZPN11	CBMZPN02
Space Group	P $\bar{1}$	P2 <sub>1</sub> /n
Z / Z'	8/2	4/1
Unit cell Dimensions	1 × 1 × 1	2 × 1 × 1
Supercell Dimensions	4 × 2 × 1	4 × 2 × 2
<b>Adenine</b>	Form I	Form II
CSD Refcode	KOBFUD	KOBFUD01
Space Group	P2 <sub>1</sub> /c	Fdd2
Z / Z'	8/2	16/1
Unit cell Dimensions	1 × 1 × 2	1 × 1 × 1
Supercell Dimensions	3 × 1 × 4	3 × 1 × 2
<b>Pyrazinamide</b>	Form $\gamma$	Form $\delta$
CSD Refcode	PYRZIN20	PYRZIN16
Space Group	Pc	P $\bar{1}$
Z / Z'	2/1	2/1
Unit cell Dimensions	1 × 2 × 1	2 × 1 × 1
Supercell Dimensions	4 × 6 × 2	4 × 3 × 4
<b>Resorcinol</b>	Form $\alpha$	Form $\beta$
CSD Refcode	RESORA03	RESORA08
Space Group	Pna2 <sub>1</sub>	Pna2 <sub>1</sub>
Z / Z'	4/1	4/1
Unit cell Dimensions	1 × 1 × 1	1 × 1 × 1

Supercell Dimensions	$2 \times 2 \times 4$	$2 \times 2 \times 4$
<b>1,4-Diiodobenzene</b>	Form $\alpha$	Form $\beta$
CSD Refcode	ZZZPRO03	ZZZPRO04
Space Group	Pbca	Pccn
Z / Z'	4/1	4/1
Unit cell Dimensions	$1 \times 1 \times 1$	$1 \times 1 \times 1$
Supercell Dimensions	$2 \times 3 \times 3$	$2 \times 3 \times 3$
<b>Paracetamol</b>	Form I	Form II
CSD Refcode	HXACAN01	HXACAN
Space Group	P2 <sub>1</sub> /a	Pcab
Z / Z'	4/1	8/1
Unit cell Dimensions	$1 \times 2 \times 1$	$1 \times 1 \times 1$
Supercell Dimensions	$2 \times 2 \times 3$	$2 \times 1 \times 3$
<b>Aripiprazole</b>	Form I	Form X
CSD Refcode	MELFIT01	MELFIT05
Space Group	P2 <sub>1</sub>	P2 <sub>1</sub>
Z / Z'	2/1	2/1
Unit cell Dimensions	$1 \times 1 \times 1$	$1 \times 1 \times 1$
Supercell Dimensions	$3 \times 4 \times 2$	$3 \times 4 \times 2$
<b>Tolbutamide</b>	Form I	Form II
CSD Refcode	ZZZPUS04	ZZZPUS05
Space Group	Pna2 <sub>1</sub>	Pc
Z / Z'	4/1	8/4
Unit cell Dimensions	$1 \times 2 \times 1$	$1 \times 1 \times 1$
Supercell Dimensions	$2 \times 3 \times 2$	$3 \times 2 \times 1$
<b>Chlorpropamide</b>	Form I	Form V
CSD Refcode	BEDMIG	BEDMIG04
Space Group	P2 <sub>1</sub> 2 <sub>1</sub> 2 <sub>1</sub>	Pna2 <sub>1</sub>
Z / Z'	4/1	4/1
Unit cell Dimensions	$1 \times 1 \times 1$	$1 \times 1 \times 1$
Supercell Dimensions	$1 \times 4 \times 2$	$1 \times 4 \times 2$

Table 3: Table of systems studied in the main paper. We have included the polymorph names, CSD reference codes, and the cell dimensions relative to the symmetric unit cell pulled down from the database.

## 1D vs. Full Anisotropic QHA

In Table 4 we report the free energy differences of the unit cell of each system using 1D and fully anisotropic QHA at the maximum temperature that all methods could

achieve  $T_{max}$ . We also report the deviation between the two methods ( $\delta(|\Delta G(T_{max})|)$ ) in the far right column, which shows that both methods are within 0.02 kcal/mol of each other for all systems except for chlorpropamide.

Differences in  $\Delta G$  of the anisotropic methods are correlated with the errors in

Table 4: Free energy differences for 1D and fully anisotropic QHA at  $T_{max}$  for the unit cells.  $T_{max}$  is the maximum temperature that both crystals and both methods can reach while still being at a free energy minimum. For all systems there is  $< 0.02$  kcal/mol difference in  $\Delta G$  with aripiprazole having the largest difference of 0.016 kcal/mol.

System	$T_{max}$ [K]	$\Delta G(T_{max})$ [kcal/mol]		$\delta( \Delta G(T_{max}) )$
		1D-QHA	Aniso.-QHA	
Piracetam	255	-1.374	-1.384	0.010
Carbamazepine	300	-0.160	-0.157	0.003
Adenine	300	1.330	1.328	0.002
Pyrazinamide	180	-0.552	-0.551	0.001
Resorcinol	300	-0.578	-0.578	0.000
1,4-Diiodobenzene	210	0.431	0.431	0.000
Paracetamol	150	-0.648	-0.652	0.004
Aripiprazole	180	-0.696	-0.712	0.016
Tolbutamide	100	-3.592	-3.593	0.001
Chlorpropamide	150	4.830	4.824	0.006

the predicted high temperature lattice geometries. Figure 11 has the absolute free energy deviations between 1D- and fully-anisotropic QHA versus the root-mean-square deviation (RMSD) between  $T_{max}$  lattice geometries for individual polymorph. The RMSD is computed as:

$$RMSD = \sqrt{\frac{1}{6} \sum_{i=1}^6 (C_i^{1D}(T_{max}) - C_i^{Full}(T_{max}))^2}$$

where the RMSD is taken between the six lattice parameters of the upper triangular crystal tensor form. From Figure 5c, we can see that as the RMSD between the 1D- and fully-anisotropic  $T_{max}$  structure becomes larger, so does the error in the computed free energy of the polymorph. The error in thermal expansion and free energy for isotropic QHA is reduced by using the 1D-QHA variant. The differences in the free energy are a direct result of the crystal expanding to a slightly different geometry, but we can see that this has little effect on the free energy differences.

The 1D-variant reduces the error of the

isotropic QHA up to 90% for the systems studied relative to the fully anisotropic approach. The deviations between 1D-QHA and fully anisotropic QHA are  $< 0.02$  kcal/mol, whereas the error for isotropic QHA is as large as 0.21 kcal/mol for individual polymorphs (Figure 11). The largest deviations in free energy for isotropic expansion come from aripiprazole form X and chlorpropamide form V. The largest deviation in free energy for 1D-QHA (0.0167 kcal/mol) is from aripiprazole form X.

## Unit vs. Supercell 1D-QHA

In Table 5 we report the free energy differences of the unit and supercell of each system using 1D-QHA at the maximum temperature all cell sizes could achieve  $T_{max}$ . We also report the deviation between the two cell sizes ( $\delta(|\Delta G(T_{max})|)$ ) in the far right column. We see that there are significant finite size errors for all crystals that range between 0.03 – 0.50 kcal/mol.

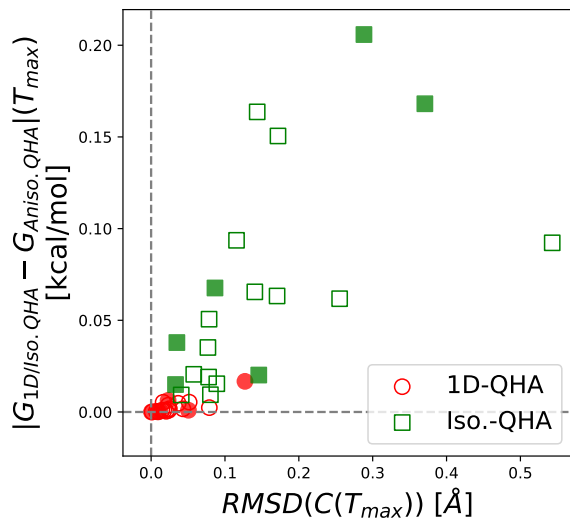


Figure 11: Deviations in the free energy of the constrained QHA (isotropic QHA and 1D-QHA) from anisotropic QHA versus the box vector RMSD from the unconstrained QHA structure. All values are reported at  $T_{max}$ . For individual free energies the 1D-variant deviates  $< 0.02$  kcal/mol, which is 10 times more precise than isotropic QHA that deviates up to 0.21 kcal/mol from the fully anisotropic approach. Filled in markers are the systems with multiple molecular conformers (tolbutamide, chlorpropamide, and aripiprazole).

Table 5: Free energy differences for unit and supercells at  $T_{max}$  using 1D-QHA are reported.  $T_{max}$  is the maximum temperature that both crystals and cell sizes can reach while still being at a free energy minimum. We find that size errors on the magnitude of 0.03 – 0.5 kcal/mol for polymorph free energy differences.

System	$T_{max}$ [K]	$\Delta G(T_{max})$ [kcal/mol]		$\delta( \Delta G(T_{max}) )$
		Unit	Super	
Piracetam	300	-1.364	-1.457	0.093
Carbamazepine	300	-0.160	0.044	0.204
Adenine	300	1.330	1.603	0.273
Pyrazinamide	300	-0.756	-0.613	0.143
Resorcinol	300	-0.578	-0.439	0.139
1,4-Diiodobenzene	300	0.427	0.389	0.038
Paracetamol	300	-1.241	-0.767	0.474
Aripiprazole	300	-0.764	-0.950	0.186
Tolbutamide	180	-3.602	-3.489	0.113
Chlorpropamide	50	5.374	5.287	0.087

For individual polymorphs, there is no trend between the differences in free energy and the RMSD in the percent expansion up to  $T_{max}$  for unit and supercells; the trends only appear for polymorph differences. Figure 12 compares the absolute deviation in free energy with the RMSD in the percent expansion for unit and supercells. The error in free energy between unit and super cells is between 0 – 3 kcal/mol and does not correlate with the cells percent expansion at  $T_{max}$ .

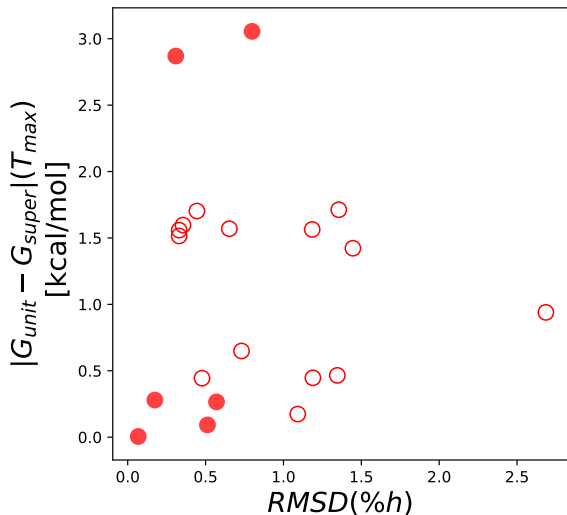


Figure 12: The deviation in the free energy between unit and super cell is shown relative to the RMSD in the percent expansion. For individual polymorphs there is no correlation between error in the free energy and the error in the high temperature lattice geometries. The filled in markers are the systems with multiple molecular conformers (tolbutamide, chlorpropamide, and aripiprazole)

The finite size errors do not correlate with the ratio of number of molecules in the unit and supercells. We have super cells that have 6 – 24 times the number of molecules in the unit cells. We would expect the systems with similar number of

molecules in the unit cell and supercell to have smaller deviations in the free energy, but that is not the case. In Figure 13 the free energy deviation between the unit and supercell at 300 K is plotted against the ratio of molecules in the super cell relative to the unit cell. The greatest error is seen for paracetamol, which is one of the systems with the most similar unit and super cells. There is no correlation between the finite size error and ratio of number of molecules ( $R^2 = 0.109$ ).

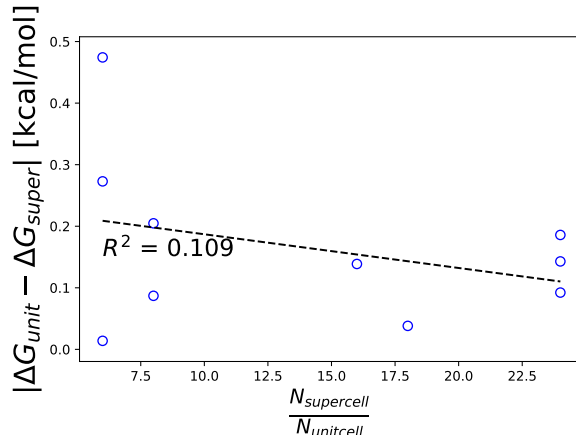


Figure 13: Plotting the finite size errors at  $T_{max}$  versus the ratio of number of molecules between the super- and unit cell.

## Re-structuring

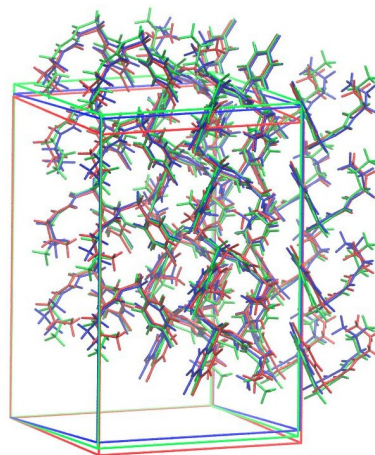


Figure 15: Lattice minimum of chlorpropamide form V from quenching the experimental structure (green), the structure used in our previous study (blue),<sup>24</sup> quenched from a 10 K replica exchange simulation (red). The RMSD between the structure quenched from experiment and from our previous paper relative to the minima found from REMD are 1.26 and 1.07 Å, respectively.

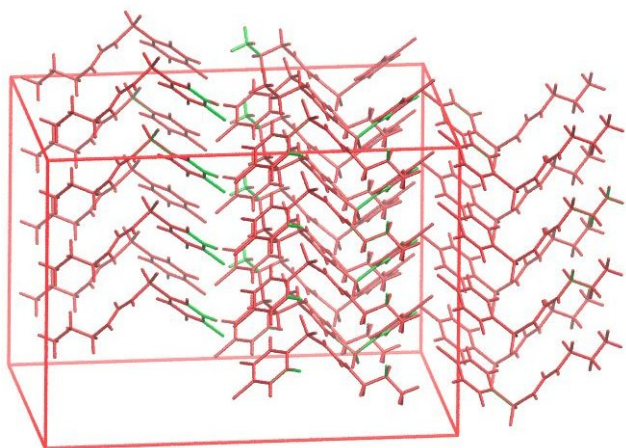


Figure 14: Lattice minimum of chlorpropamide form I from quenching the experimental structure (green), the structure used in our previous study (blue),<sup>24</sup> quenched from a 10 K replica exchange simulation (red). The RMSD between all structures is  $< 0.0001$  Å.

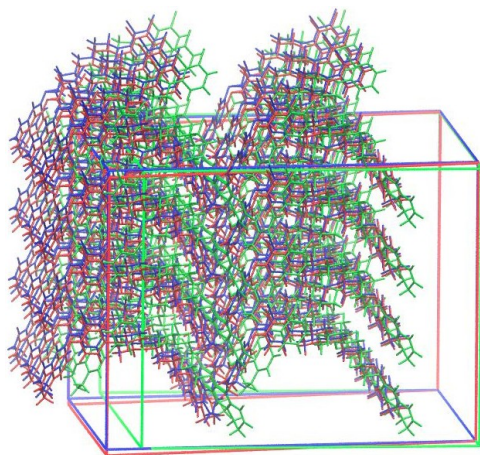


Figure 16: Lattice minimum of aripiprazole form I from quenching the experimental structure (green), the structure used in our previous study (blue),<sup>24</sup> quenched from a 10 K replica exchange simulation (red). The RMSD between the structure from our previous paper relative to the minima found from REMD is 0.36 Å.

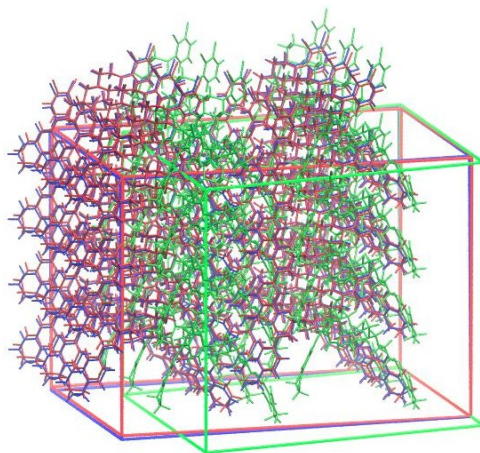


Figure 17: Lattice minimum of aripiprazole form X from quenching the experimental structure (green), the structure used in our previous study (blue),<sup>24</sup> quenched from a 10 K replica exchange simulation (red). The RMSD between the structure from our previous paper relative to the minima found from REMD is 0.51 Å.

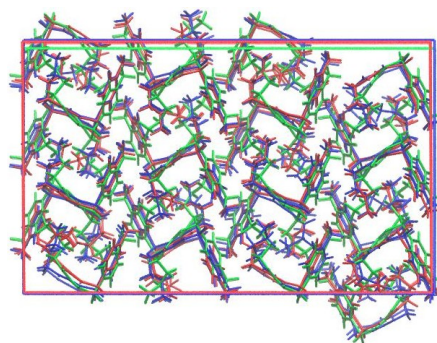


Figure 18: Lattice minimum of tolbutamide form I from quenching the experimental structure (green), the structure used in our previous study (blue),<sup>24</sup> quenched from a 10 K replica exchange simulation (red). The RMSD between the structure quenched from experiment and from our previous paper relative to the minima found from REMD are 1.48 and 1.09 Å, respectively.

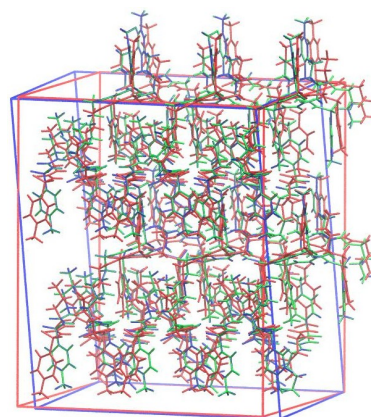


Figure 19: Lattice minimum of tolbutamide form I from quenching the experimental structure (green), the structure used in our previous study (blue),<sup>24</sup> quenched from a 10 K replica exchange simulation (red). The RMSD between the structure quenched from experiment and from our previous paper relative to the minima found from REMD are 1.35 and 1.35 Å, respectively.

## Free Energy Differences and Expansion with Temperature

The original MD data for several systems were run with constraints that prevented the angles from changing. While there fluctuations in the angles should have been considered, the angles remain  $90^\circ$  across the en-

tire temperature range. For the following systems the MD angles were fixed at  $90^\circ$ : adenine from II, resorcinol from  $\alpha$  and  $\beta$ , diiodobenzene form  $\alpha$  and  $\beta$ -restructured, and paracetamol form II. For all crystals where the angles are fixed at  $90^\circ$ , we ran 1 ns simulations at 50, 100, 200, and 300 K with the angles unfixed and verified that average value of the angle remains at  $90^\circ$ .

### Piracetam

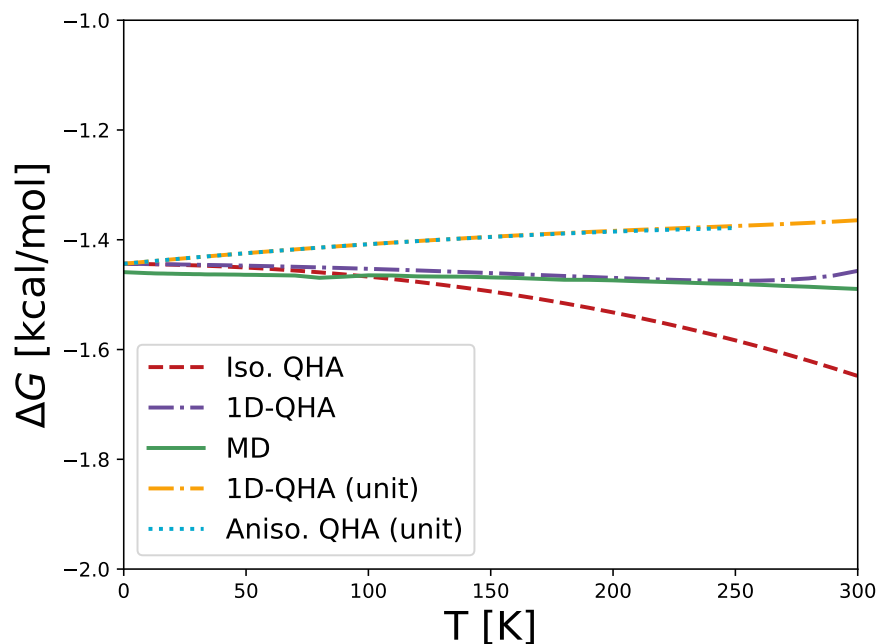


Figure 20: Polymorph free energy differences of piracetam form I relative to form III

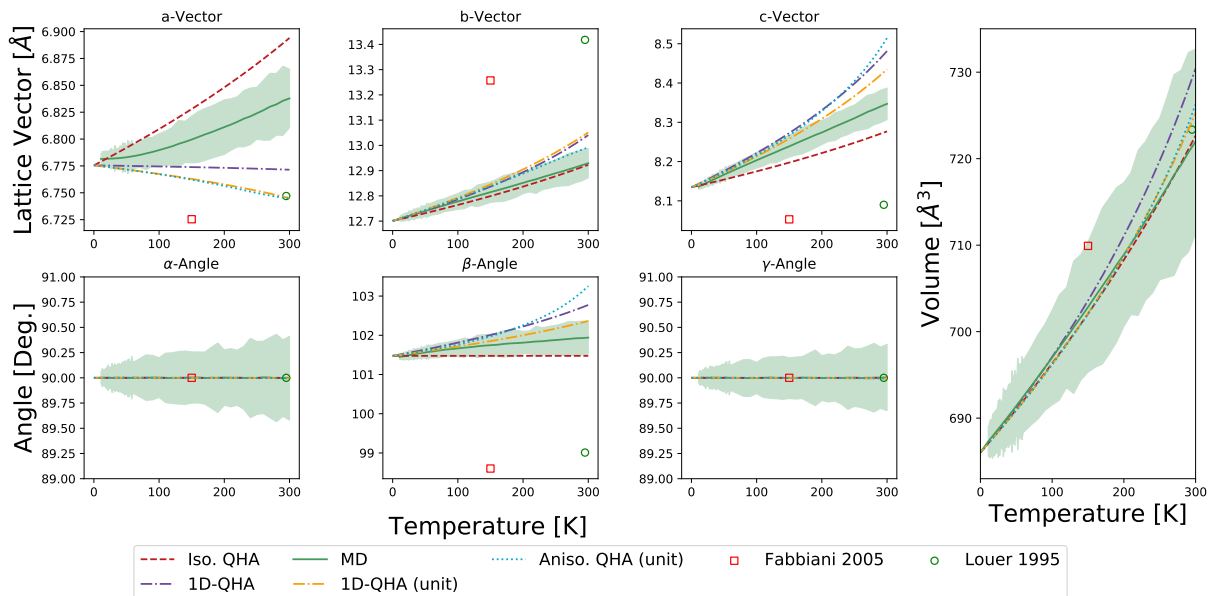


Figure 21: Piracetam form I percent expansion from 0 K with experimental results.<sup>59,60</sup>

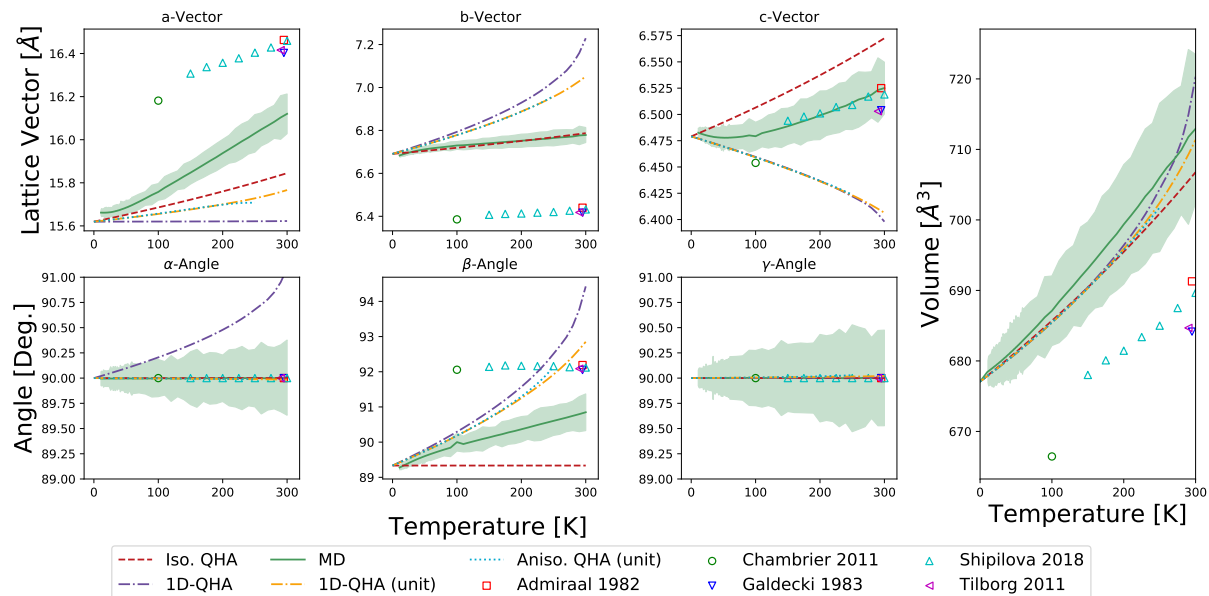


Figure 22: Piracetam form III percent expansion from 0 with experimental results.<sup>61-65</sup>

## Carbamazepine

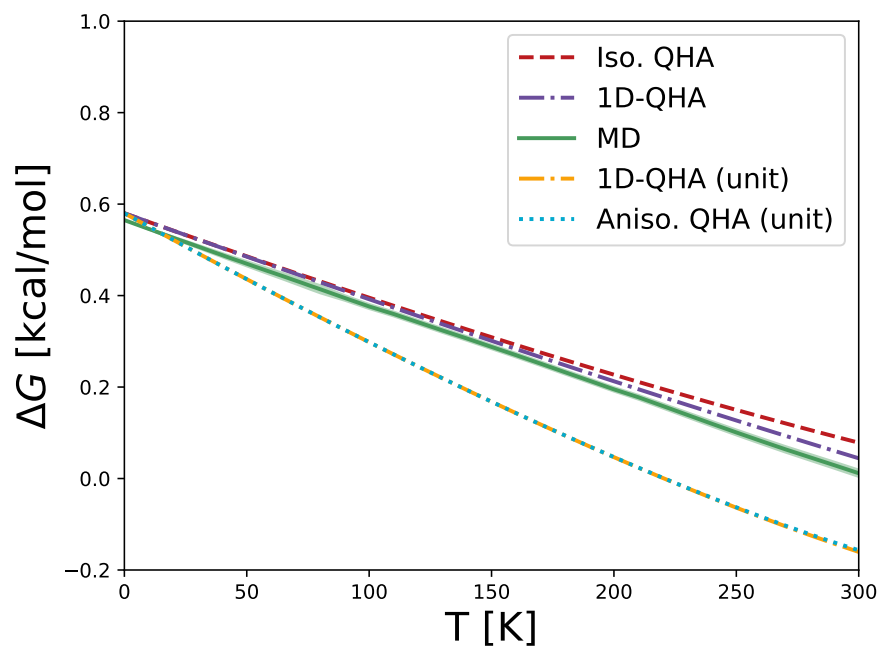


Figure 23: Polymorph free energy differences of carbamazepine form I relative to form III

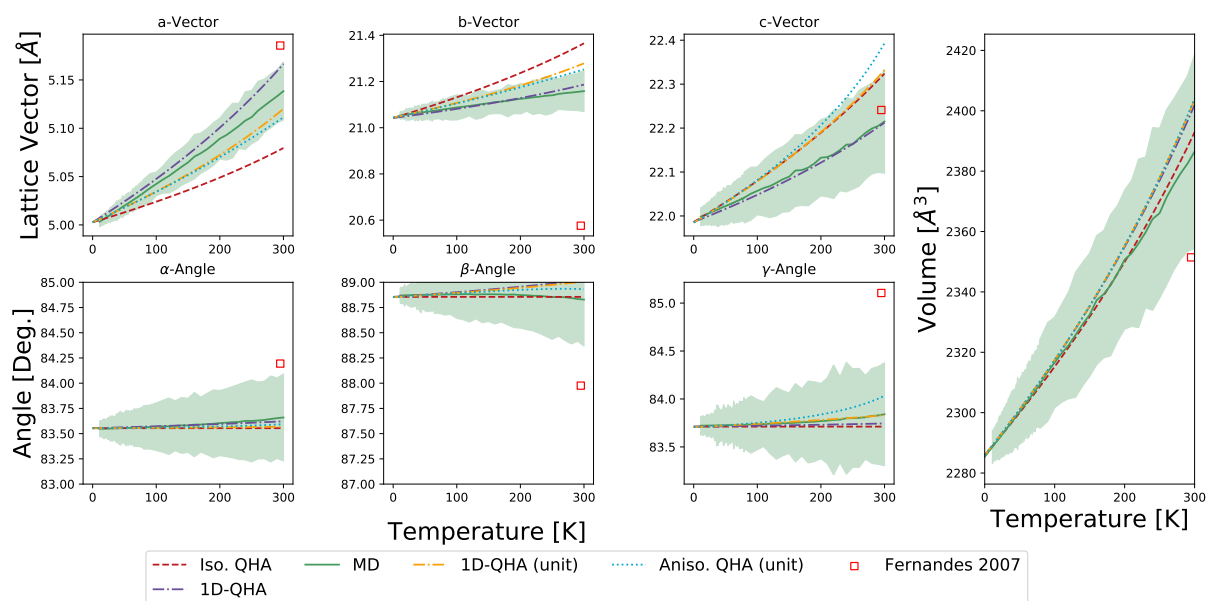


Figure 24: Carbamazepine form I percent expansion from 0 K with experimental results.<sup>66</sup>

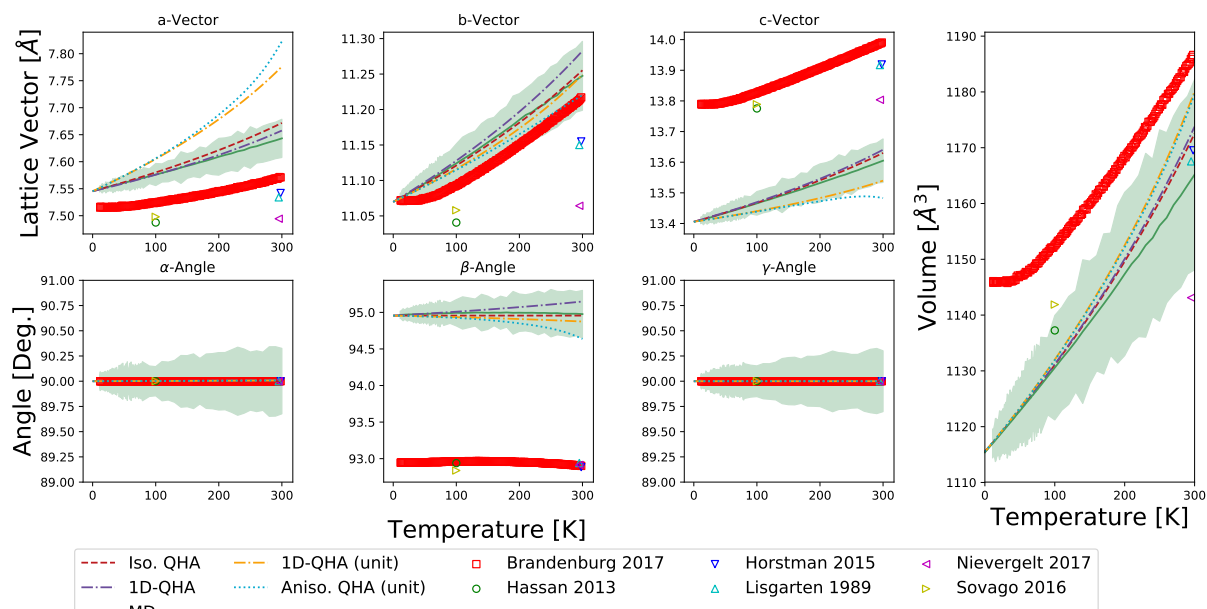


Figure 25: Carbamazepine form III percent expansion from 0 K with experimental results.<sup>47,49–53</sup>

# Adenine

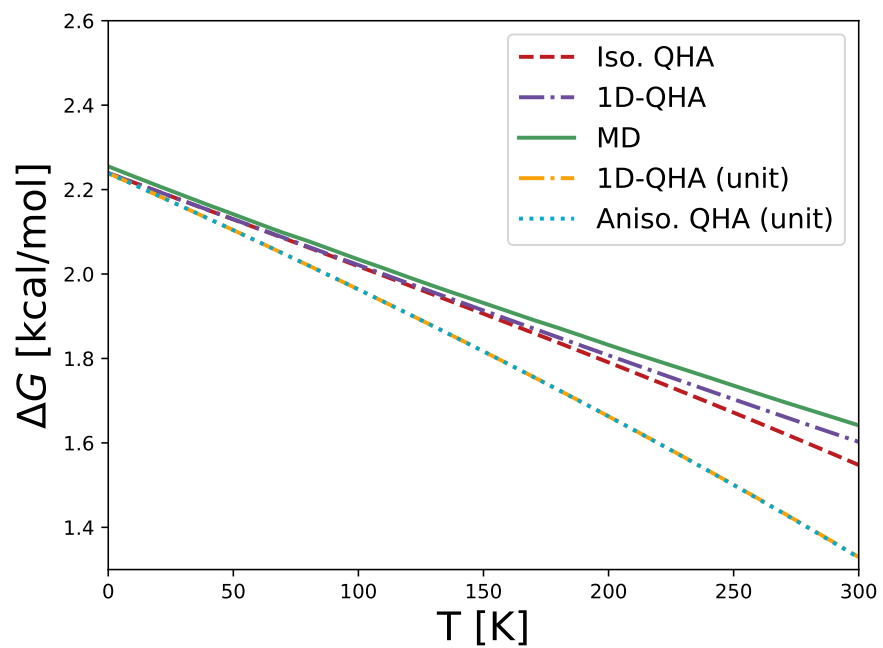


Figure 26: Polymorph free energy differences of adenine form II relative to form I

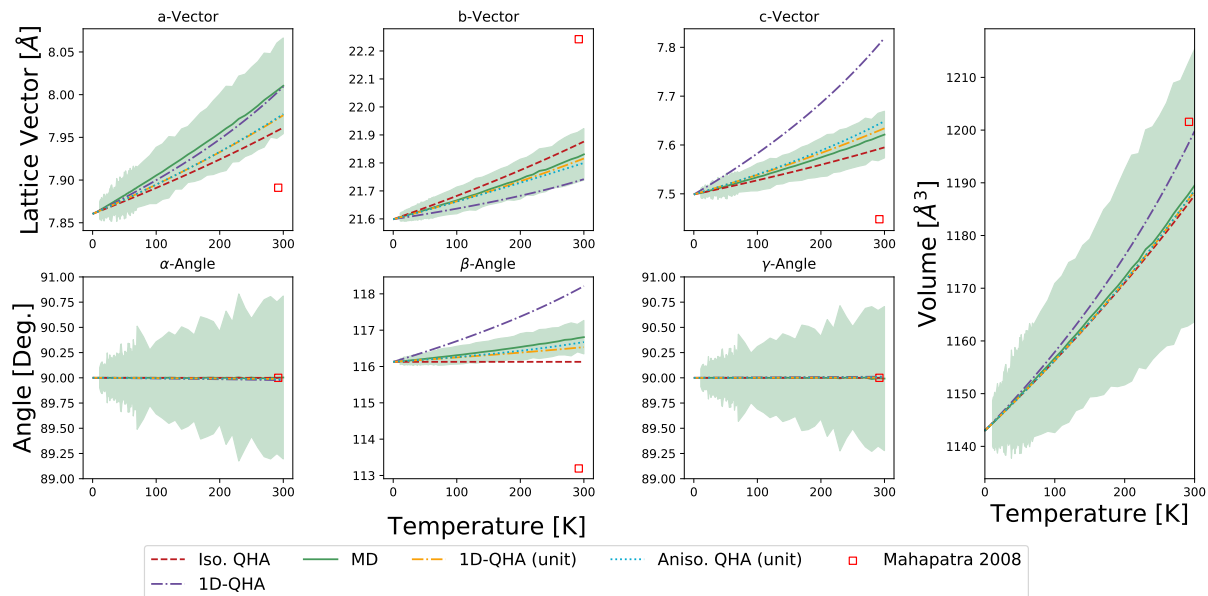


Figure 27: Adenine form I percent expansion from 0 K with experimental results.<sup>67</sup>

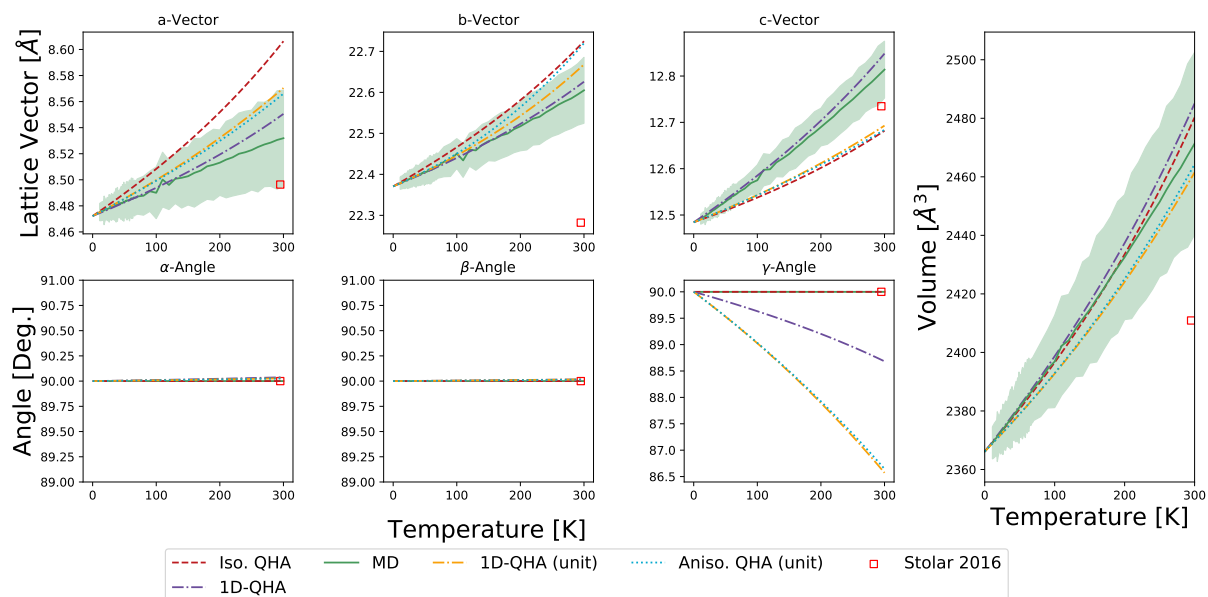


Figure 28: Adenine form II percent expansion from 0 K with experimental results.<sup>16</sup>

## Pyrazinamide

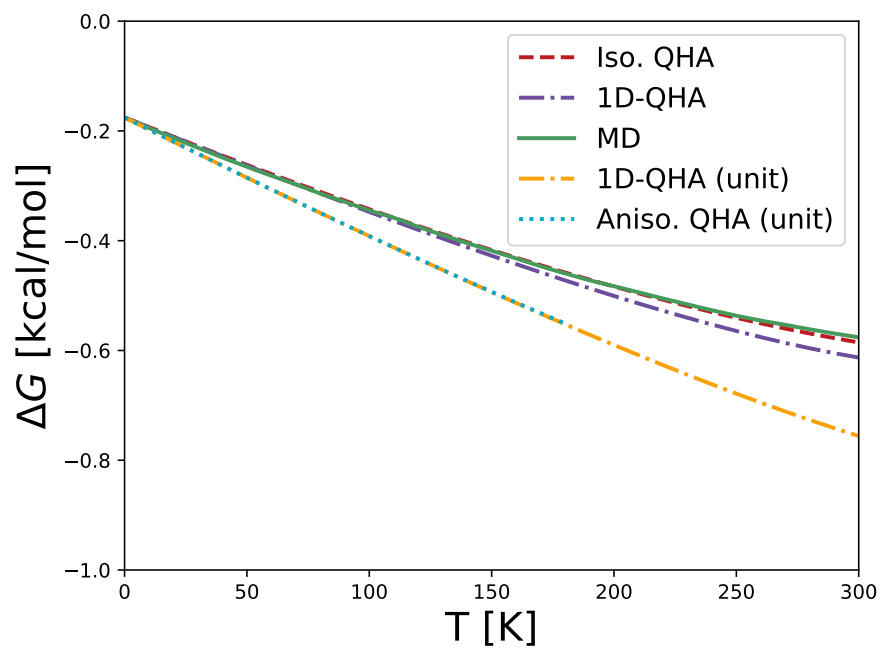


Figure 29: Polymorph free energy differences of pyrazinamide form  $\gamma$  relative to form  $\delta$

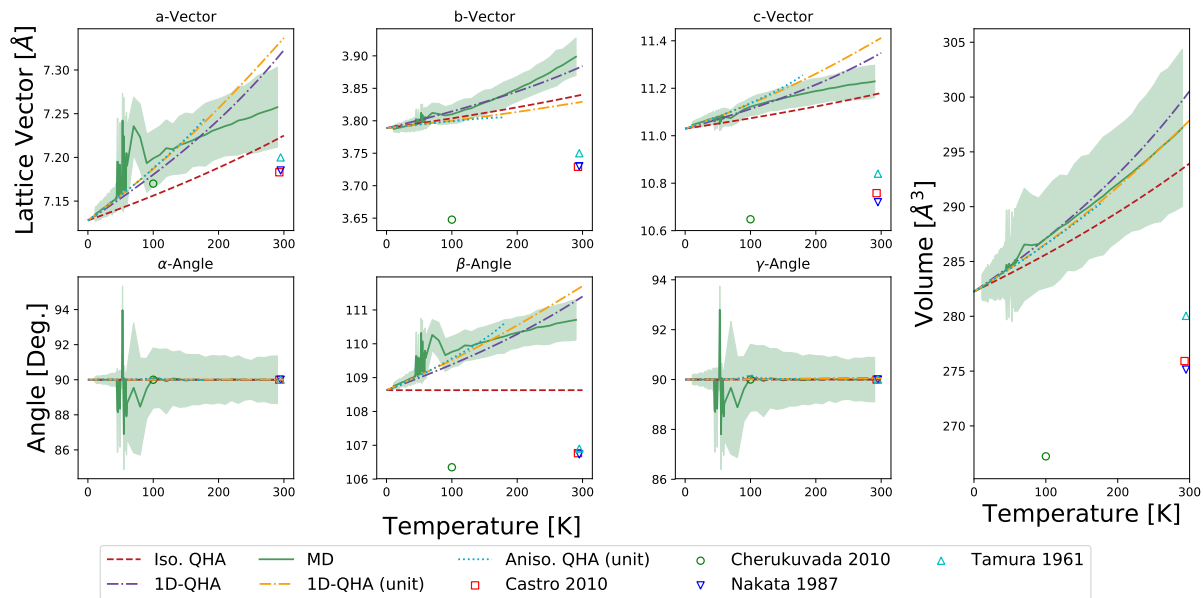


Figure 30: Pyrazinamide form  $\gamma$  percent expansion from 0 K with experimental results.<sup>68,69</sup>

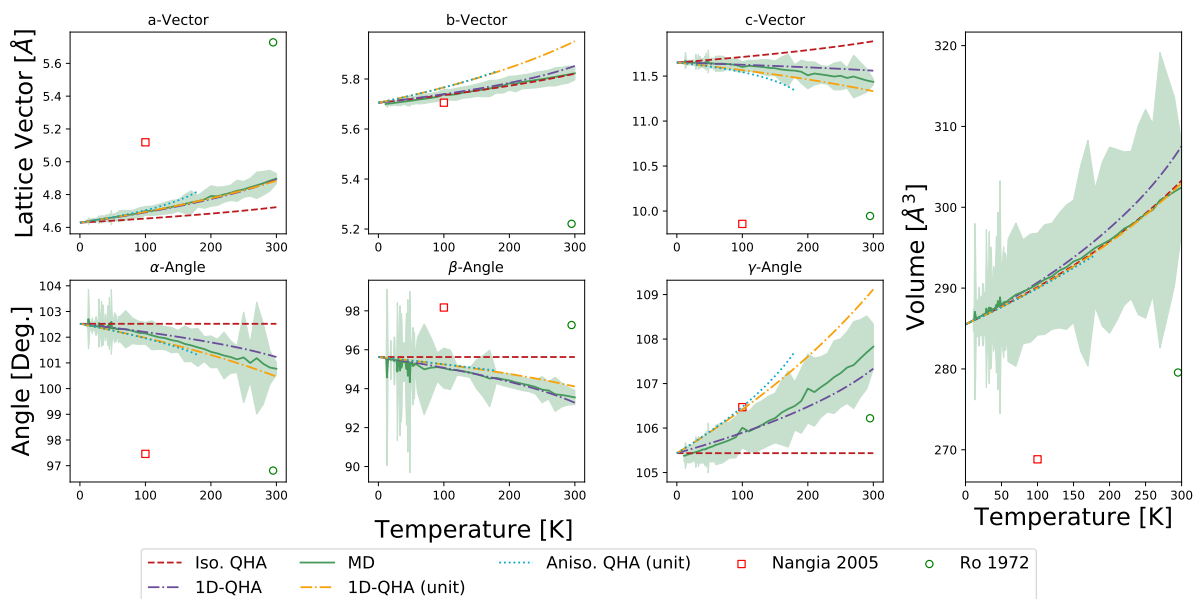


Figure 31: Pyrazinamide form  $\delta$  percent expansion from 0 K with experimental results.<sup>14,70-72</sup>

## Resorcinol

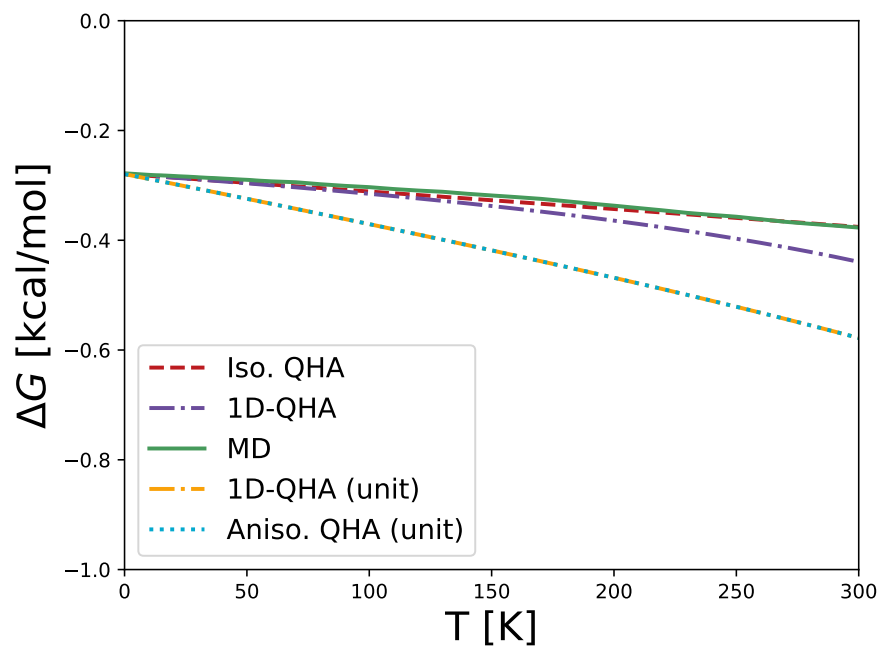


Figure 32: Polymorph free energy differences of carbamazepine form  $\beta$  relative to form  $\alpha$

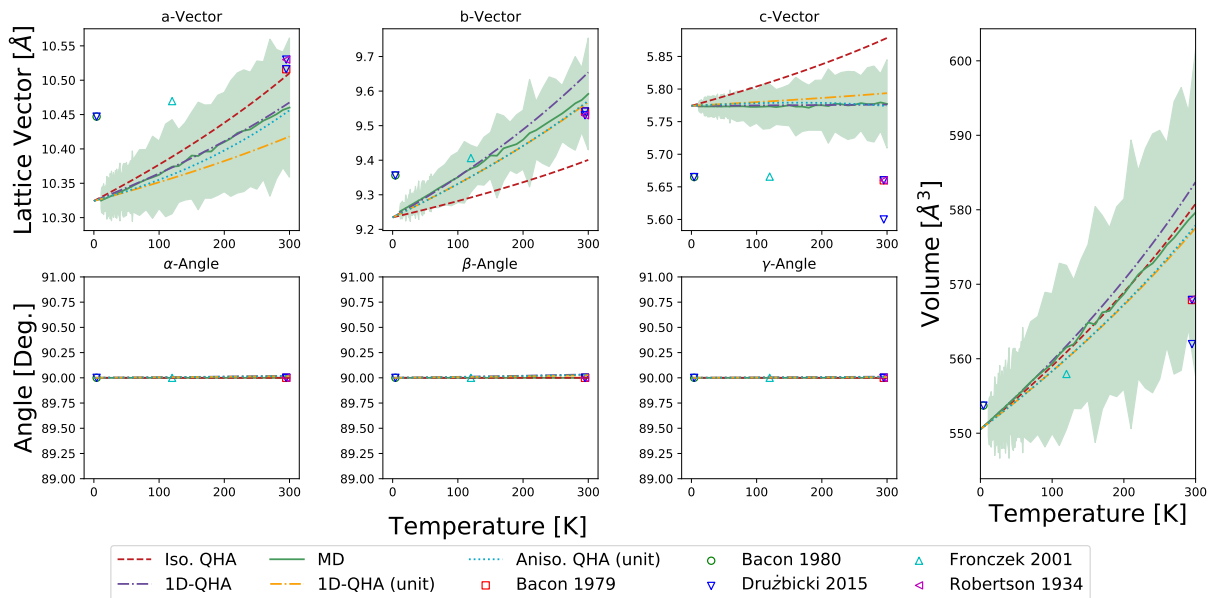


Figure 33: Resorcinol form  $\alpha$  percent expansion from 0 K with experimental results.<sup>73-77</sup>

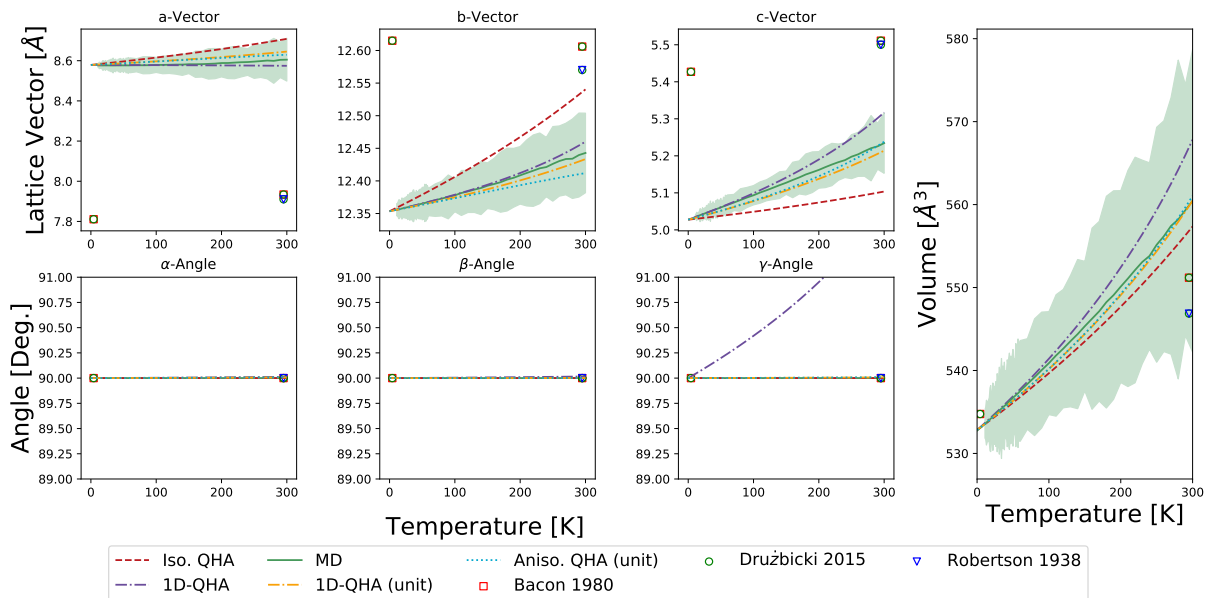


Figure 34: Resorcinol form  $\beta$  percent expansion from 0 K with experimental results.<sup>74,75,77</sup>

## 1,4-Diiodobenzene

For MD, form  $\beta$  was found to restructure at high temperature to form  $\beta$ -restructured. We show the results for form  $\beta$  using QHA only, where the lattice minimum was found by directly quenching the experimen-

tal crystal structure. The results for form  $\beta$  were used for the comparison of the 1D variant and fully anisotropic QHA, as well as the error with cell size. Form  $\beta$ -restructured was used for the comparison to MD.

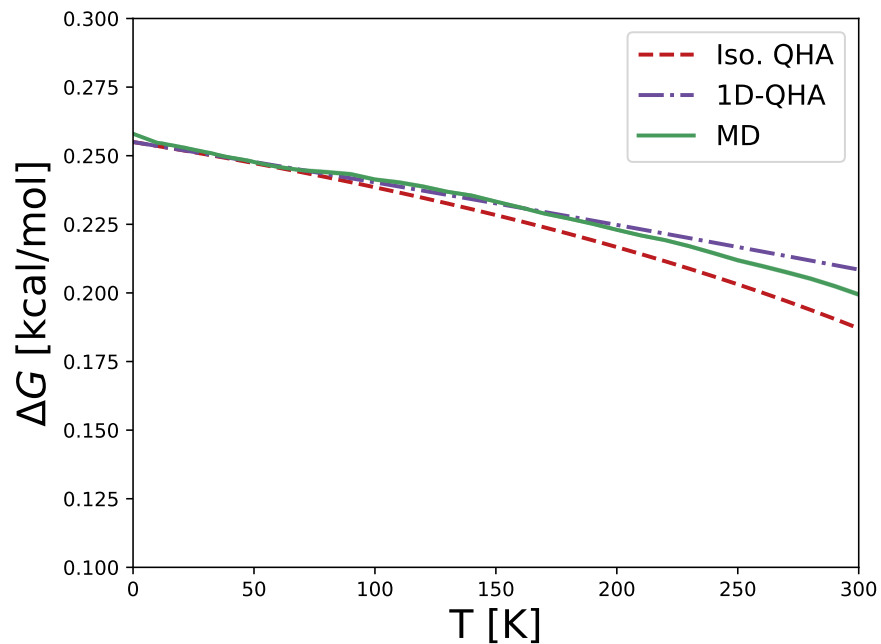


Figure 35: Polymorph free energy differences of diiodobenzene form  $\beta$ -restructured relative to form  $\alpha$

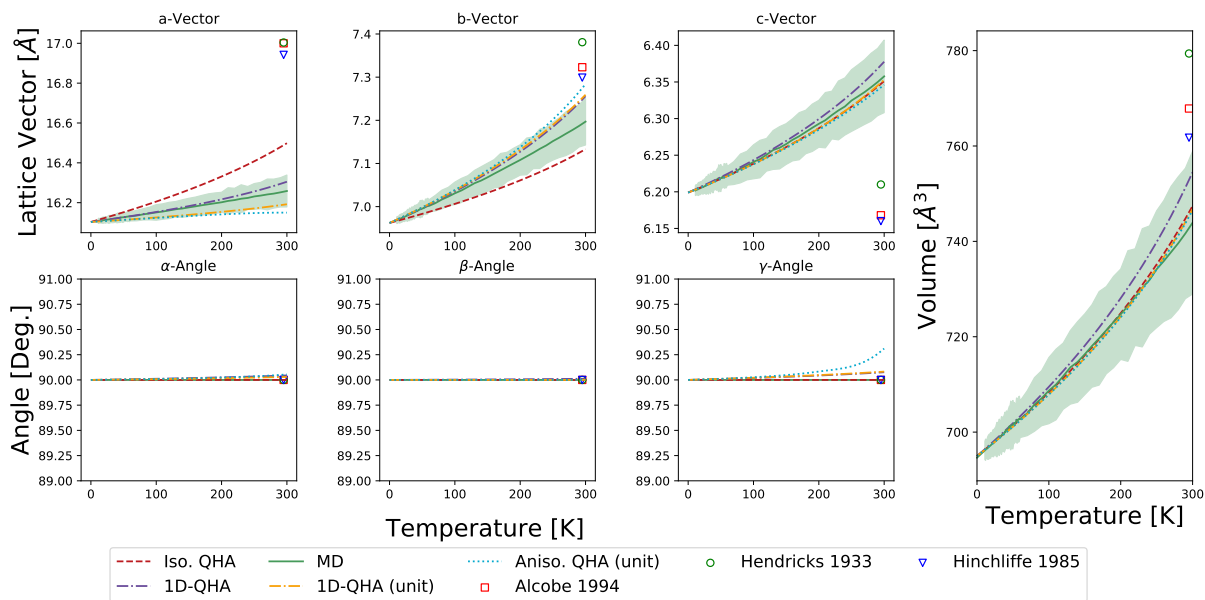


Figure 36: Diiodobenzene form  $\alpha$  percent expansion from 0 K with experimental results.<sup>17,78,79</sup>

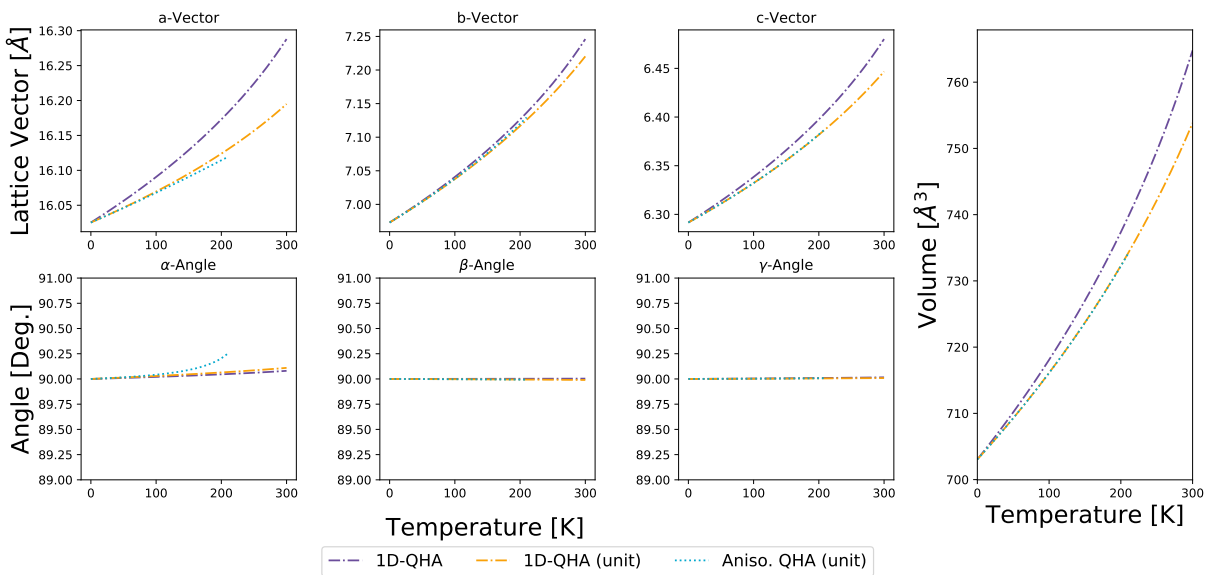


Figure 37: Diiodobenzene form  $\beta$  percent expansion from 0 K with experimental results. MD is not shown for the original structure of  $\beta$  because the system restructured at high temperature.

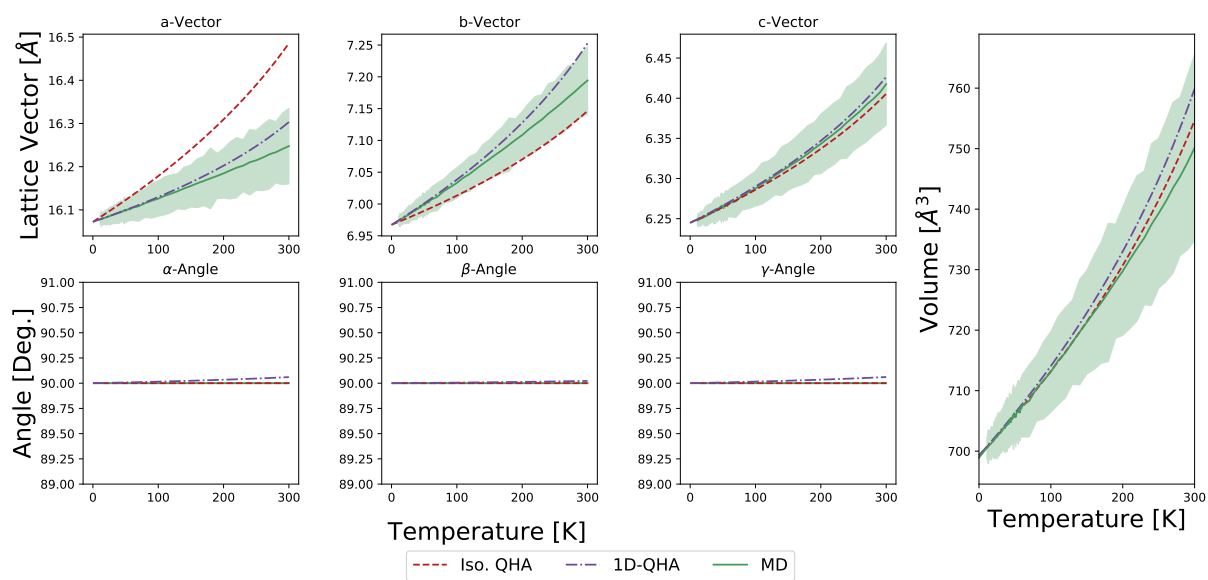


Figure 38: Diiodobenzene form  $\beta$ -restructured percent expansion from 0 K with experimental results.

## Paracetamol

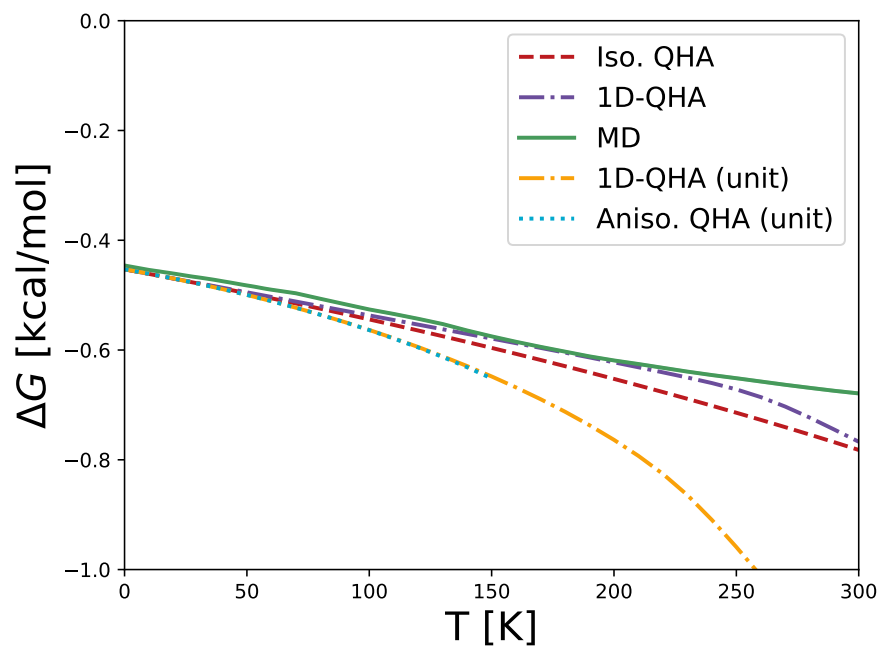


Figure 39: Polymorph free energy differences of paracetamol form I relative to form II

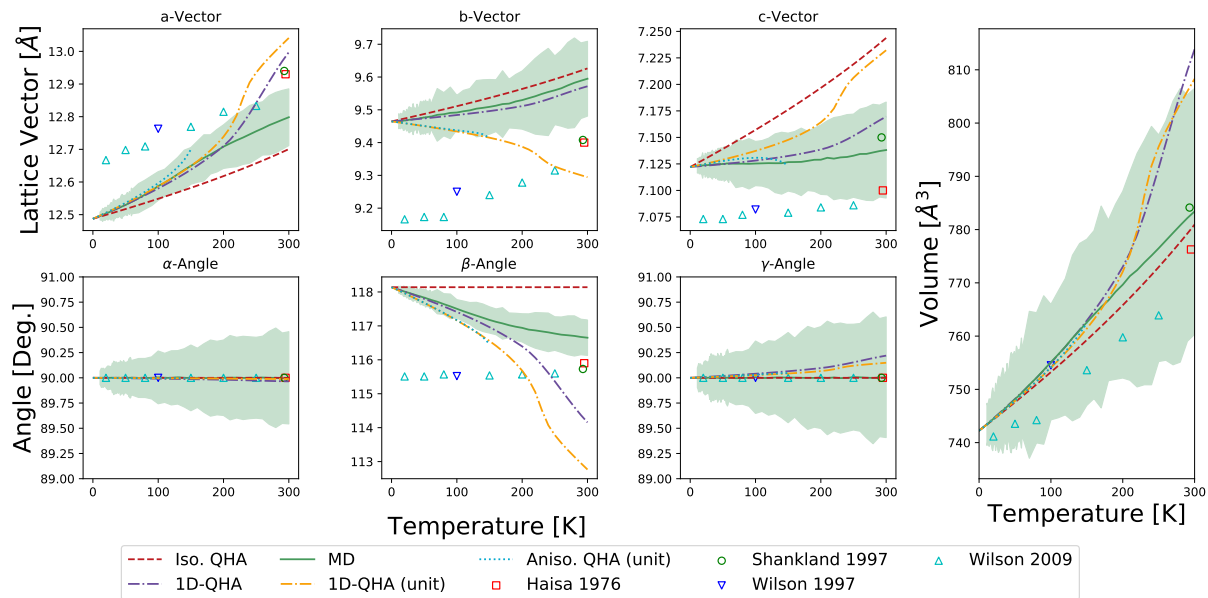


Figure 40: Paracetamol form I percent expansion from 0 K with experimental results.<sup>48,54–56</sup>

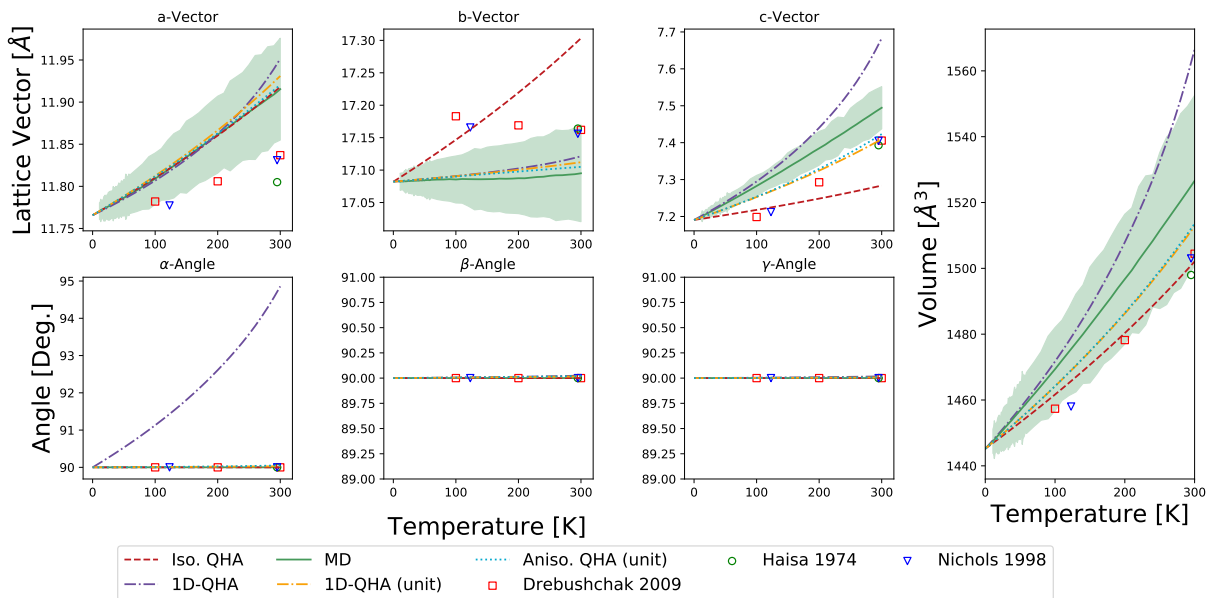


Figure 41: Paracetamol form II percent expansion from 0 K with experimental results.<sup>80–82</sup>

## Aripiprazole

For MD, both crystal structures were found to restructure at high temperature to form. We show the results for for I and X using QHA only, where the lattice minimum was found by directly quenching the experimental crystal structure. These results were

used for the comparison of the 1D variant and fully anisotropic QHA, as well as the error with cell size. Form I-restructured and form X-restructured were used for the comparison to MD.

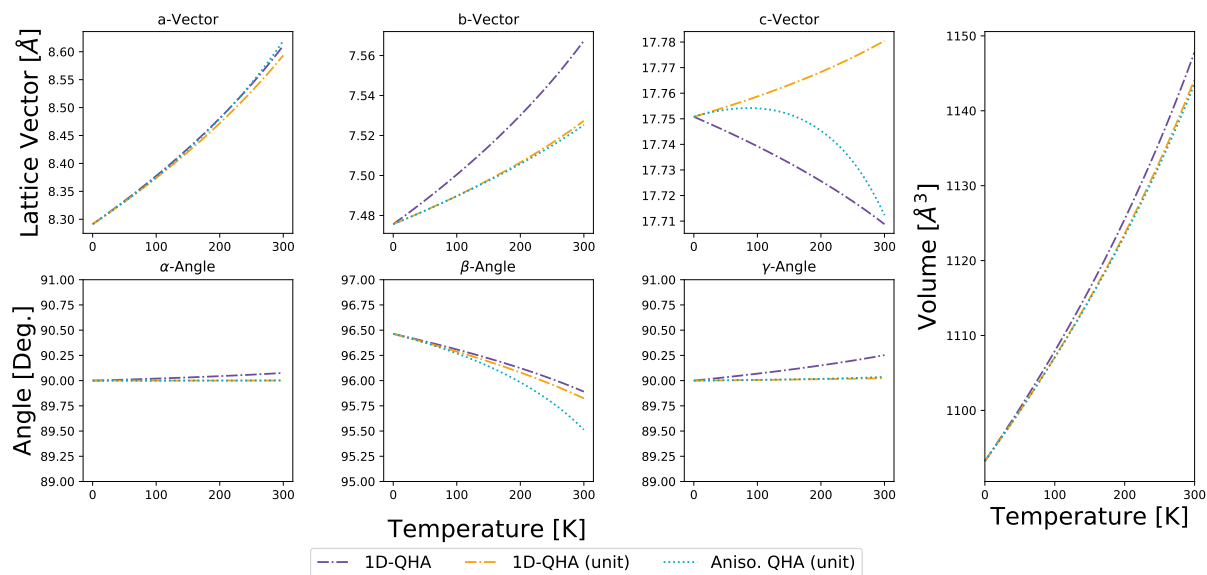


Figure 42: Aripiprazole form I percent expansion from 0 K. MD is not shown for the original structure of I because the system restructured at high temperature.

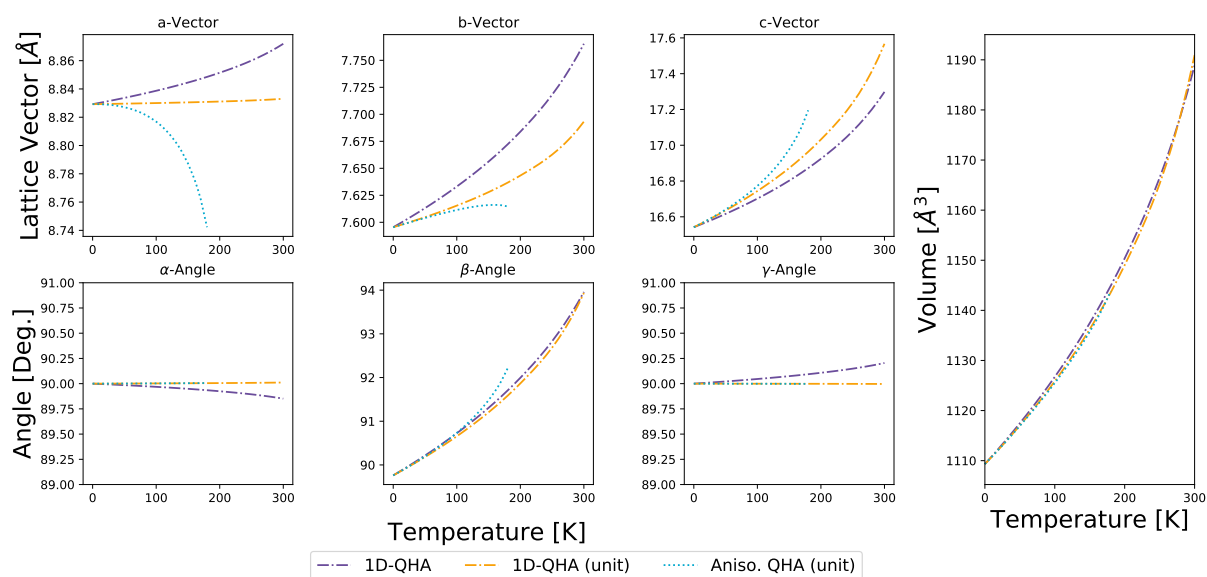


Figure 43: Aripiprazole form X percent expansion from 0 K. MD is not shown for the original structure of X because the system restructured at high temperature.

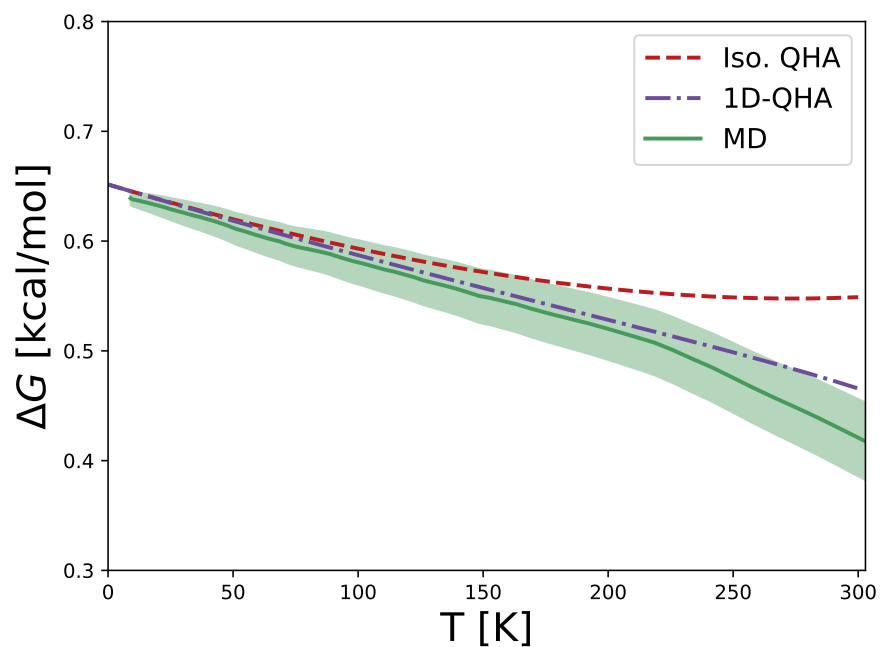


Figure 44: Polymorph free energy differences of aripiprazole form X-restructured relative to form I-restructured

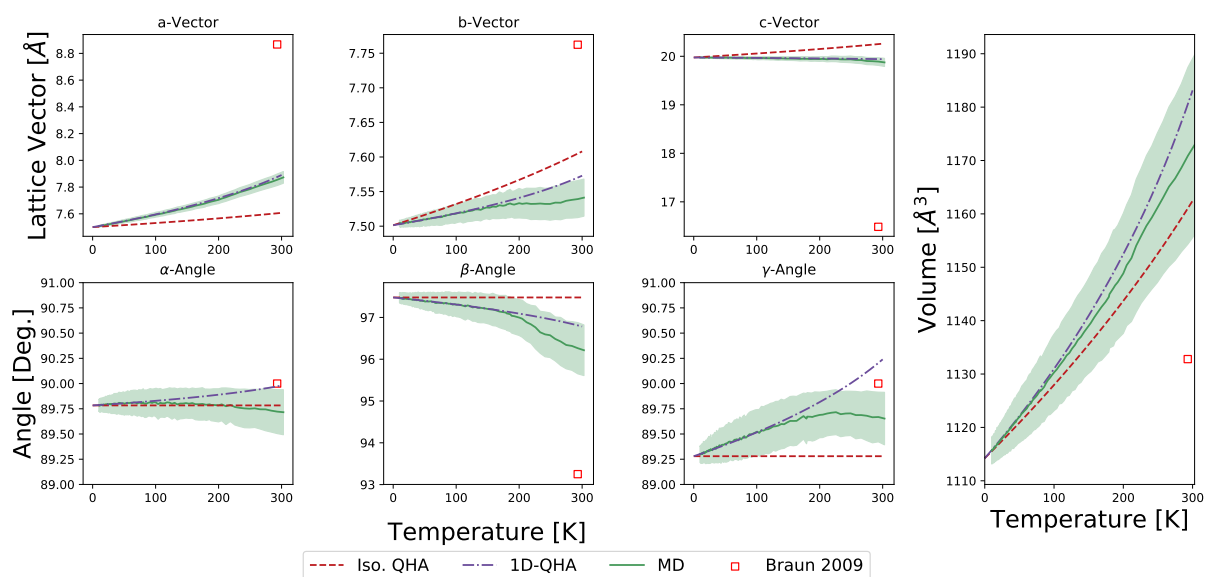


Figure 45: Aripiprazole form X-restructured percent expansion from 0 K with experimental results.<sup>44</sup>

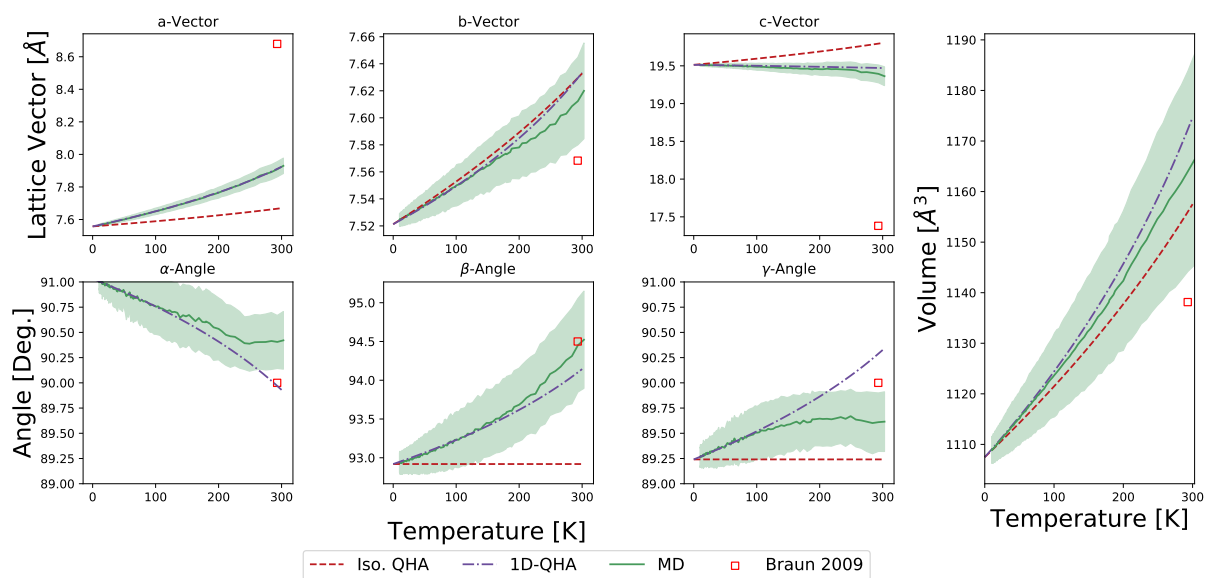


Figure 46: Aripiprazole form I-restructured percent expansion from 0 K with experimental results.<sup>44</sup>

## Tolbutamide

For MD, form I was found to restructure at high temperature to form I-restructured. We show the results for form I using QHA only, where the lattice minimum was found by directly quenching the experimen-

tal crystal structure. The results for form I were used for the comparison of the 1D variant and fully anisotropic QHA, as well as the error with cell size. Form I-restructured was used for the comparison to MD.

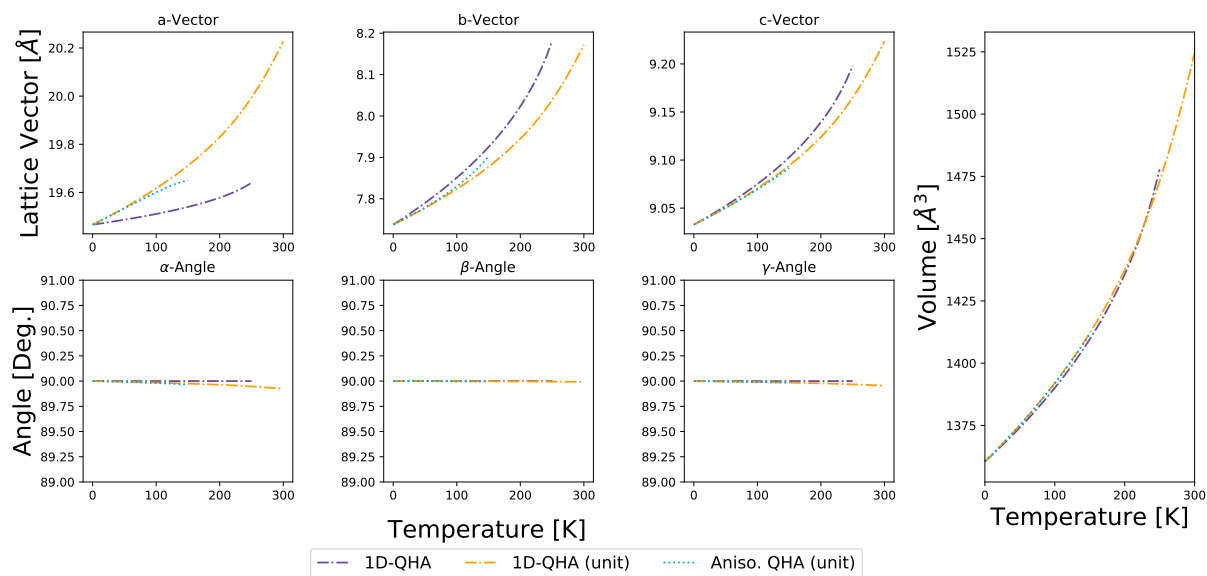


Figure 47: Tolbutamide form I percent expansion from 0 K. MD is not shown for the original structure of I because the system restructured at high temperature.

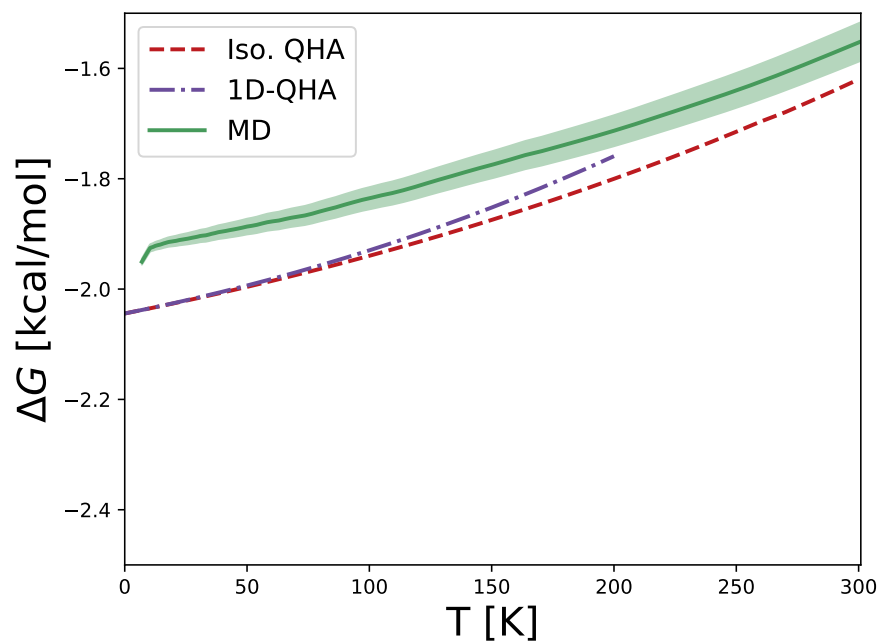


Figure 48: Polymorph free energy differences of tolbutamide form II relative to form I-restructured.

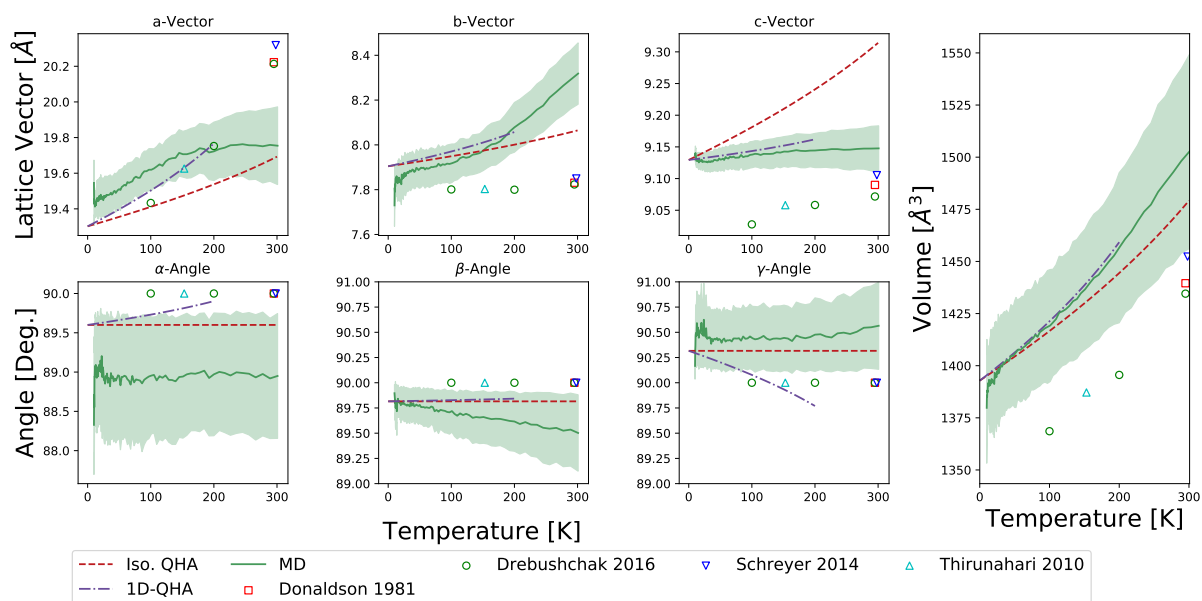


Figure 49: Tolbutamide form I-restructured percent expansion from 0 K with experimental results.<sup>83–86</sup>

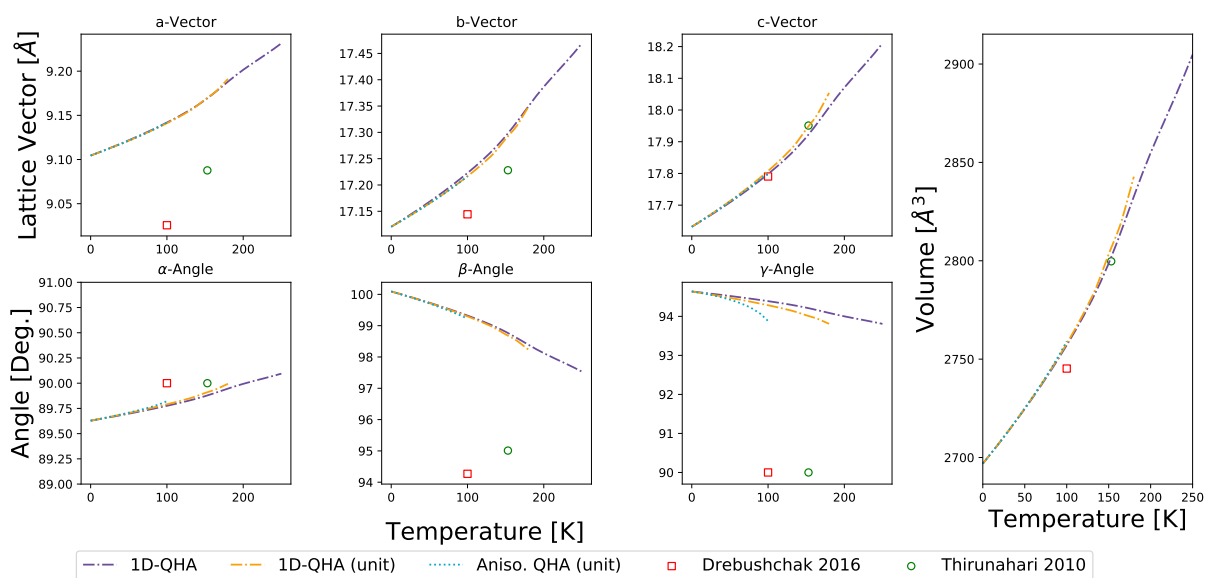


Figure 50: Tolbutamide form II percent expansion from 0 K with experimental results.<sup>43,84,86</sup>

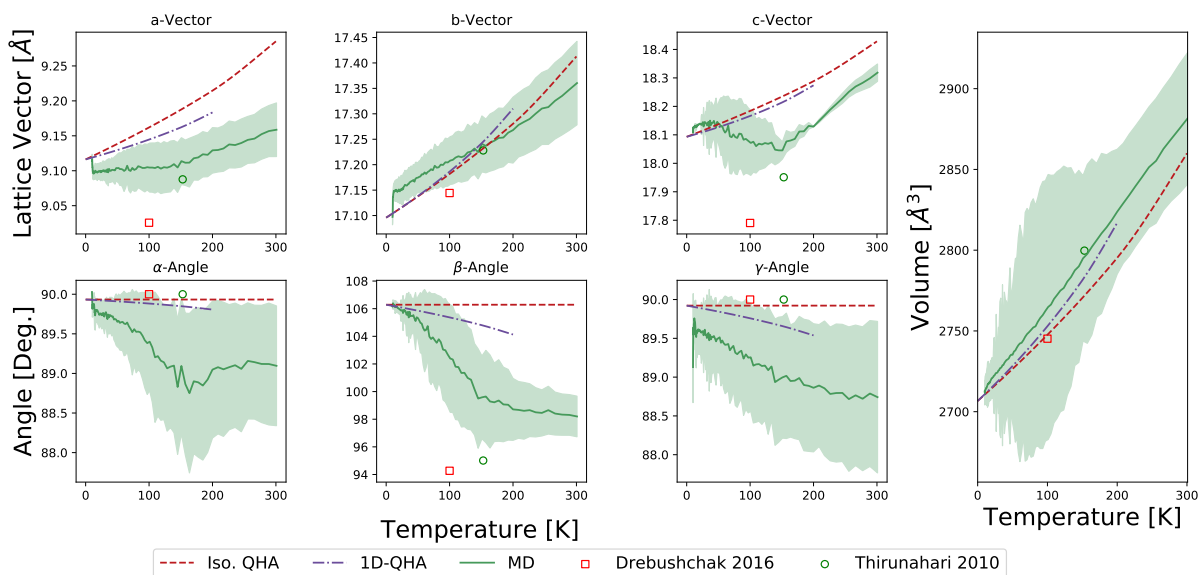


Figure 51: Tolbutamide form II-restructured percent expansion from 0 K with experimental results.<sup>43,84,86</sup>

## Chlorpropamide

For MD, form V was found to restructure at high temperature to form V-restructured. We show the results for form V using QHA only, where the lattice minimum was found by directly quenching the experimental crystal structure. The results

for form V were used for the comparison of the 1D variant and fully anisotropic QHA, as well as the error with cell size. Form V-restructured was used for the comparison to MD.

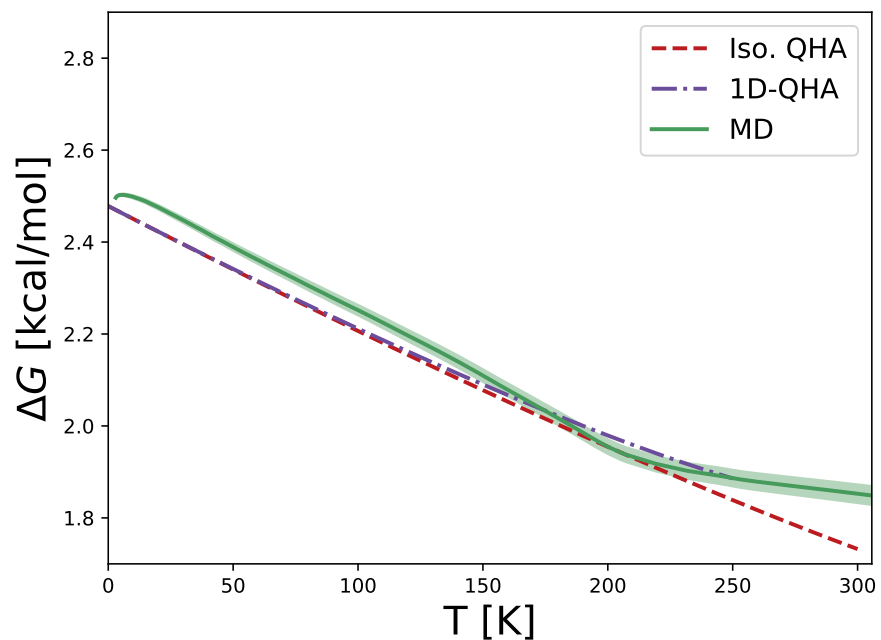


Figure 52: Polymorph free energy differences of chlorpropamide form V-restructured relative to form I-Restructured

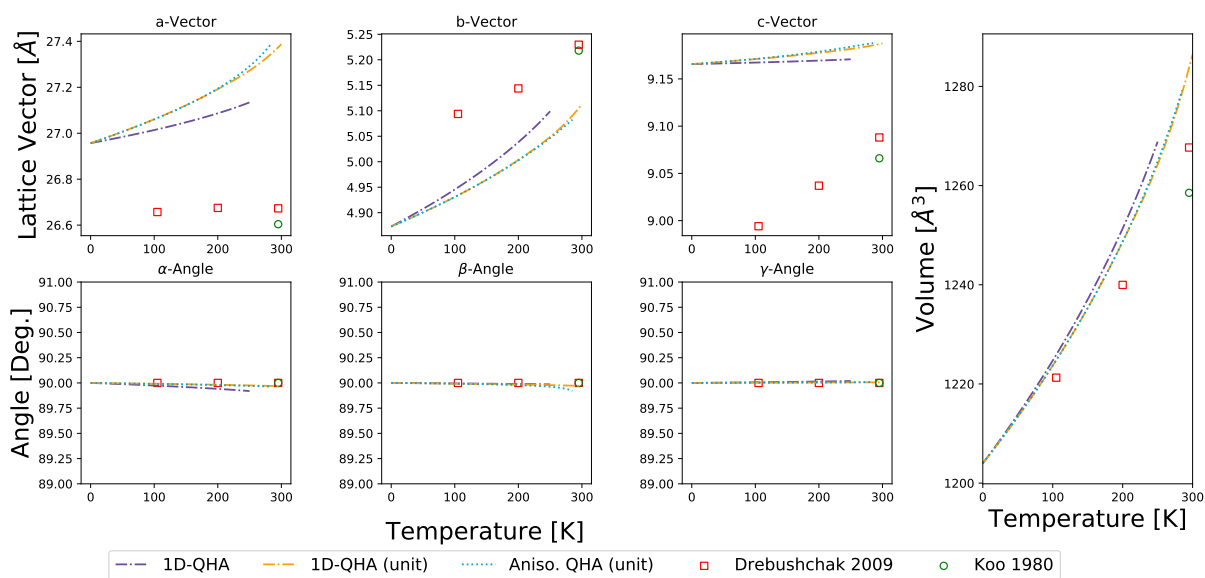


Figure 53: Chlorpropamide form I percent expansion from 0 K with experimental results.<sup>87,88</sup> MD is not shown here because this is QHA using the minima directly quenched from the experimental structure, which does not correspond with the 0 K minima found with MD.

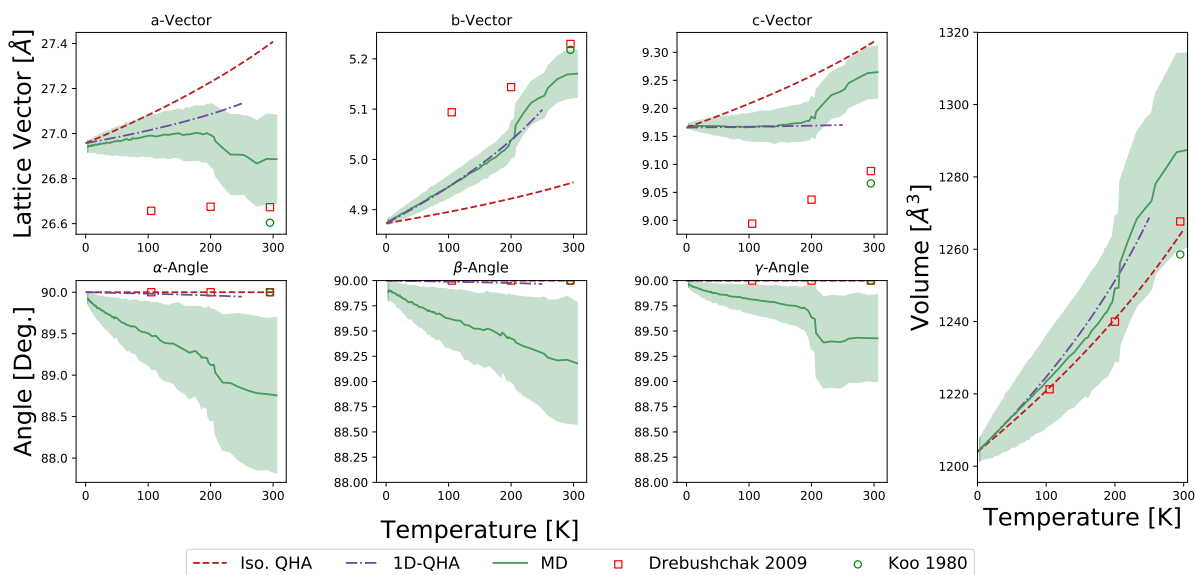


Figure 54: Chlorpropamide form I-Restructured percent expansion from 0 K with experimental results.<sup>87,88</sup>

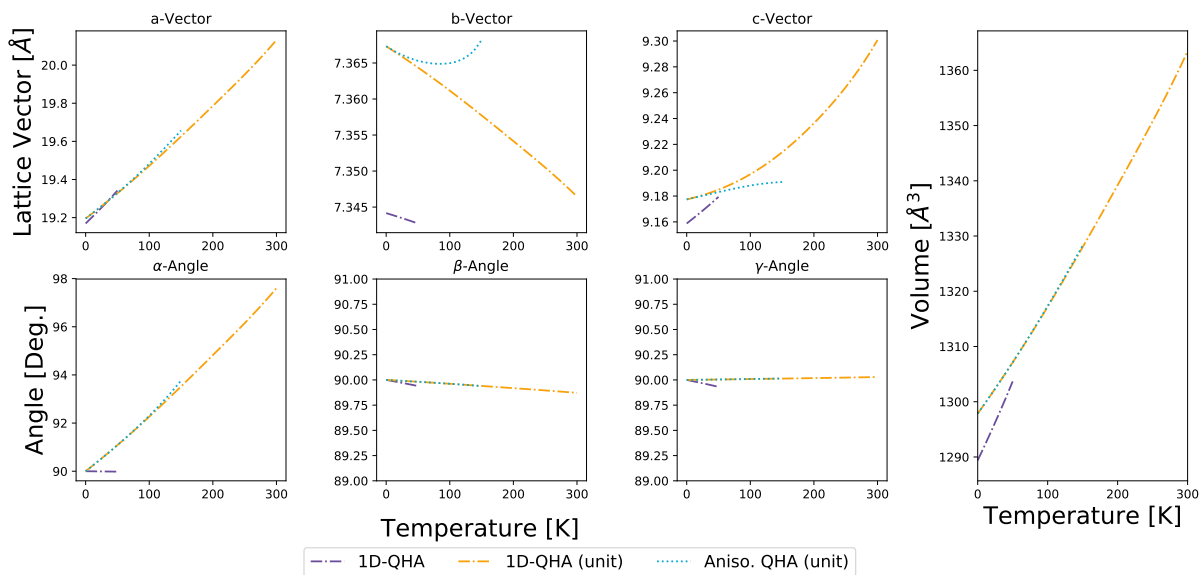


Figure 55: Chlorpropamide form V percent expansion from 0 K. MD is not shown here because this is QHA using the minima directly quenched from the experimental structure, which does not correspond with the 0 K minima found with MD.

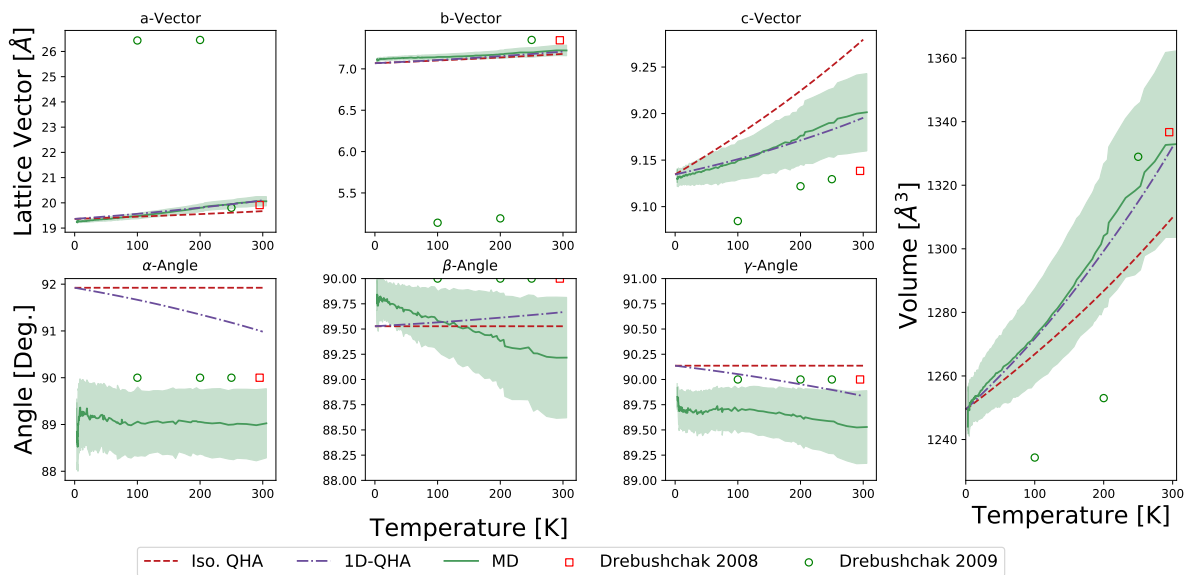


Figure 56: Chlorpropamide form V-restructured percent expansion from 0 K with experimental results.<sup>87,89</sup>

## Summary of Results

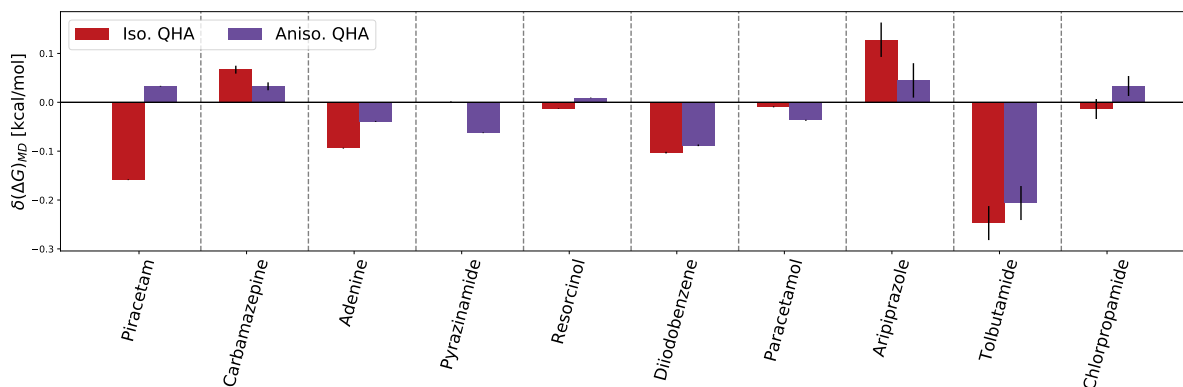


Figure 57: Deviations in the free energy differences from MD at 300 K (except for tolbutamide at 200 K, and chlorpropamide at 250 K). We report results for isotropic QHA and 1D-anisotropic QHA relative to MD. Overall, there is no evidence that a more complex thermal expansion model reduces the error between QHA and MD.

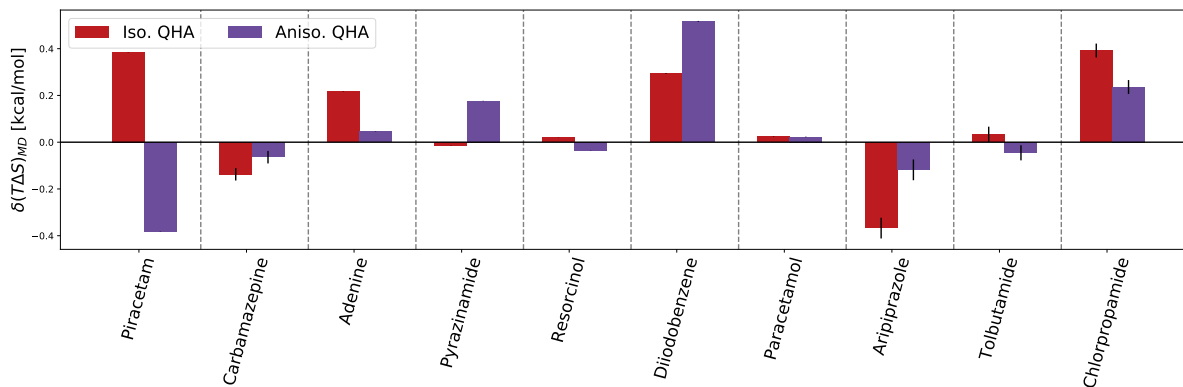


Figure 58: Deviations in the entropic contribution to the Gibbs free energy differences from MD at 300 K (except for tolbutamide at 200 K, and chlorpropamide at 250 K). We report results for isotropic QHA and 1D-anisotropic QHA relative to MD. The entropy differences between methods are compensated by a larger enthalpy difference, resulting in a smaller free energy differences.

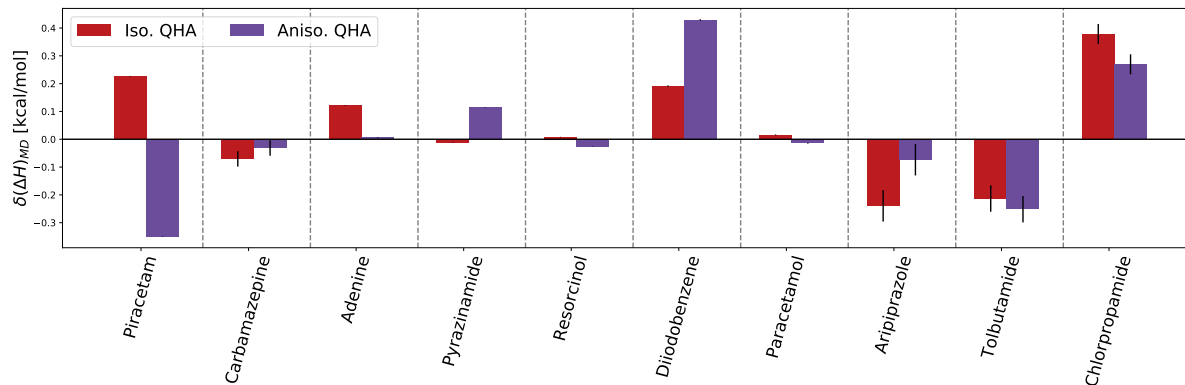


Figure 59: Deviations in the enthalpic contribution to the Gibbs free energy differences from MD at 300 K (except for tolbutamide at 200 K, and chlorpropamide at 250 K). We report results for isotropic QHA and 1D-anisotropic QHA relative to MD. The enthalpy differences between methods are compensated by a larger enthalpy difference, resulting in a smaller free energy differences.

# Replica Exchange

System	Simulation Time [ns]	Temperatures Sampled [K]
Aripiprazole	20	10.0, 10.2, 10.4, 10.6, 10.8, 11.0, 11.2, 11.5, 11.8, 12.1, 12.4, 12.7, 13.0, 13.3, 13.6, 13.9, 14.2, 14.6, 15.0, 15.4, 15.8, 16.2, 16.6, 17.0, 17.4, 17.9, 18.4, 18.9, 19.4, 19.9, 20.4, 21.0, 21.6, 22.2, 22.8, 23.4, 24.1, 24.8, 25.5, 26.2, 27.0, 27.8, 28.6, 29.4, 30.3, 31.2, 32.1, 33.1, 34.1, 35.1, 36.2, 37.3, 38.4, 39.6, 40.8, 42.0, 43.3, 44.6, 46.0, 47.4, 48.9, 50.4, 52.0, 53.6, 55.3, 57.0, 58.8, 60.7, 62.6, 64.6, 66.6, 68.7, 70.9, 73.2, 75.5, 77.9, 80.4, 81.1, 83.0, 85.7, 88.5, 91.4, 94.4, 97.5, 100.7, 104.0, 107.4, 110.9, 114.5, 118.2, 122.1, 126.1, 130.2, 134.5, 138.9, 143.5, 148.2, 153.1, 158.1, 163.3, 168.7, 174.3, 179.1, 180.0, 185.9, 188.1, 192.0, 200.0, 204.9, 211.7, 218.7, 225.9, 233.4, 241.1, 249.1, 257.4, 265.9, 274.7, 283.8, 293.2, 302.9, 313.0, 323.4, 334.2, 345.3, 350.0
Tolbutamide	20	10.0, 10.30, 10.6, 10.9, 11.2, 11.5, 11.8, 12.1, 12.5, 12.9, 13.3, 13.7, 14.1, 14.5, 15.0, 15.5, 16.0, 16.5, 17.0, 17.6, 18.2, 18.8, 19.4, 20.1, 20.8, 21.5, 22.3, 23.1, 23.9, 24.8, 25.7, 26.6, 27.6, 28.6, 29.7, 30.8, 31.9, 33.1, 34.3, 35.6, 36.9, 38.3, 39.8, 41.3, 42.9, 44.6, 46.3, 48.1, 50.0, 52.0, 54.0, 56.1, 58.3, 60.6, 63.0, 65.5, 68.1, 70.8, 73.6, 76.6, 79.7, 82.9, 86.2, 89.7, 93.3, 97.1, 101.0, 105.1, 109.4, 113.9, 118.6, 123.4, 128.5, 133.8, 139.3, 145.0, 151.0, 157.2, 163.7, 170.5, 177.5, 184.8, 192.4, 200.0, 208.7, 217.3, 226.3, 235.7, 245.5, 255.7, 266.3, 277.4, 288.9, 300.9, 313.4, 326.5, 340.1, 350.0

Chlorpropamide	30	3.00, 3.12, 3.25, 3.38, 3.52, 3.67, 3.83, 4.00, 4.18, 4.37, 4.57, 4.78, 5.00, 5.24, 5.49, 5.75, 6.03, 6.32, 6.63, 6.96, 7.31, 7.68, 8.07, 8.48, 8.92, 9.38, 9.87, 10.39, 10.94, 11.52, 12.13, 12.78, 13.46, 14.10, 14.18, 14.94, 15.75, 16.20, 16.60, 17.50, 18.46, 19.47, 20.54, 21.67, 22.87, 24.14, 25.48, 26.9, 28.4, 29.98, 31.65, 33.42, 35.29, 37.27, 39.36, 41.58, 43.92, 45.80, 46.40, 49.02, 51.79, 54.72, 57.82, 61.10, 64.57, 67.30, 68.24, 72.12, 74.80, 75.10, 76.22, 80.56, 85.15, 90.00, 95.13, 100.56, 106.30, 112.37, 118.79, 125.58, 132.76, 140.36, 148.39, 156.89, 160.90, 165.88, 175.38, 183.60, 185.43, 187.90, 194.40, 196.06, 200.00, 205.30, 207.30, 219.19, 231.76, 245.06, 253.20, 259.13, 274.01, 289.74, 305.70, 306.38, 323.98, 332.20, 333.50, 342.59, 362.27, 382.20, 383.09, 390.70, 400.00
----------------	----	--

Table 6: Systems that replica exchange we run on, the amount of time run for, and the temperatures used for exchange. Chlorpropamide was run to lower temperatures to validate our findings at low temperatures and therefore required 10 ns longer of simulation time for these low temperatures to converge conformationally.

## Comparison of Gas & Crystal Torsions

For all molecules that contain 1 or more free rotating torsions, we compared the torsional

distributions in the gas state with the crystals at 300 K. The gas states were run with REMD from 300 to 1000 K with about 0.2 probability exchange between replica.

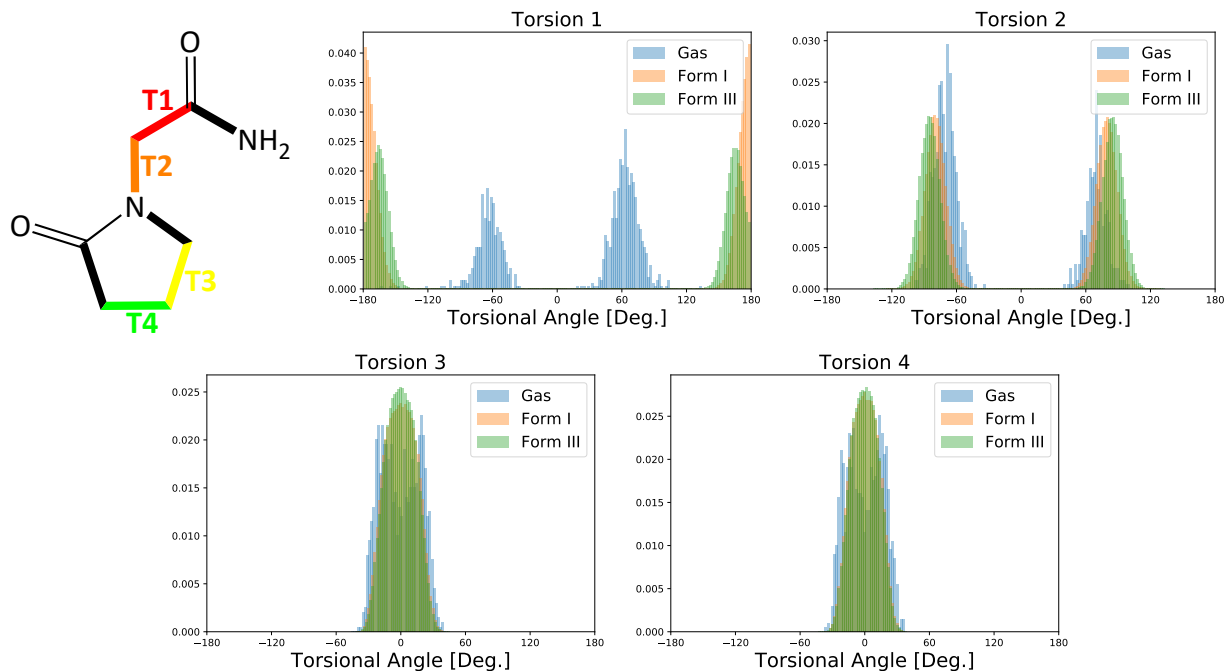


Figure 60: Torsional distributions of piracetam at 300 K for the molecule in gas and both polymorphs.

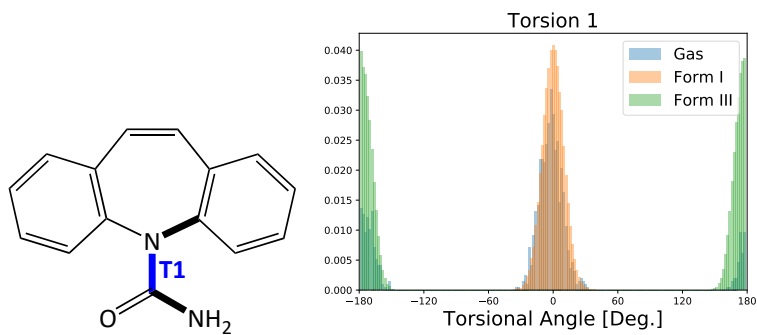


Figure 61: Torsional distributions of carbamazepine at 300 K for the molecule in gas and both polymorphs.

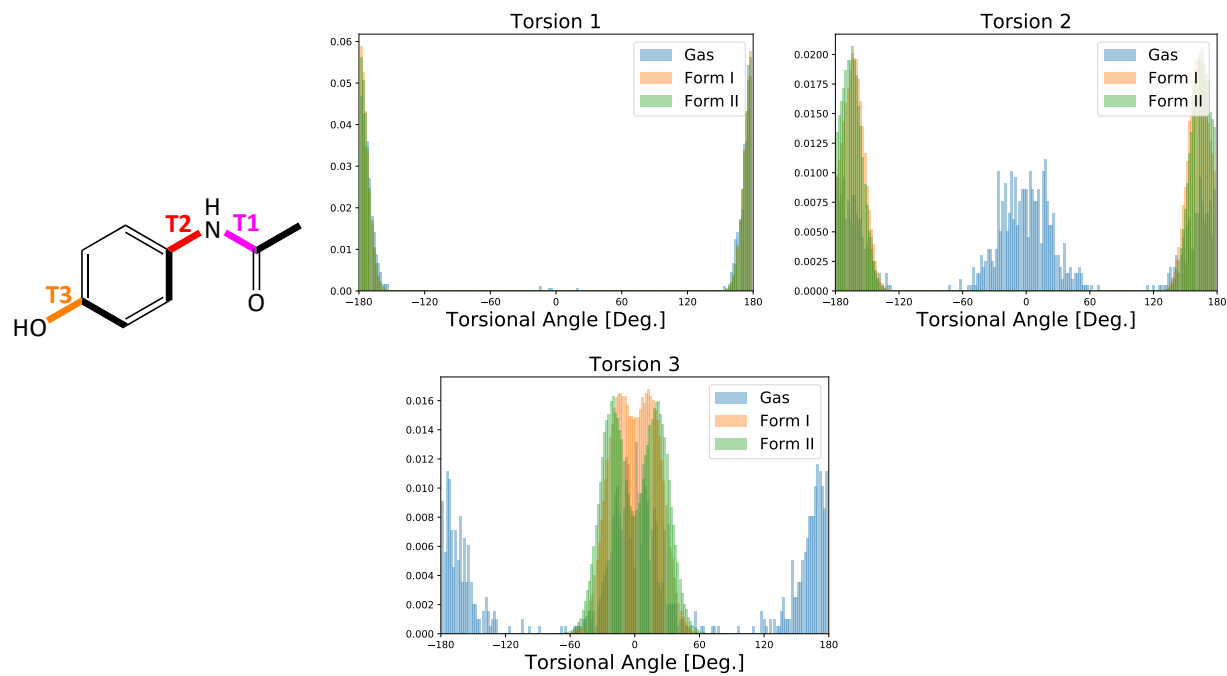


Figure 62: Torsional distributions of paracetamol at 300 K for the molecule in gas and both polymorphs.

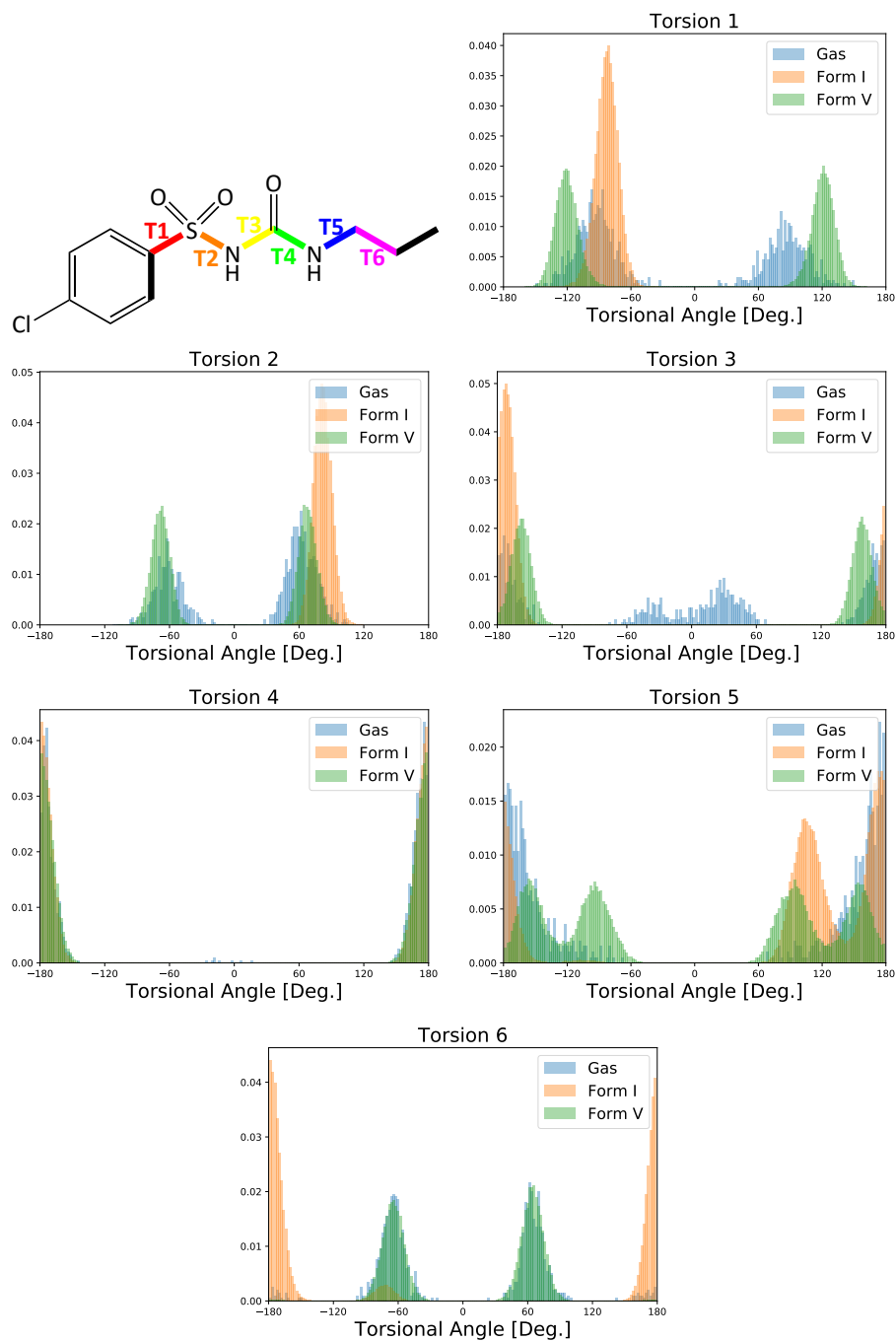


Figure 63: Torsional distributions of chlorpropamide at 300 K for the molecule in gas and both polymorphs.

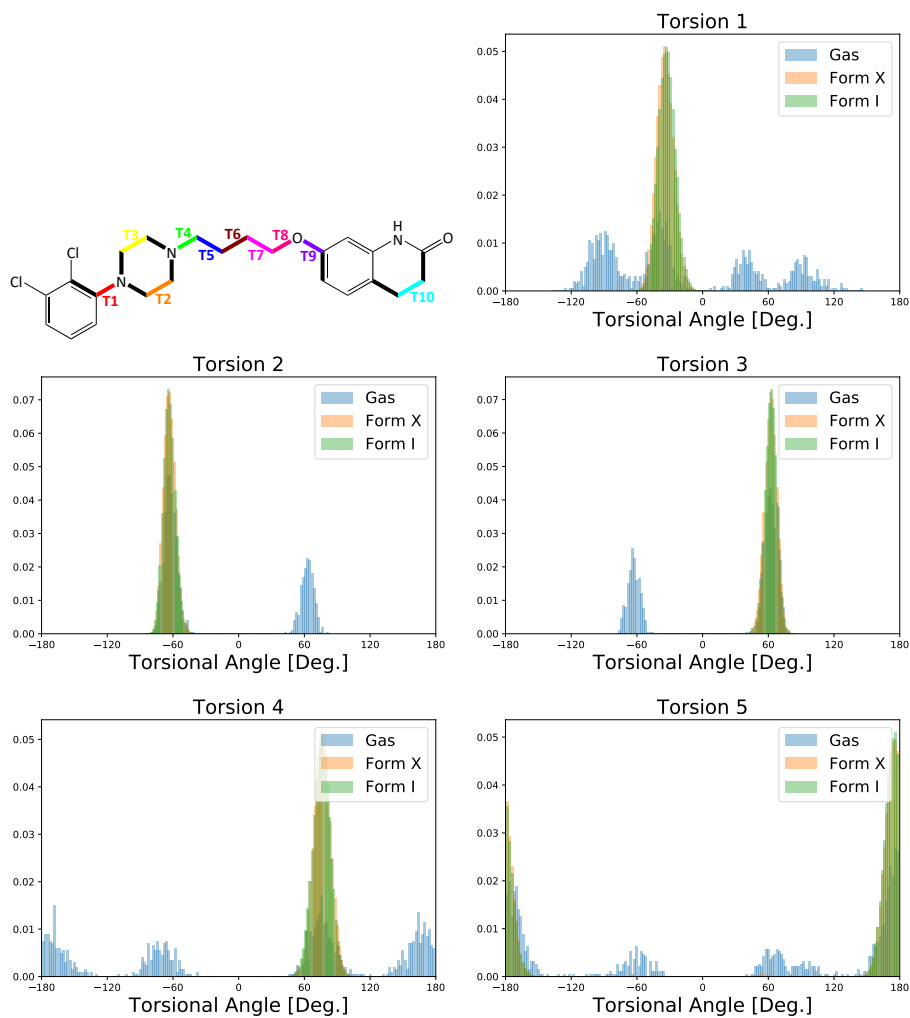


Figure 64: Torsional distributions of aripiprazole at 300 K for the molecule in gas and both polymorphs for torsions 1 – 5.

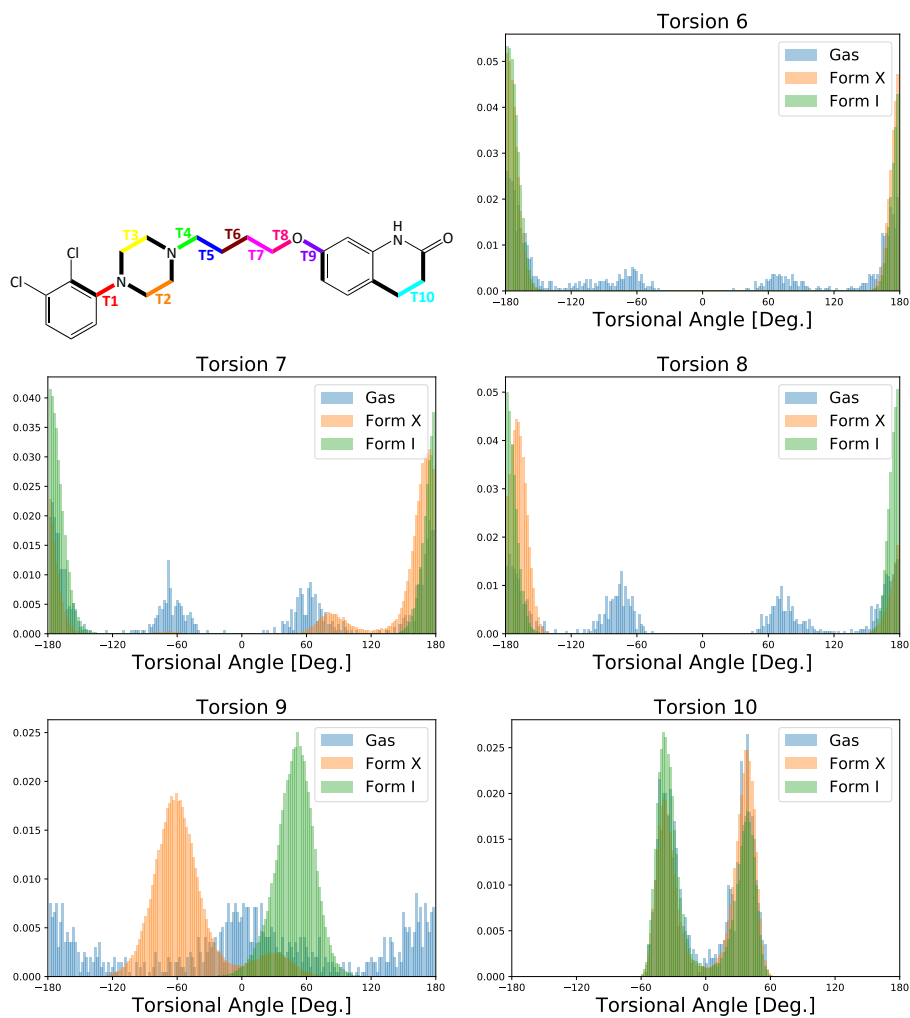


Figure 65: Torsional distributions of aripiprazole at 300 K for the molecule in gas and both polymorphs for torsions 6 – 10.

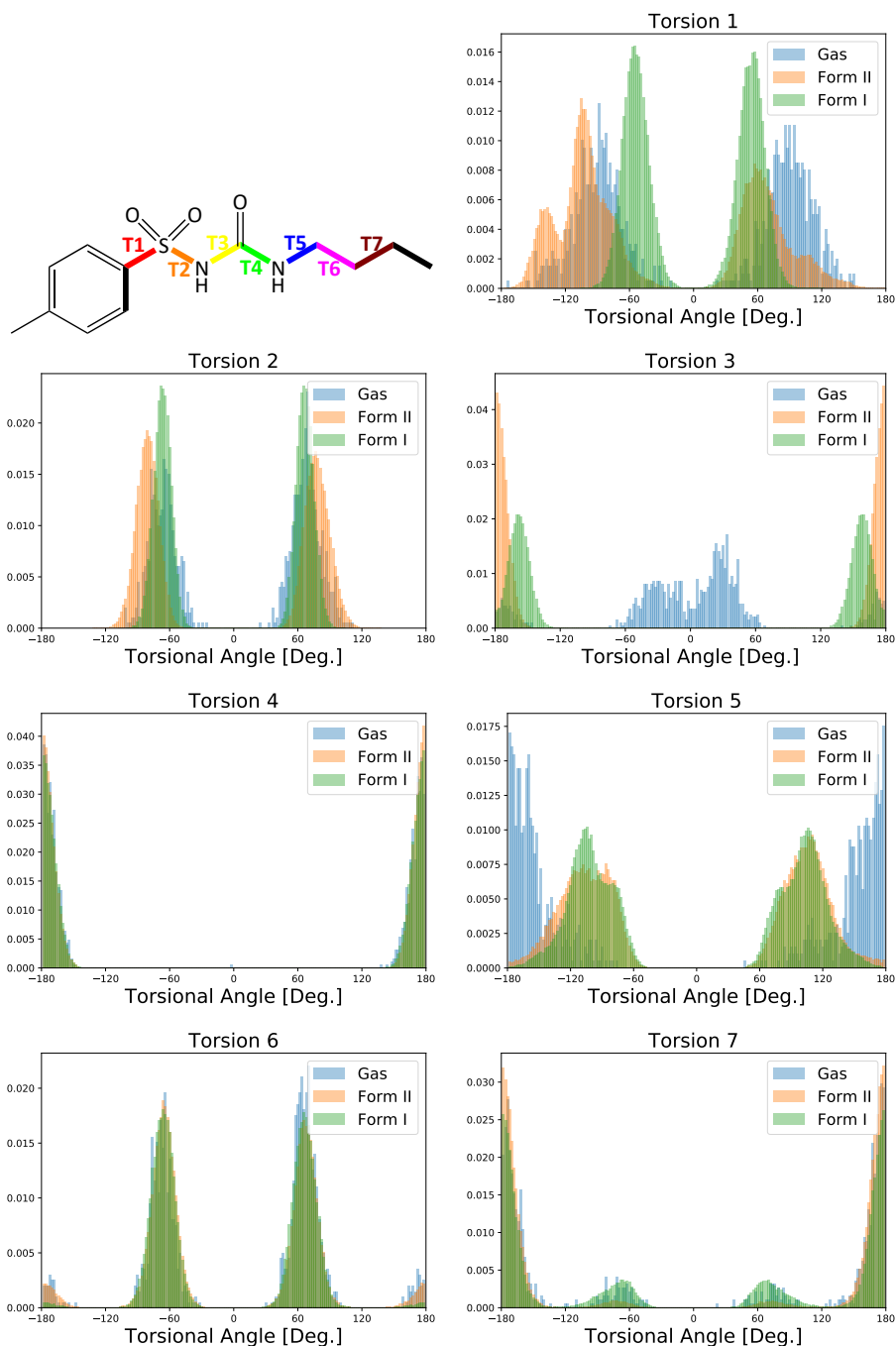


Figure 66: Torsional distributions of tolbutamide at 300 K for the molecule in gas and both polymorphs.

## Error in QHA due to Hydrogen Bonds

We found that there was little to no correlation between the hydrogen bonds and

the error in anisotropic QHA relative to MD. We determine the number of hydrogen bonds on a per molecule basis for the lattice minimum (Figure 67) and the per-

cent of hydrogen bonds remaining at 300 K (Figure 68) for MD for all systems to see if there was any correlation between error in 1D-QHA from MD ( $\delta(\Delta G_{QHA})$ ) and the number of hydrogen bonds. Despite having no hydrogen bonds present, diiodobenzene has the lowest error in the QHA free energy difference and we therefore left it out of both Figure 67 and 68. In both cases, a linear fit shows the  $R^2$  value is less than 0.1 showing that there is little to no correlation.

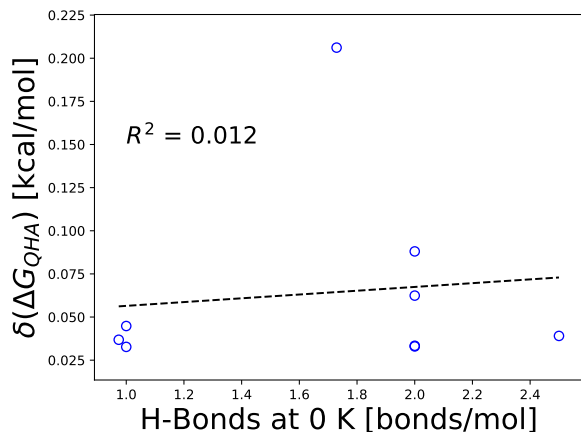


Figure 67: Error in the polymorph free energy differences for 1D-QHA from MD versus the number of hydrogen bonds in the lattice minimum structure. There is no correlation between QHA error and 0 K hydrogen bonds.

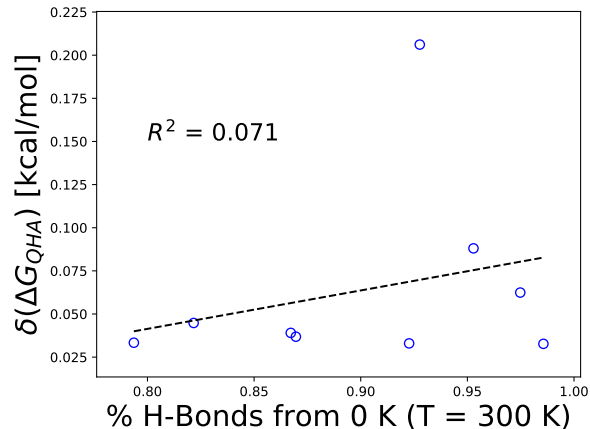


Figure 68: Error in the polymorph free energy differences for 1D-QHA from MD versus the percent of hydrogen bonds remaining at 300 K relative to the lattice minimum. There is no correlation between QHA error and 300 K hydrogen bonds.

## References

- (1) Cheuk, D.; Khamar, D.; McArdle, P.; Rasmuson, . C. Solid Forms, Crystal Habits, and Solubility of Danthron. *J. Chem. Eng. Data* **2015**, *60*, 2110–2118.
- (2) Maher, A.; Rasmuson, . C.; Croker, D. M.; Hodnett, B. K. Solubility of the Metastable Polymorph of Piracetam (Form II) in a Range of Solvents. *J. Chem. Eng. Data* **2012**, *57*, 3525–3531.
- (3) Valle, R. G. D.; Brillante, A.; Farina, L.; Venuti, E.; Masino, M.; Girlando, A. Organic Semiconductors: Polymorphism, Phonon Dynamics and Carrier-Phonon Coupling in Pentacene. *Mol. Cryst. Liq. Cryst. Sci.* **2004**, *416*, 145–154.
- (4) Stevens, L. A.; Goetz, K. P.; Fonari, A.; Shu, Y.; Williamson, R. M.; Brdas, J.-L.; Coropceanu, V.; Jurchescu, O. D.; Collis, G. E. Temperature-Mediated Polymorphism in Molecular Crystals: The Impact on Crystal Packing and Charge Transport. *Chem. Mater.* **2015**, *27*, 112–118.
- (5) Singhal, D.; Curatolo, W. Drug polymorphism and dosage form design: a practical perspective. *Adv. Drug Deliv. Rev* **2004**, *56*, 335–347.
- (6) Ghosh, M.; Banerjee, S.; Khan, S.; Sikder, N.; Sikder, A. Understanding Metastable Phase Transformation during Crystallization of RDX, HMX and CL-20: Experimental and DFT Studies. *Phys. Chem. Chem. Phys.* **2016**, 23554–23571.
- (7) Dreger, Z. A.; Tao, Y.; Gupta, Y. M. Phase Diagram and Decomposition of 1,1-Diamino-2,2-dinitroethene Single Crystals at High Pressures and Temperatures. *J. Phys. Chem. C* **2016**, 11092–11098.
- (8) van der Heijden, A. E. D. M.; Bouma, R. H. B. Crystallization and Characterization of RDX, HMX, and CL-20. *Cryst. Growth Des.* **2004**, *4*, 999–1007.
- (9) Grzesiak, A. L.; Lang, M.; Kim, K.; Matzger, A. J. Comparison of the Four Anhydrous Polymorphs of Carbamazepine and the Crystal Structure of Form I. *J. Pharm. Sci.* **2003**, *92*, 2260–2271.
- (10) Yoshino, M.; Takahashi, K.; Okuda, Y.; Yoshizawa, T.; Fukushima, N.; Naoki, M. Contribution of Hydrogen Bonds to Equilibrium Transition of Resorcinol. *J. Phys. Chem. A* **1999**, *103*, 2775–2783.
- (11) Vemavarapu, C.; Mollan, M. J.; Needham, T. E. Crystal doping aided by rapid expansion of supercritical solutions. *AAPS PharmSciTech* **2002**, *3*, 17.
- (12) Badea, E.; Blanco, I.; Della Gatta, G. Fusion and solid-to-solid transitions of a homologous series of alkane-, dinitriles. *J. Chem. Thermodyn.* **2007**, *39*, 1392–1398.
- (13) Yu, L.; Huang, J.; Jones, K. J. Measuring Free-Energy Difference between Crystal Polymorphs through Eutectic Melting. *J. Phys. Chem. B* **2005**, *109*, 19915–19922.

- (14) Cherukuvada, S.; Thakuria, R.; Nangia, A. Pyrazinamide Polymorphs: Relative Stability and Vibrational Spectroscopy. *Cryst. Growth Des.* **2010**, *10*, 3931–3941.
- (15) Torrisi, A.; Leech, C. K.; Shankland, K.; David, W. I. F.; Ibberson, R. M.; Benet-Buchholz, J.; Boese, R.; Leslie, M.; Catlow, C. R. A.; Price, S. L. Solid Phases of Cyclopentane: Combined Experimental and Simulation Study. *J. Phys. Chem. B* **2008**, *112*, 3746–3758.
- (16) Stolar, T.; Lukin, S.; Poar, J.; Rubi, M.; Day, G. M.; Biljan, I.; Jung, D. .; Horvat, G.; Uarevi, K.; Metrovi, E.; Halasz, I. Solid-State Chemistry and Polymorphism of the Nucleobase Adenine. *Cryst. Growth Des.* **2016**, *16*, 3262–3270.
- (17) Alcob, X.; Estop, E.; Aliev, A. E.; Harris, K. D. M.; Rodriguez-Carvajal, J.; Rius, J. Temperature-Dependent Structural Properties of p-Diiodobenzene: Neutron Diffraction and High-Resolution Solid State  $^{13}\text{C}$  NMR Investigations. *J. Solid State Chem.* **1994**, *110*, 20–27.
- (18) Sacchetti, M. Thermodynamic Analysis of DSC Data for Acetaminophen Polymorphs. *J. Therm. Anal. Calorim* **2000**, *63*, 345–350.
- (19) Cesaro, A.; Starec, G. Thermodynamic properties of caffeine crystal forms. *J. Phys. Chem.* **1980**, *84*, 1345–1346.
- (20) Seryotkin, Y. V.; Drebuschak, T. N.; Boldyreva, E. V. A high-pressure polymorph of chlorpropamide formed on hydrostatic compression of the -form in saturated ethanol solution. *Acta Cryst B* **2013**, *69*, 77–85.
- (21) Boldyreva, E. V.; Shakhtshneider, T. P.; Ahsbahs, H.; Sowa, H.; Uchtmann, H. Effect of High Pressure on the Polymorphs of Paracetamol. *J. Therm. Anal. Calorim* **2002**, *68*, 437–452.
- (22) Cansell, F.; Fabre, D.; Petitet, J. Phase transitions and chemical transformations of benzene up to 550C and 30 GPa. *J. Chem. Phys.* **1993**, *99*, 7300–7304.
- (23) Gajda, R.; Katrusiak, A. Pressure-Promoted CHO Hydrogen Bonds in Formamide Aggregates. *Cryst. Growth Des.* **2011**, *11*, 4768–4774.
- (24) Dybeck, E. C.; Abraham, N. S.; Schieber, N. P.; Shirts, M. R. Capturing Entropic Contributions to Temperature-Mediated Polymorphic Transformations Through Molecular Modeling. *Cryst. Growth Des.* **2017**, *17*, 1775–1787.
- (25) Abraham, N. S.; Shirts, M. R. Thermal Gradient Approach for the Quasi-harmonic Approximation and Its Application to Improved Treatment of Anisotropic Expansion. *J. Chem. Theory Comput.* **2018**, *14*, 5904–5919.
- (26) Erba, A.; Shahrokhi, M.; Moradian, R.; Dovesi, R. On how differently the quasi-harmonic approximation works for two isostructural crystals: Thermal properties of periclase and lime. *J. Chem. Phys.* **2015**, *142*, 044114.
- (27) Erba, A.; Maul, J.; Demichelis, R.; Dovesi, R. Assessing thermochemical

- properties of materials through ab initio quantum-mechanical methods: the case of  $\alpha$ -Al<sub>2</sub>O<sub>3</sub>. *Phys. Chem. Chem. Phys.* **2015**, *17*, 11670–11677.
- (28) Erba, A.; Maul, J.; De La Pierre, M.; Dovesi, R. Structural and elastic anisotropy of crystals at high pressures and temperatures from quantum mechanical methods: The case of Mg<sub>2</sub>SiO<sub>4</sub> forsterite. *J. Chem. Phys.* **2015**, *142*, 204502.
- (29) Erba, A. On combining temperature and pressure effects on structural properties of crystals with standard ab initio techniques. *J. Chem. Phys.* **2014**, *141*, 124115.
- (30) Maul, J.; Santos, I. M. G.; Sambrano, J. R.; Erba, A. Thermal properties of the orthorhombic CaSnO<sub>3</sub> perovskite under pressure from ab initio quasi-harmonic calculations. *Theor. Chem. Acc* **2016**, *135*, 36.
- (31) Dybeck, E. C.; Schieber, N. P.; Shirts, M. R. Effects of a More Accurate Polarizable Hamiltonian on Polymorph Free Energies Computed Efficiently by Reweighting Point-Charge Potentials. *J. Chem. Theory Comput.* **2016**, *12*, 3491–3505.
- (32) Hore, S.; Dinnebier, R.; Wen, W.; Hanson, J.; Maier, J. Structure of plastic crystalline succinonitrile: High-resolution in situ powder diffraction. *Z. Anorg. Allg. Chem.* **2009**, *635*, 88–93.
- (33) Heit, Y. N.; Nanda, K. D.; Beran, G. J. O. Predicting finite-temperature properties of crystalline carbon dioxide from first principles with quantitative accuracy. *Chem. Sci.* **2015**, *7*, 246–255.
- (34) Ramirez, R.; Neuerburg, N.; Fernandez-Serra, M.-V.; Herrero, C. P. Quasi-harmonic approximation of thermodynamic properties of ice Ih, II, and III. *J. Chem. Phys.* **2012**, *137*, 044502.
- (35) Nath, P.; Plata, J. J.; Usanmaz, D.; Al Rahal Al Orabi, R.; Fornari, M.; Nardelli, M. B.; Toher, C.; Curtarolo, S. High-throughput prediction of finite-temperature properties using the quasi-harmonic approximation. *Comput. Mater. Sci* **2016**, *125*, 82–91.
- (36) Huang, L.-F.; Lu, X.-Z.; Tennessen, E.; Rondinelli, J. M. An efficient ab-initio quasiharmonic approach for the thermodynamics of solids. *Comput. Mater. Sci* **2016**, *120*, 84–93.
- (37) Choy, C. L.; Wong, S. P.; Young, K. Thermal expansion and Grüneisen parameters for anisotropic solids. *Phys. Rev. B* **1984**, *29*, 1741–1747.
- (38) Gould, S.; Fernando, B.; Cherian, A.; Anderson, P.; Cruz, R. S.; Guo, E. On Differentiating Parameterized Argmin and Argmax Problems with Application to Bi-level Optimization. *arXiv:1607.05447 [cs, math]* **2016**, arXiv: 1607.05447.
- (39) Zhang, W.; Wu, C.; Duan, Y. Convergence of replica exchange molecular dynamics. *J. Chem. Phys.* **2005**, *123*, 154105.
- (40) Robertson, M. J.; Tirado-Rives, J.; Jorgensen, W. L. Improved Peptide and Protein Torsional Energetics with the OPLS-AA Force Field. *J. Chem. Theory Comput.* **2015**, *11*, 3499–3509.
- (41) Jorgensen, W. L.; Maxwell, D. S.; Tirado-Rives, J. Development and Testing of the OPLS All-Atom Force

- Field on Conformational Energetics and Properties of Organic Liquids. *J. Am. Chem. Soc.* **1996**, *118*, 11225–11236.
- (42) Hairer, E.; Nørsett, S. P.; Wanner, G. *Solving Ordinary Differential Equations I: Nonstiff Problems*; Springer Science & Business Media, 2008.
- (43) Kimura, K.; Hirayama, F.; Uekama, K. Characterization of tolbutamide polymorphs (burger's forms II and IV) and polymorphic transition behavior. *J. Pharm. Sci.* **1999**, *88*, 385–391.
- (44) Braun, D. E.; Gelbrich, T.; Kahlenberg, V.; Tessadri, R.; Wieser, J.; Griesser, U. J. Conformational polymorphism in aripiprazole: Preparation, stability and structure of five modifications. *J. Pharm. Sci.* **2009**, *98*, 2010–2026.
- (45) van Miltenburg, J. C.; Oonk, H. A. J.; van den Berg, G. J. K. Low-Temperature Heat Capacities and Derived Thermodynamic Functions of Para-Substituted Halogen Benzenes. 2. p-Bromiodobenzene and p-Diiodobenzene. *J. Chem. Eng. Data* **2001**, *46*, 84–89.
- (46) Drebuschak, V. A.; Drebuschak, T. N.; Chukanov, N. V.; Boldyreva, E. V. Transitions among five polymorphs of chlorpropamide near the melting point. *J. Therm. Anal. Calorim.* **2008**, *93*, 343–351.
- (47) Brandenburg, J. G.; Potticary, J.; Sparkes, H. A.; Price, S. L.; Hall, S. R. Thermal Expansion of Carbamazepine: Systematic Crystallographic Measurements Challenge Quantum Chemical Calculations. *J. Phys. Chem. Lett.* **2017**, *8*, 4319–4324.
- (48) Wilson, C. Variable temperature study of the crystal structure of paracetamol (p-hydroxyacetanilide), by single crystal neutron diffraction. *Z. Kristallogr. Cryst. Mater.* **2009**, *215*, 693–701.
- (49) Horstman, E. M.; Goyal, S.; Pawate, A.; Lee, G.; Zhang, G. G. Z.; Gong, Y.; Kenis, P. J. A. Crystallization Optimization of Pharmaceutical Solid Forms with X-ray Compatible Microfluidic Platforms. *Cryst. Growth Des.* **2015**, *15*, 1201–1209.
- (50) Lisgarten, J. N.; Palmer, R. A.; Saldanha, J. W. Crystal and molecular structure of 5-carbamyl-5H-dibenzo[b,f]azepine. *J. Crystallogr. Spectrosc. Res.* **1989**, *19*, 641–649.
- (51) Nievergelt, P. P.; Spingler, B. Growing single crystals of small molecules by thermal recrystallization, a viable option even for minute amounts of material? *CrystEngComm* **2017**, *19*, 142–147.
- (52) Sovago, I.; Gutmann, M. J.; Senn, H. M.; Thomas, L. H.; Wilson, C. C.; Farrugia, L. J. Electron density, disorder and polymorphism: high-resolution diffraction studies of the highly polymorphic neuralgic drug carbamazepine. *Acta Cryst B* **2016**, *72*, 39–50.
- (53) El Hassan, N.; Ikni, A.; Gillet, J.-M.; Spasojevic-de Bir, A.; Ghermani, N. E. Electron Properties of Carbamazepine Drug in Form III. *Cryst. Growth Des.* **2013**, *13*, 2887–2896.
- (54) Haisa, M.; Kashino, S.; Kawai, R.; Maeda, H. The Monoclinic Form of p-Hydroxyacetanilide. *Acta Cryst B* **1976**, *32*, 1283–1285.

- (55) Wilson, C. C.; Shankland, N.; Florence, A. J.; Frampton, C. S. Single-crystal neutron diffraction of bioactive small molecules. *Physica B* **1997**, *234-236*, 84–86.
- (56) Wilson, C. C. Neutron diffraction of p-hydroxyacetanilide (Paracetamol): libration or disorder of the methyl group at 100 K. *J. Mol. Struct* **1997**, *405*, 207–217.
- (57) Nyman, J.; Day, G. M. Static and lattice vibrational energy differences between polymorphs. *CrystEngComm* **2015**, *17*, 5154–5165.
- (58) Dybeck, E. C.; McMahon, D. P.; Day, G. M.; Shirts, M. R. Exploring the Multi-minima Behavior of Small Molecule Crystal Polymorphs at Finite Temperature. *Crystal Growth & Design* **2019**, *19*, 5568–5580.
- (59) Fabbiani, F. P. A.; Allan, D. R.; Parsons, S.; Pulham, C. R. An exploration of the polymorphism of piracetam using high pressure. *CrystEngComm* **2005**, *7*, 179–186.
- (60) Louër, D.; Louër, M.; Dzyabchenko, V. A.; Agafonov, V.; Ceolin, R. Structure of a metastable phase of piracetami from X-ray powder diffraction using the atom–atom potential method. *Acta Cryst B* **1995**, *51*, 182–187.
- (61) Admiraal, G.; Eikelenboom, J. C.; Vos, A. Structures of the triclinic and monoclinic modifications of (2-oxo-1-pyrrolidinyl)acetamide. *Acta Cryst B* **1982**, *38*, 2600–2605.
- (62) Chambrier, M.-H.; Bouhmada, N.; Bonhomme, F.; Lebègue, S.; Gillet, J.-M.; Jelsch, C.; Ghermani, N. E. Electron and Electrostatic Properties of Three Crystal Forms of Piracetam. *Cryst. Growth Des.* **2011**, *11*, 2528–2539.
- (63) Galdecki, Z.; Glowka, M. L. *Pol. J. Chem.* **1983**, *57*, 1307.
- (64) Shipilova, A. S.; Knyazev, A. V.; Gusarova, E. V.; Amosov, A. A.; Knyazeva, S. S. X-ray studies of piracetam in a wide range of temperatures. *J. Solid State Chem.* **2018**, *2*, 51–56.
- (65) Tilborg, A.; Jacquemin, D.; Norberg, B.; Perpète, E.; Michaux, C.; Wouters, J. Structural study of piracetam polymorphs and cocrystals: crystallography redetermination and quantum mechanics calculations. *Acta Cryst B* **2011**, *67*, 499–507.
- (66) Fernandes, P.; Shankland, K.; Florence, A. J.; Shankland, N.; Johnston, A. Solving Molecular Crystal Structures from X-ray Powder Diffraction Data: The Challenges Posed by  $\gamma$ -Carbamazepine and Chlorothiazide N,N,-Dimethylformamide (1/2) Solvate. *J. Pharm. Sci* **2007**, *96*, 1192–1202.
- (67) Mahapatra, S.; Nayak, S. K.; Prathapa, S. J.; Guru Row, T. N. Anhydrous Adenine: Crystallization, Structure, and Correlation with Other Nucleobases. *Cryst. Growth Des.* **2008**, *8*, 1223–1225.
- (68) Nangia, A.; Srinivasulu, A. *CSD Comm.* **2005**,
- (69) Rø, G.; Sørum, H. The crystal and molecular structure of  $\delta$ -pyrazinecarboxamide. *Acta Cryst B* **1972**, *28*, 1677–1684.

- (70) Castro, R. A. E.; Maria, T. M. R.; Évora, A. O. L.; Feiteira, J. C.; Silva, M. R.; Beja, A. M.; Cantilho, J.; Eusébio, M. E. S. A New Insight into Pyrazinamide Polymorphic Forms and their Thermodynamic Relationships. *Cryst. Growth Des.* **2010**, *10*, 274–282.
- (71) Nakata, K.; Takaki, Y. *Memoirs of Osaka Kyoiku University* **1987**, *36*, 93.
- (72) Tamura, C.; Kuwano, H. Crystallographic data of carboxylic acids and carboxyamides of picoline and pyrazine derivatives. *Acta Cryst* **1961**, *14*, 693.
- (73) Bacon, G. E.; Lisher, E. J.; Pawley, G. S. A neutron powder diffraction study of deuterated  $\alpha$ -resorcinol: a test of profile refinement using TLS constraints. *Acta Cryst B* **1979**, *35*, 1400–1403.
- (74) Bacon, G. E.; Lisher, E. J. A neutron powder diffraction study of deuterated  $\alpha$ - and  $\beta$ -resorcinol. *Acta Cryst B* **1980**, *36*, 1908–1916.
- (75) Druzbicki, K.; Mikuli, E.; Pałka, N.; Zalewski, S.; Ossowska-Chruściel, M. D. Polymorphism of Resorcinol Explored by Complementary Vibrational Spectroscopy (FT-RS, THz-TDS, INS) and First-Principles Solid-State Computations (Plane-Wave DFT). *J. Phys. Chem. B* **2015**, *119*, 1681–1695.
- (76) Fronczek, F. R. *CSD Comm.* **2001**,
- (77) Robertson J. Monteath,; Ubbelohde A. R., A New Form of Resorcinol. I. Structure Determination by X-Rays. *Proc. Royal Soc. Lond.* **1938**, *167*, 122–135.
- (78) Hendricks, S. B.; Maxwell, L. R.; Mosley, V. L.; Jefferson, M. E. X-Ray and Electron Diffraction of Iodine and the Diiodobenzenes. *J. Chem. Phys.* **1933**, *1*, 549–565.
- (79) Hinchliffe, A.; Munn, R. W.; Pritchard, R. G.; Spicer, C. J. The structure of a solution-grown crystal of 1,4-diiodobenzene. *J. Mol. Struct* **1985**, *130*, 93–96.
- (80) Haisa, M.; Kashino, S.; Maeda, H. The orthorhombic form of p-hydroxyacetanilide. *Acta Cryst B* **1974**, *30*, 2510–2512.
- (81) Drebuschak, T. N.; Boldyreva, E. V. Variable temperature (100–360 K) single-crystal X-ray diffraction study of the orthorhombic polymorph of paracetamol (p-hydroxyacetanilide). *Z. Kristallogr. Cryst. Mater.* **2009**, *219*, 506–512.
- (82) Nichols, G.; Frampton, C. S. Physicochemical Characterization of the Orthorhombic Polymorph of Paracetamol Crystallized from Solution. *J. Pharm. Sci.* **1998**, *87*, 684–693.
- (83) Donaldson, J. D.; Leary, J. R.; Ross, S. D.; Thomas, M. J. K.; Smith, C. H. The structure of the orthorhombic form of tolbutamide (1-n-butyl-3-p-toluenesulphonylurea). *Acta Cryst B* **1981**, *37*, 2245–2248.
- (84) Drebuschak, T. N.; Drebuschak, V. A.; Pankrushina, N. A.; Boldyreva, E. V. Single-crystal to single-crystal conformational polymorphic transformation in tolbutamide at 313 K. Relation to other polymorphic transformations in tolbutamide and chlorpropamide. *CrystEngComm* **2016**, *18*, 5736–5743.

- (85) Schreyer, M.; Guo, L.; Thirunahari, S.; Gao, F.; Garland, M. Simultaneous determination of several crystal structures from powder mixtures: the combination of powder X-ray diffraction, band-target entropy minimization and Rietveld methods. *J Appl Cryst* **2014**, *47*, 659–667.
- (86) Thirunahari, S.; Aitipamula, S.; Chow, P. S.; Tan, R. B. H. Conformational Polymorphism of Tolbutamide: A Structural, Spectroscopic, and Thermodynamic Characterization of Burger's Forms I–IV. *J. Pharm. Sci.* **2010**, *99*, 2975–2990.
- (87) Drebuschak, T. N.; Chesalov, Y. A.; Boldyreva, E. V. A conformational polymorphic transition in the high-temperature  $\epsilon$ -form of chlorpropamide on cooling: a new  $\epsilon'$ -form. *Acta Cryst B* **2009**, *65*, 770–781.
- (88) Koo, C. H.; Cho, S. I.; Yeon, Y. H. The crystal and molecular structure of chlorpropamide. *Arch. Pharm. Res.* **1980**, *3*, 37–49.
- (89) Drebuschak, T. N.; Chukanov, N. V.; Boldyreva, E. V. Two polymorphs of chlorpropamide: the  $\delta$ -form and the high-temperature  $\epsilon$ -form. *Acta Cryst C* **2008**, *64*, o623–o625.